PHYSICS

STUDY OF THE REACTIONS $K^-N \to \pi^-\pi^-\pi^+\Lambda$, $K^-N \to \pi^-\pi^-\pi^+\Sigma^\circ$, AND $K^-N \to \pi^-\pi^-\pi^+\pi^\circ\Lambda$ AT 4.91 GeV/c

RONALD ELDEN BERG

Dissertation under the direction of Professor Alfred Weinberg

The reactions (1) $K^-N \to \pi^-\pi^-\pi^+\Lambda$, (2) $K^-N \to \pi^-\pi^-\pi^+\Sigma^\circ$, and (3) $K^-N \to \pi^-\pi^-\pi^+\pi^\circ\Lambda$ at a beam momentum of (4.910 ± 0.007) GeV/c have been studied. The cross-sections for these reactions and for resonance production in them have been measured. The observed single particle production angular distributions show good qualitative but not quantitative agreement with the Reggeized multiperipheral model of Chan, Loskiewicz, and Allison. We found strong disagreement between the amounts of observed resonance production and the multiperipheral model of Plahte and Roberts that is based on the models of Chan *et al.* and Veneziano. However we included isospin effects only in an approximate manner.

Approved_____ Date_____
Adviser

A STUDY OF THE REACTIONS $K^-N \rightarrow \pi^-\pi^-\pi^+\Lambda$, $K^-N \rightarrow \pi^-\pi^-\pi^+\Sigma^\circ$, AND $K^-N \rightarrow \pi^-\pi^-\pi^+\pi^\circ\Lambda$ AT 4.9 GeV/c

By

Ronald Elden Berg

Dissertation

Submitted to the Faculty of the

Graduate School of Vanderbilt University

in partial fulfillment of the requirements

for the degree of

DOCTOR OF PHILOSOPHY

in

Physics

August, 1971

Nashville, Tennessee

Approved: Date:

_____ _____

_____ _____

_____ _____

_____ _____

_____ _____

To my parents, Elmer and Inga Berg

ACKNOWLEDGMENTS

The work presented here is the result of the efforts of many people.

The continuous interest, dedication, and guidance of Dr. Alfred Weinberg has been a major factor in the completion of this work and is gratefully acknowledged by the author.

The assistance and encouragement of the other faculty members of the high energy research group which included Drs. E. O. Salant, M. S. Webster, E. J. Moses, F. M. Bomse, and J. W. Waters is greatly appreciated. I particularly wish to thank Dr. Salant for his support. I thank Drs. T. C. Bacon, W. J. Fickinger, and H. W. K. Hopkins for contributing work prior to and necessary for this experiment.

I wish especially to thank my fellow graduate student, Ronald R. Price, for an enjoyable association and innumerable contributions to this work.

The company of the other high energy graduate students--T. B. Borak, W. R. Burdett, W. E. Ellis, J. H. Hanlon, and J. Mandzy--has been most profitable.

I thank A. D. Kellner for work on the early part of the experiment.

I thank W. Rice, Jr. for building and maintaining much of the electronic equipment necessary to do the experiment and W. Akin for electronics work prior to and necessary for the experiment.

Without the generous help and enthusiasm of Anastasia Koshakji, Chief Supervisor, and many other scanners and measurers this experiment could not have been completed.

I acknowledge with thanks the work of the crews of the Brookhaven National Laboratory alternating-gradient synchrotron and the 80-inch bubble chamber.

Thanks are due to H. W. Carlton and the other members of the Vanderbilt University Science Shop for building and maintaining the scanning and measuring machines.

The financial support of Vanderbilt University and the continuous cooperation of the Vanderbilt University Computing Center are greatly appreciated. The services of the Atomic Energy Commission Computation Center at Courant Institute for Mathematical Sciences, New York University and specifically those of Robert Malchie at this installation are greatly appreciated.

This work was supported by a National Science Foundation research contract to the Vanderbilt University Bubble Chamber Group headed by Dr. E. O. Salant and Dr. M. S. Webster.

TABLE OF CONTENTS

	Page
ACKNOWLEDGMENTS	iii
LIST OF TABLES	vii
LIST OF FIGURES	viii
Chapter	
I. INTRODUCTION	1
II. DATA COLLECTION	3
A. Exposing, Scanning, and Measuring Bubble Chamber Film	3
B. Geometrical Reconstruction and Kinematic Fitting	7
III. EXPERIMENTAL DETAILS	14
A. Beam Momentum and Magnetic Field	14
B. Spectator Protons	17
C. Determining the Events of Each Reaction	20
1. Vee decision	20
2. Separating events of the reactions $K^-N \to \pi^-\pi^-\pi^+\Lambda$ and $K^-N \to \pi^-\pi^-\pi^+\Sigma^\circ$	21
3. The reaction $K^-N \to \pi^-\pi^-\pi^+\Lambda\pi^\circ$	33
D. Small Corrections for Lost Vees	38
1. Vees lost out end of bubble chamber	38
2. Vees lost due to slow π^-	39
3. Vees lost near main vertex	44

Chapter Page

IV. MODELS 51

A. The Multiperipheral Model of Chan, Loskiewicz and Allison 51

B. The Veneziano-Type Multiperipheral Model of Plahte and Roberts 58

V. DATA AND RESULTS OF THE CLA CALCULATIONS 64

A. Resonance Production 67

B. Single Particle Distributions 128

VI. COMPARISON OF DATA WITH MODEL OF PLAHTE AND ROBERTS 151

VII. CONCLUSIONS 159

APPENDIX 162

LIST OF REFERENCES 168

LIST OF TABLES

Table		Page
1.	Number of Events, Percentage Contributions and Cross-Sections for Resonant and Non-Resonant Events Observed in Reactions (I-1) and (I-2)	113
2.	Number of Events, Percentage Contributions, and Cross-Sections for Resonant and Non-Resonant Events Observed in Reaction (I-3)	114
3.	Description of Peaking in Resonance Production Angular Distributions, Signal to Background Ratios, and Mass Cuts for Resonances and Control Regions	126
4.	Average Values and Errors for Transverse (P_T) and Longitudinal (P_L) Momenta of the Single Particles in the Overall Center of Mass as Obtained from the Data and Given by the CLA Model	147
5.	Chi-Squared Probability that CLA Model Agrees with Data for Single Particle Cos θ Distributions	148
6.	Fraction of Baryons in the Forward Hemisphere of the Center of Mass System	149
7.	Cross-Sections and Percentages for Resonances Observed in the Reaction $K^-N \rightarrow \Lambda\pi^-\pi^-\pi^+\pi^\circ$ at an Incident Beam Momentum of Three GeV/c[27].	160
8.	Cross-Section Data for Rolls 765 and 766	163
9.	Total Cross-Sections[7,30] for K^-P, K^-D and K^-N for Various Beam Momenta	166

LIST OF FIGURES

Figure		Page
1.	The Fiducial Volume Boundaries as Seen by Bubble Chamber Camera Number One	5
2.	Illustration of Angles ϕ and λ Used by Geometry Program	9
3.	Distribution of Measured Beam Momentum	15
4.	Measured Spectator Momentum Distribution for All Events Having a Lambda Fit Probability of Greater than One Per Cent. There are 1246 Measured Protons with Momentum Less than 0.500 GeV/c and 2536 Unseen Protons	18
5.	Distribution of Baryon Missing Mass Squared for Events Ambiguous between Reactions (I-1) and (I-2)	24
6.	Distribution of Cosine of Angle between Λ and Σ° Direction in Σ° Rest Frame for (A) Unambiguous Σ°, (B) Ambiguous Λ/Σ° Called Σ°, (C) Ambiguous Λ/Σ° Called Λ	26
7.	Distribution of Baryon Missing Mass Squared for Reaction (I-1)	29
8.	(A) Distribution of the Deviation of the Missing Mass Squared, F_2, for Events Having Fit Probabilities as Follows: Reaction (I-2) > One Per Cent, [Reaction (I-2)/Reaction (I-3)] > 0.5, and [Reaction (I-2)/Reaction (I-1)] > 2.0 (B) Distribution of Baryon $(MM)^2$ for Events in (A) Having $\lvert F_2 \rvert < 2.0$	31
9.	Distribution of F_3 for All Events Not Taken as Reaction (I-1) or (I-2) but Having Fit Probability for Reaction (I-3) Greater than One Per Cent. The Smooth Curve is a Gaussian Normalized to the 644 Events Having $F_3 < 0.0$	34

Figure | Page

10. Distribution of Missing Boson Mass Squared Minus π° Mass Squared for All Events Not Included in Reaction (I-1) or (I-2). Shaded Portion Corresponds to Events Included in Reaction (I-3). Cross-Hatched Portion Corresponds to Events Having a Fit Probability to Reaction (I-3) of Greater than one Per Cent and F_3 Greater than 1.25 36

11. Distribution of the Cosine of the Angle between the π^- Momentum and Λ Direction in the Λ Rest System for the Events in Reaction (I-3) for Various Λ Momenta 40

12. Distribution of Lambda Laboratory Momentum for the Events of Reaction (I-3) 42

13. Distribution of Probability that Lambda Would Go as Far as It Did or Farther for Reaction (I-3) for Various Intervals of Lambda Laboratory Momentum 46

14. For Reaction (I-3) the Distribution of Probability that Lambda Would Go as Far as It Did or Farther for All Values of Lambda Laboratory Momentum and for Values Greater than 2.2 GeV/c 48

15. The Multiperipheral Graph for the Collision Process $A + B \rightarrow 1 + 2 + 3 + \cdots + n$ 52

16. (A) A typical diagram. (B) Method of Including Clebsch-Gordan Coefficients 61

17. The Thirteen Diagrams Which Were Calculated for Reaction (I-1) Using the CLA Model 65

18. For the Reaction $K^-N \rightarrow \pi^-\pi^-\pi^+\Lambda$ [Reaction (I-1)] with 479 Events (A) Gives the Effective Mass Distributions for the Particle Combinations $\Lambda^\circ\pi^-$ [Hereafter Denoted as the Distribution of $M(\Lambda\pi^-)$], and (B) Distribution of $M(\Lambda\pi^+)$. The Smooth Curves on These and All Subsequent Graphs (Unless Otherwise Indicated) Are the Results of the CLA Model Normalized to the Data 69

Figure | Page

19. Center of Mass Production Cosine Distribution of Reaction (I-1) for the Particle Combinations
(A) $\Lambda\pi^-$ Where Cross-Hatched Portion Corresponds to 137 Combinations Obtained by Demanding $M(\Lambda\pi^-)$ in the Mass Interval [1.342, 1.442] GeV/c^2. If Both Possible Combinations Had Masses in the Interval of Interest We Plotted Only the Combination Having the Mass Closer to the Resonance of Interest [In This Case the $Y^{*-}(1385)$]. Unless Otherwise Indicated This Procedure Will Be Adhered To in Subsequent Graphs Where Mass Cuts Are Made and an Ambiguity Exists between π^- Combinations.
(B) $\Lambda\pi^+$ Where Cross-Hatched Portion Corresponds to 78 Combinations Obtained by Demanding $M(\Lambda\pi^+)$ in the Mass Interval [1.342, 1.442] GeV/c^2 71

20. Cross-Section Versus Beam Momentum as Predicted by CLA Model for $Y^{*\pm}(1385)$ and $Y^{*\pm}(1626)$. Curves Are Normalized to the Purdue Data at 4.5 GeV/c 75

21. Mass Distributions for Reaction (I-1) When We Attempted to Reduce Background by Using BNL Criteria[18] for
(A) $M(\Lambda\pi^\pm)$, (B) $M(\Lambda\pi^-)$ with 518 Combinations, and
(C) $M(\Lambda\pi^+)$ with 246 Combinations 79

22. For Reaction (I-1) (A) $\pi^-\pi^+$ Center of Mass Production Angular Distribution Where Cross-Hatched Region Corresponds to 245 Combinations Having $M(\pi^-\pi^+)$ in the Mass Interval [0.667, 0.867] GeV/c^2.
(B) $M(\pi^-\pi^+)$ Distribution 81

23. For $K^-N \rightarrow \pi^-\pi^-\pi^+\Sigma^\circ$ [Reaction (I-2)] with 201 Events
(A) Is the Center of Mass Production Angular Distribution for the $\pi^-\pi^+$ Combinations Where the Cross-Hatched Area Corresponds to the 107 Events Obtained by Demanding $M(\pi^-\pi^+)$ in the Mass Interval [0.667, 0.867] GeV/c^2, and
(B) the $M(\pi^-\pi^+)$ Distribution 83

24. The 3π Mass Distribution for (A) Reaction (I-1) and
(B) Reaction (I-2) 86

25. The 3π Mass Distribution Where We Have Demanded that at Least One $\pi^-\pi^+$ Mass Combination be in the Mass Interval from 0.666 to 0.866 GeV/c^2 for
(A) Reaction (I-1) Giving 248 Events and
(B) Reaction (I-2) Giving 107 Events 88

Figure | Page

26. For the Reaction $K^-N \rightarrow \pi^-\pi^-\pi^+\pi^\circ\Lambda$ [Reaction (I-3)] with 1347 Events (A) the Center of Mass Production Angular Distribution for the $\Lambda\pi^-$ Combinations Where the Cross-Hatched Area Corresponds to the 495 Events Obtained by Demanding a $\Lambda\pi^-$ Mass Combination in the Mass Interval from 1.342 to 1.442 GeV/c^2
(B) Distribution in $M(\Lambda\pi^-)$ 90

27. For the Particle Combination $\Lambda\pi^+$ of Reaction (I-3)
(A) Gives the Center of Mass Production Angular Distribution Where the Cross-Hatched Area Corresponds to the 238 Events Obtained by Demanding $M(\Lambda\pi^+)$ be in the Mass Interval [1.342, 1.442] GeV/c^2
(B) The Distribution of $M(\Lambda\pi^+)$ 92

28. For the Particle Combination $\Lambda\pi^\circ$ of Reaction (I-3)
(A) Gives the Center of Mass Production Angular Distribution Where the Cross-Hatched Area Corresponds to the 281 Events Obtained by Requiring $M(\Lambda\pi^\circ)$ be in the Mass Interval [1.300, 1.450] GeV/c^2
(B) The Distribution of $M(\Lambda\pi^\circ)$ 94

29. For the Particle Combination $\pi^-\pi^+$ of Reaction (I-3)
(A) Gives the Center of Mass Production Angular Distribution Where the Cross-Hatched Area Corresponds to the 599 Events Obtained by Requiring $M(\pi^-\pi^+)$ be in the Interval from 0.680 to 0.880 GeV/c^2
(B) Distribution of $M(\pi^-\pi^+)$ Where the Dashed Line Shows the Result of the CLA Model Computed without Including Any Diagrams for $\rho(765)$ Production and Normalized to the Number of Observed Combinations in the Mass Intervals [0.480 to 0.680] and [0.880 to 1.580] GeV/c^2. The Solid Line Gives the CLA Result Where All Diagrams for ρ Production Are Included 98

30. For the Particle Combinations $\pi^-\pi^\circ$ for Reaction (I-3)
(A) Gives the Center of Mass Production Angular Distribution Where the Cross-Hatched Area Corresponds to the 607 Events Obtained by Requiring $M(\pi^-\pi^\circ)$ to be in the Interval 0.675 to 0.875 GeV/c^2
(B) Distribution of $M(\pi^-\pi^\circ)$ Where the Dashed Line Shows the Result of the CLA Model Computed Without Including Diagrams for $\rho(765)$ and Normalized to the Number of Events in the Mass Intervals [0.475 to 0.675] and [0.875 to 1.575] GeV/c^2 100

Figure | Page

31. For Reaction (I-3) the Mass Distributions of the Particle Combinations (A) $\pi^-\pi^-$ and (B) $\pi^+\pi^\circ$ Where Dashed Line Shows the Distribution Given by the CLA Model Computed without Including Diagrams for $\rho(765)$ and Normalized to the Number of Events in the Mass Intervals [0.475 to 0.675] and [0.875 to 1.575] GeV/c^2 102

32. For the Particle Combination $\pi^-\pi^+\pi^\circ$ of Reaction (I-3) (A) Gives the Center of Mass Production Angular Distribution Where the Cross-Hatched Area Corresponds to the 239 Events Obtained by Requiring $M(\pi^-\pi^+\pi^\circ)$ in the Mass Interval [0.740 to 0.840] GeV/c^2 (B) The $M(\pi^-\pi^+\pi^\circ)$ Distribution Where the Dashed Curve in the Region of the $\omega^\circ(784)$ is a Linear Estimate of the Background 105

33. The Mass Distribution of the Particle Combination $\pi^-\pi^-\pi^+\pi^\circ$ for Reaction (I-3) 108

34. For the 267 Events Obtained for the Reaction $K^-N \rightarrow \omega^\circ(784)\pi^-\Lambda$ by Requiring $M(\pi^-\pi^+\pi^\circ)$ to be in the Interval [0.740 to 0.840] GeV/c^2
(A) Gives the Center of Mass Production Angular Distribution Where the Cross-Hatched Area Corresponds to 76 Events Obtained by Requiring $M(\pi^-\pi^-\pi^+\pi^\circ)$ to be in the Interval [1.130, 1.330] GeV/c^2
(B) Gives the Distribution in $M(\pi^-\pi^-\pi^+\pi^\circ)$ 110

35. For Reaction (I-1) the Center of Mass Production Angular Distributions Where Background Has Been Subtracted for (A) $Y^{*-}(1385)$ with 71 Events, (B) $Y^{*+}(1385)$ with 44 Events and (C) $\rho^\circ(765)$ with 101 Events 115

36. For Reaction (I-3) the Center of Mass Production Angular Distributions Where Background Has Been Subtracted for (A) $Y^{*-}(1385)$ with 188 Events, (B) $Y^{*\circ}(1385)$ with 50 Events, and (C) $\rho^\circ(765)$ with 128 Events 117

37. For Reaction (I-3) the Center of Mass Production Angular Distributions Where Background Has Been Subtracted for (A) $B^-(1235)$ with 40 Events and (B) $\omega^\circ(784)$ with 62 Events 119

Figure | Page

38. For Reaction (I-1) the Center of Mass Production Angular Distribution for the 141 Events Obtained by Demanding $M(\pi^-\pi^+)$ in the Mass Interval [1.092, 1.417] GeV/c^2 122

39. For Reaction (I-3) the Center of Mass Production Angular Distribution for the 178 Events Obtained by Demanding $M(\Lambda\pi^\circ)$ in the Mass Interval [1.725, 1.825] GeV/c^2 124

40. The Single Particle Center of Mass Longitudinal Momentum (P_L) Distributions of Reaction (I-1) for (A) Λ, (B) π^-, and (C) π^+ 129

41. The Single Particle Center of Mass Transverse Momentum (P_T) Distributions of Reaction (I-1) for (A) Λ, (B) π^- and (C) π^+ 131

42. The Single Particle Center of Mass Production Angular Distributions of Reaction (I-1) for (A) Λ, (B) π^-, and (C) π^+, Where Dashed Lines Give the CLA Model Results When We Use Values for b_i That Are 0.5 Times the Ones We Regularly Used 133

43. The Single Particle Center of Mass Longitudinal Momentum Distributions of Reaction (I-2) for (A) Σ°, (B) π^-, and (C) π^+ 135

44. The Single Particle Center of Mass Transverse Momentum Distributions of Reaction (I-2) for (A) Σ°, (B) π^-, and (C) π^+ 137

45. The Single Particle Center of Mass Production Angular Distributions of Reaction (I-2) for (A) Σ°, (B) π^-, and (C) π^+. The Dashed Lines Give the CLA Model Results When We Use Values for b_i That Are 0.5 Times the Ones We Regularly Used 139

46. The Single Particle Center of Mass Longitudinal Momentum Distributions of Reaction (I-3) for (A) Λ, (B) π^-, (C) π°, and (D) π^+ 141

47. The Single Particle Center of Mass Transverse Momentum Distributions of Reaction (I-3) for (A) Λ, (B) π^-, (C) π°, and (D) π^+ 143

Figure Page

48. The Single Particle Center of Mass Production Angular Distributions of Reaction (I-3) for (A) Λ, (B) π^-, (C) π°, and (D) π^+ Where the Dashed Lines Give the CLA Model Results When We Use Values for b_i That Are 0.5 Times the Ones We regularly Used 145

49. Mass Distributions of Reaction (I-1) Where the Smooth Curve is the Prediction of the Plahte and Roberts Model Normalized to the Data for the Particle Combinations (A) $\Lambda\pi^-$ and (B) $\Lambda\pi^+$ 152

50. The $\pi^+\pi^-$ Invariant Mass Distribution for Reaction (I-1) Where the Smooth Curve is the Prediction of the Model of Plahte and Roberts Normalized to the Data 154

51. The Distribution in $M(\pi^+\pi^\circ)$ for Reaction (I-3) Where the Smooth Curve is the Prediction of the Plahte and Roberts Model Normalized to the Data 156

CHAPTER I

INTRODUCTION

Resonance production and peripheralism (glancing collisions) are two of the most prominent features of high-energy interactions which have emerged as a result of intensive study over the last decade. The list of sub-atomic particles has grown to more than 100.

For quasi-two body reactions models using the idea of one-particle-exchange have had a large degree of success in explaining the data. These ideas have been extended into multiperipheral models to include three or more particles in the final state. It is interesting to compare these models with the data. This may eventually lead to better understanding and a complete theory.

This work is an experimental study of the reactions

$$K^-d \rightarrow P_s\pi^-\pi^-\pi^+\Lambda, \qquad \text{(I-1)}$$

$$K^-d \rightarrow P_s\pi^-\pi^-\pi^+\Sigma^\circ, \qquad \text{(I-2)}$$

and

$$K^-d \rightarrow P_s\pi^-\pi^-\pi^+\pi^\circ\Lambda \qquad \text{(I-3)}$$

where the K^- has an incident laboratory momentum of (4.910 ± 0.007) GeV/c. The target neutron is in a deuterium nucleus and the symbol P_s refers to a spectator proton that does not take part in the reaction. The experimental results are based on data obtained from analysis of approximately 100,000 pictures taken at Brookhaven National Laboratory.

The details of data collection including scanning and measuring of the bubble chamber film and geometrical reconstruction and kinematic fitting are discussed. The details of selecting the events for these reactions are discussed. Small corrections due to lost vees are given. The cross-sections and production angular distributions for these reactions and for resonance production in them are given. The data are compared to two phenomenological Reggeized multiperipheral models.[1,2]

CHAPTER II

DATA COLLECTION

A. Exposing, Scanning and Measuring Bubble Chamber Film

Our 100,000 triads were obtained by exposing the deuterium filled 80 inch Brookhaven National Laboratory Bubble Chamber[3] to an electrostatically separated beam of K^- mesons having laboratory momentum of (4.910 ± .007) GeV/c. The magnetic field of the chamber was 17,000 Gauss. The chamber was viewed by three cameras. Their lenses were at the corners of a square whose edge was 63.5 cm long. The plane of this square was parallel to the plane of the bubble chamber window and 206.6 cm from its wet surface.

The film was scanned on all three views. This experiment used events having a main vertex with a beam track and three or four outgoing prongs. In order for four-prong events to be accepted, they had to have a proton that stopped in the bubble chamber, i.e. a spectator proton candidate (see Chapter III, Section B). In order for the event to be measured, it had to have an associated vee candidate. By using conservation of linear momentum a crude check was made at the scanning table for vee association by demanding that a straight line drawn from the main vertex through the vee vertex pass within the area defined by the initial directions of the two tracks comprising the vee. If the vee failed to meet this criterion in one or more of the three views it was considered not associated with the main vertex under consideration.

Also, if the scanner was sure that the curvatures and angles of the vee prongs and conservation of momentum implied that it was not associated, she discarded it.

The fiducial volume boundaries, as seen by bubble chamber camera number one, are shown in Figure 1. The main vertex fiducial volume at the median beam depth is 146 cm long and the additional vee vertex volume is 7.5 cm long.

Each roll of film was scanned and then twenty per cent of it was immediately rescanned by another person, who was a very good scanner. The two scans were then compared by a third person, who was one of our best workers and acted as an arbiter on the points of disagreement and as a teacher of the other workers. This method resulted in constant supervision of our workers and in their being shown mistakes they had made. If more than about 15 per cent of the events were missed on the first scan, the roll was rescanned.

Nearly all the measurements were made on image plane digitizers. These machines projected an image of the 70 millimeter film onto a plane surface parallel to the film and with a magnification of approximately ten. There were no mirrors between the film and the image plane. This provided simplicity of construction and eliminated a possible source of distortion. Each machine had a target point that was free to move in the image plane. Its position was determined by rack and pinion gears or wires, relative encoders, and up-down scalers. The least count of our most inaccurate machine was about four microns, as seen on the film, while the inherent accuracy of the bubble chamber system is about seven microns. The location of a bubble was measured by putting the target

Figure 1.--The fiducial volume boundaries as seen by bubble chamber camera number one.

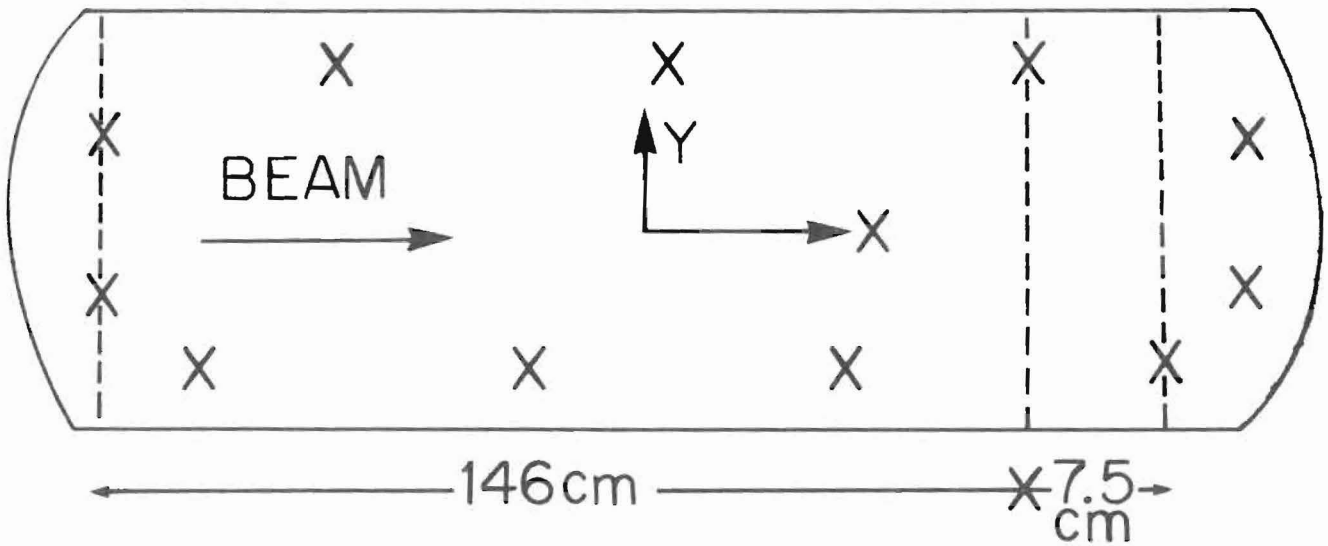
BEAM
Y
X
146cm
7.5
cm

point beneath its image. The measurement of events was done on line to an IBM 1800 computer. The measurer positioned the target at about six approximately equal intervals along the length of a given track. The coordinates of each point were entered directly into the computer. The 1800 checked that the separation between fiducial marks was correct in order to see if the worker measured the correct fiducial marks and also to check the electronics. The on-line computer reminded the measurer to measure all the tracks in all the views. The 1800 was programmed to check that the points measured for each track lay on a smooth curve. The data for the completed event were stored on a magnetic disk and were then punched onto cards at a later convenient time. The data were then transposed onto magnetic tape by an IBM 1401 computer. This tape was shipped to the AEC Computing Center at New York University to be processed by the geometrical reconstruction and kinematical fitting programs. If an event failed to be reconstructed by the geometry program, the event was measured a second time and another attempt was made at reconstruction. About 96 per cent of the events passed through the geometry and kinematics programs.

B. Geometrical Reconstruction and Kinematic Fitting

The geometrical reconstruction and kinematical fitting of the events were done on a Control Data Corporation 6600 computer at the AEC Computing Center of New York University using the program package KGEOM-HKINE-KINC3 which originated at the Rutherford High Energy Laboratory. These programs have been described in detail elsewhere[4] and therefore we shall only briefly summarize the descriptions.

The purpose of the geometrical reconstruction program HGEOM is to calculate the three-momentum with errors for each track of a given event and in addition find the space coordinates with errors for all vertices. A left-handed rectangular coordinate system is used. The origin is at the center of the wet surface of the bubble chamber window. The directions of the x- and y-axes are shown in Figure 2 and the z-axis points into the deuterium. The tracks are reconstructed in three-dimensions by a two-stage process. In the first stage points in space on a track are found by the method of corresponding points. Then a curve which is either a circle, a parabola or a straight line (the choice depends on the magnitude of the angle through which the track has turned) is fitted to the x- and y-coordinates of the space points on the track. The z-coordinates are used to find the dip. In the second stage a helix fit with a mass-dependent correction for slowing down in the liquid is made to the rays of the measured points of all three views by minimizing the sum of the squares of the distances of the rays from the projection of the helix onto a nominal film plane. From the parameters of the fitted helix and the scatter of the rays from the projected helix, the momentum variables with errors for use in the kinematic fitting are calculated. Both the measurement errors calculated from the helix fit and the uncertainties caused by multiple Coulomb scattering are included in the calculation of errors in the momentum variables. The variables are illustrated in Figure 2. The first variable is the azimuthal angle ϕ between the x-axis and the perpendicular projection of the momentum vector into the xy-plane. The second is the dip angle λ between the xy-plane and the momentum vector. The third is the reciprocal of the

Figure 2.--Illustration of angles ϕ and λ used by geometry program.

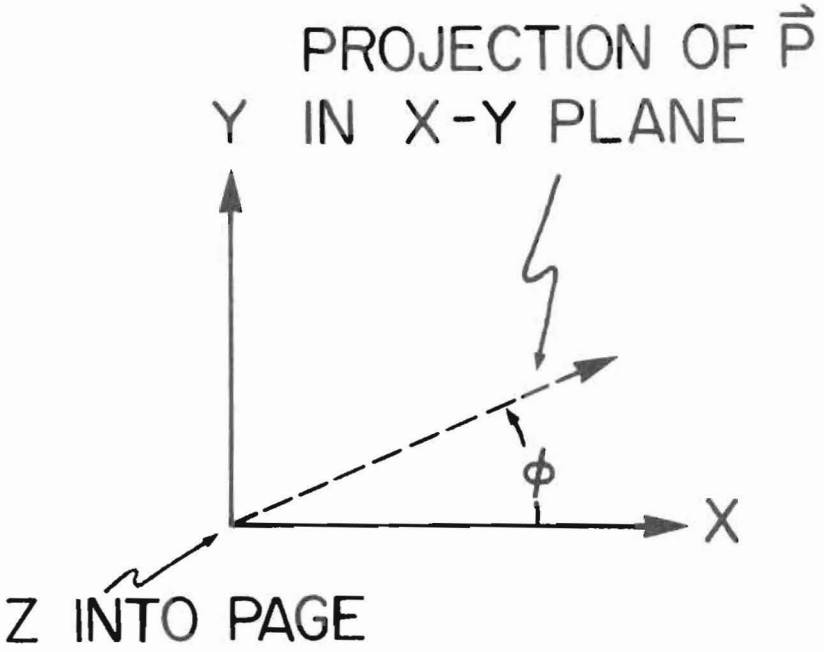
PROJECTION OF $\vec{P}$
IN X-Y PLANE
Y
X
ϕ
Z INTO PAGE

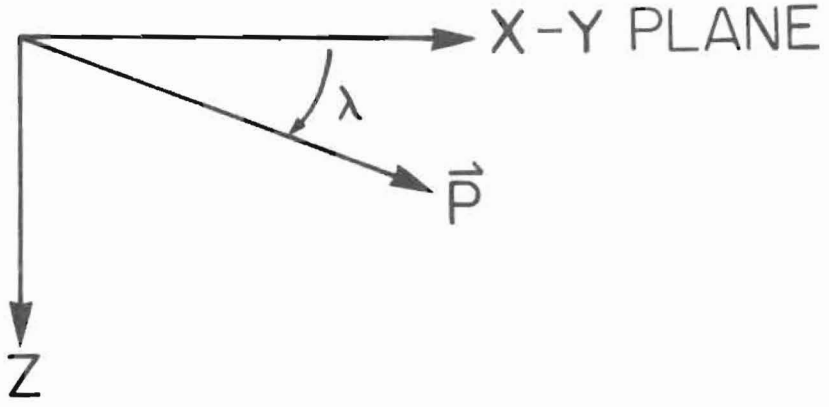
X-Y PLANE
λ
$\vec{P}$
Z

momentum, (1/P). These are used because their deviations are approximately Gaussian. The magnitude of the momentum P (in GeV/c) is found from the radius of curvature r (in cm) of the helix by

$$P = \frac{0.3\ Br}{\cos\lambda} \times 10^{-3} \qquad \text{(II-1)}$$

where B is the z-component of the magnetic field in kilogauss.

The measured track variables and their errors given by the geometrical reconstruction program are then used by the kinematic fitting program HKINE to find fitted track variables and their errors. This is done by minimizing

$$\chi^2 = \sum_i \frac{(v_i^m - v_i^f)^2}{\sigma_i^{\,2}} \qquad \text{(II-2)}$$

subject to the constraints of energy and momentum conservation. The quantity v_i^m is the measured value of a track variable, σ_i is its error, and v_i^f is its fitted value. The sum is taken over the measured quantities. There are three reasons for doing this. The first is that the three-momentum vector of an undetected neutral particle, such as the π^o of Reaction (I-3), is determined. The second is that more accurate values are obtained for the three-momenta of the charged tracks. The third is that the minimum value of χ^2 is useful in determining if the assignment of particle types to the tracks is correct. The particle types fix the masses and the energies depend on these masses. The decay

$$\Lambda \rightarrow P\pi^- \qquad \text{(II-3)}$$

has three constraints since the magnitude of the momentum of the Λ is not measured. Suppose the Λ momentum has been determined by fitting to this decay. Reaction (I-1) has four constraints since there are no undetected neutrals, while Reaction (I-3) has only one constraint, since the π° is not detected. Consider Reaction (I-2) and the subsequent decay

$$\Sigma^\circ \rightarrow \Lambda\gamma. \qquad \text{(II-4)}$$

Since four-momentum is conserved in both the production process and the decay, there are eight constraint equations. Since neither the Σ° or γ are detected, six variables are unmeasured. Therefore Reaction (I-2) has a two-constraint fit.

Sixty-eight per cent of our events had spectator protons with such low momenta that they could not be seen (see Section B of Chapter III). For these, HKINE used rectangular components of momentum with values $P_x = P_y = (0 \pm 30)$ MeV/c and $P_z = (0 \pm 41)$ MeV/c.

KINC3 transferred the results of HGEOM and HKINE to magnetic tapes that were returned to Vanderbilt. These data were then written on buffered tapes by the Vanderbilt Sigma-7 computer which was the only machine used subsequently. The information in this buffered binary form described approximately 17,300 events and comprised 12 magnetic tapes. A single buffered tape was prepared from these and it contained all necessary information for subsequent analysis of Reactions (I-1), (I-2), and (I-3). For a given event the information describing a fit with a chi-squared probability of greater than one per cent for Reaction (I-1) or (I-2) was always transcribed. If there was not such a fit to either

of these, then the information describing a fit with a probability of greater than one per cent for Reaction (I-3) was transcribed. Regardless of whether or not such a fit existed, measured quantities and also fitted quantities for the vee were still written on this single tape provided there was a fit to a lambda vee or an anti-lambda vee with a probability greater than one per cent. (See Section C of Chapter III for the reason behind our interest in anti-lambda fits.) Events which had no fits meeting these criteria were passed over.

CHAPTER III

EXPERIMENTAL DETAILS

A. Beam Momentum and Magnetic Field

The beam momentum was determined by measuring long beam tracks on a film plane measuring machine at Oak Ridge National Laboratory. Permission to use the machine was kindly granted by Dr. H. Cohen and Dr. W. Bugg of Oak Ridge National Laboratory. For an incident track to be measured as a beam track we required that it travel more than halfway through the chamber, be parallel to the other beam tracks and have an interaction. We demanded the interaction in order to avoid possible muon contamination. The measured beam tracks were processed through HGEOM, the geometry program. Since momentum and azimuthal angle ϕ will change for a given beam track as it passes through the chamber these quantities were calculated for each track at $x = 0$ in the bubble chamber coordinate system. The dip angle λ (angle with respect to the xy-plane) will remain essentially unchanged for a beam track as it passes through the chamber because to a good approximation the magnetic field only has a z-component. Histograms showing the λ and ϕ distributions were made. Then appropriate cuts on these quantities were taken to ensure a good beam sample. The resulting distribution of beam momenta is shown in Figure 3. We discarded the tracks below 4.760 GeV/c. Based on the remaining 137 tracks we obtained (4.910 ± .007) GeV/c for the average beam momentum at the center of the bubble chamber. As a check on this value an

Figure 3.--Distribution of Measured Beam Momentum.

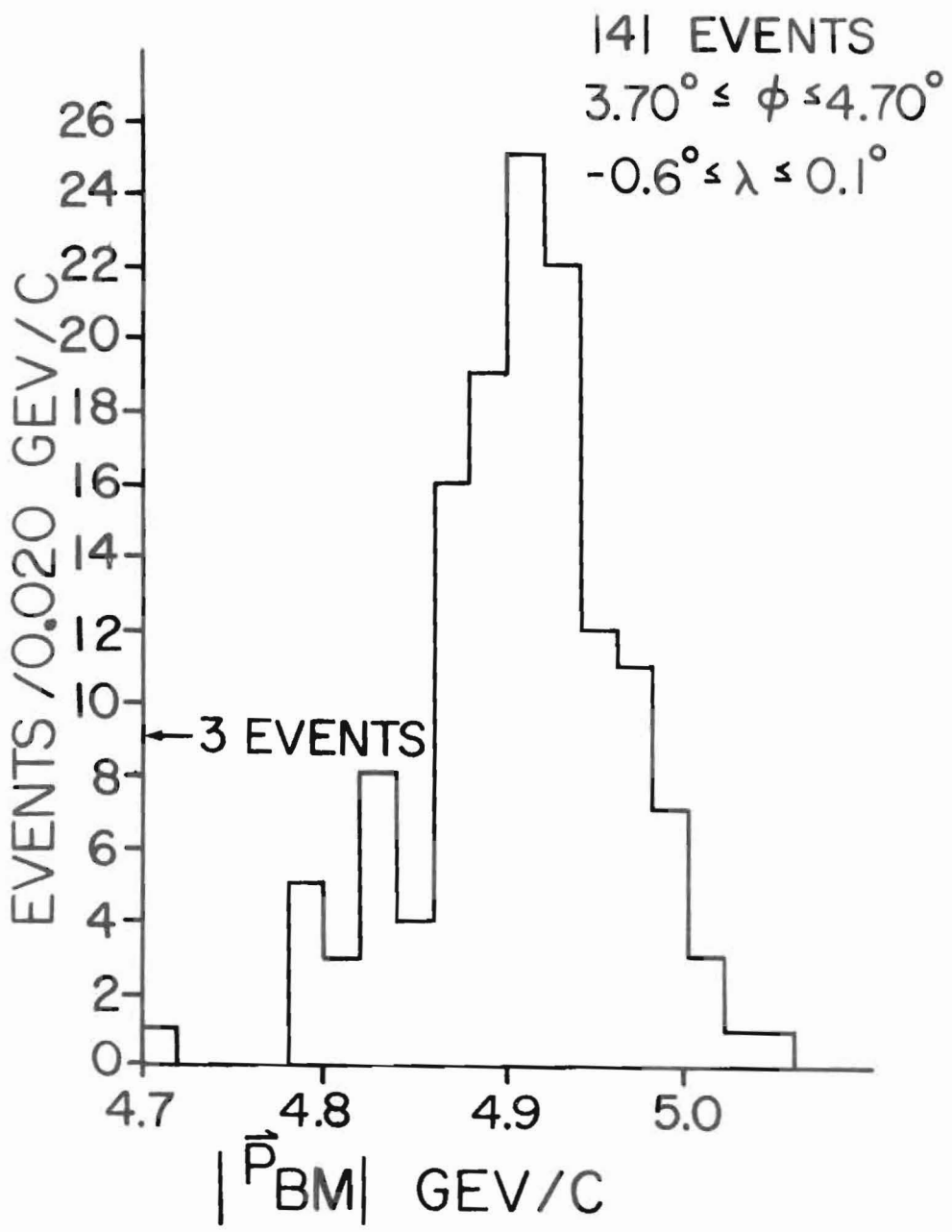
141 EVENTS
3.70° ≤ φ ≤ 4.70°
-0.6° ≤ λ ≤ 0.1°
EVENTS /0.020 GEV/C
26
24
22
20
18
16
14
12
10
8
6
4
2
0
3 EVENTS
4.7
4.8
4.9
5.0
|P_BM| GEV/C

examination of the distribution of initial state energy minus total final state measured energy for the four-constraint events $K^-d \rightarrow p_s\pi^-\pi^-p\overline{K}^\circ$ was made and within statistics no bias was observed.[5]

A check on the value of the magnetic field used in the geometry program was made by plotting the measured invariant mass distribution of the $\overline{K}^\circ$ vee. The mean value obtained for the mass of the $\overline{K}^\circ$ was consistent with the accepted value thus indicating that the magnetic field was free of bias.[5]

B. Spectator Protons

We use the neutron in the deuterium nucleus to study K^-N interactions because the binding energy of the deuteron nucleus is very small (~ 2 MeV) as compared with the energy of the beam (~ 5 GeV). Also the separation of the proton and neutron is sufficiently large so that corrections for hiding and rescattering are small.[6,7] Thus, for the events under consideration we have made the assumption that the proton is a spectator to the interaction. Of the events having a lambda vee fit with a chi-squared probability of greater than one per cent, 67 per cent had spectators with such low momenta that they could not be detected by the scanners. The distribution of the measured spectator momenta for the remaining 33 per cent is shown in Figure 4. The smooth curve is the momentum distribution for the proton in the deuterium nucleus as predicted by the Hulthén wave function [8,9] where we have normalized to the number of events in the momentum interval [0.125, 0.175] GeV/c. For a spectator momentum of greater than 0.275 GeV/c there is an excess of events. We interpret this excess as due to a

Figure 4.--Measured spectator momentum distribution for all events having a lambda fit probability of greater than one per cent. There are 1246 measured protons with momentum less than 0.500 GeV/c and 2536 unseen protons.

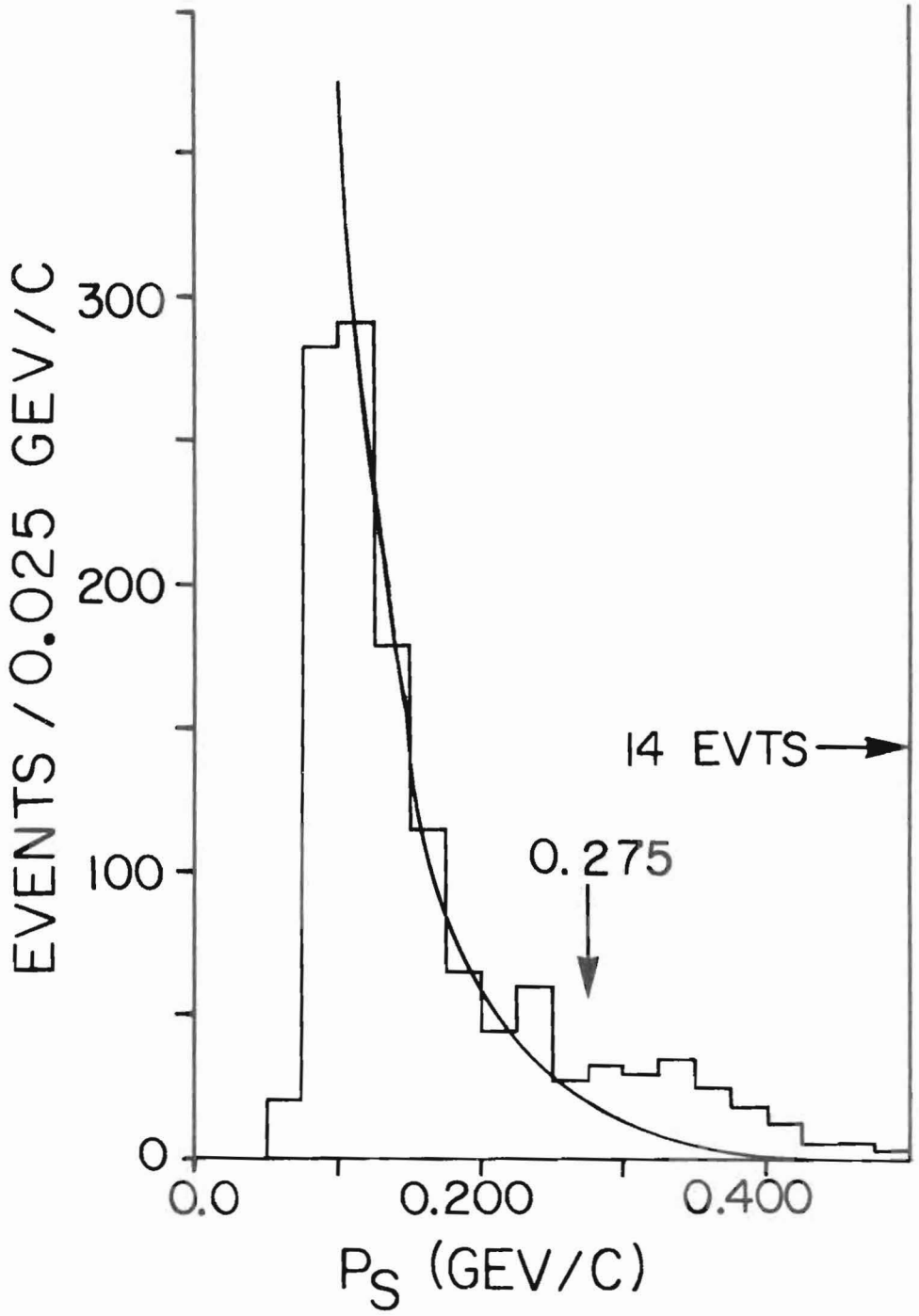
EVENTS / 0.025 GEV/C
300
200
100
0
0.0
0.200
0.400
P_S (GEV/C)
14 EVTS
0.275

rescattering off the spectator proton. Therefore we use only those events having a spectator momentum of less than 0.275 GeV/c for studying Reactions (I-1), (I-2), and (I-3). When calculating cross-sections we include a factor of 1.057 to account for this spectator momentum cut.

C. Determining the Events of Each Reaction

1. Vee decision

Vees that looked like definite electron pairs were never classed as lambdas. Definite electron pairs showed essentially zero opening angle and the characteristic curling of at least one prong. All other vees that had a three-constraint lambda fit with a probability greater than one per cent were called lambdas and only their production vertices were candidates for Reactions (I-1) through (I-3). This classification held regardless of whether or not the vee also fit the three-constraint $\overline{K}^{\circ}$ decay. This was done because an actual $\overline{K}^{\circ}$ decay has a much smaller probability of fitting Λ decay than an actual Λ decay has of fitting $\overline{K}^{\circ}$ decay.[10] We determined the fraction of Λ vee fits due to $\overline{K}^{\circ}$ decays by including an anti-lambda among the attempted vee fits. Our beam momentum is too low for anti-lambda production. There should be no difference in the distributions of laboratory variables for the π^+ and π^- resulting from $\overline{K}^{\circ}$ decay. Thus the real number of $\overline{K}^{\circ}$ decays fitting lambda decays should equal the number of anti-lambda fits. There were 107 vees which had both a $\overline{K}^{\circ}$ fit and an anti-lambda fit of greater than one per cent probability while 3,779 vees were found which had a lambda fit of greater than one per cent probability. Therefore we conclude that the $\overline{K}^{\circ}$ contamination in the lambda vee sample is only (3.0 ± 0.4) per cent. Demanding a fit

to a production reaction should reduce the $\overline{K}^\circ$ contamination much further.

A further test of the purity of the lambda vee sample was made by examining the distribution of the cosine of the decay angle. This is the angle between the lambda laboratory momentum and the momentum of its daughter pi-minus, as seen in the hyperon rest system. For a sample of pure lambdas this distribution should be flat. The proof that this distribution is flat can be constructed from the conservation of parity in the production reaction and the fact that the Λ° has spin 1/2. This is done in detail in the next subsection for the analogous case of Σ° production and decay. The resulting distribution for those lambda vees belonging to the sample for Reaction (I-3) is shown in Figure 11. It is indeed seen to be flat except for a small loss due to slow pi-minus tracks. (This small loss is discussed in Section D of this chapter.) We thus see that our lambda vee sample was very pure and thus no correction was needed for contamination.

2. Separating events of the reactions $K^-N \to \pi^-\pi^-\pi^+\Lambda$ and $K^-N \to \pi^-\pi^-\pi^+\Sigma^\circ$

To facilitate the separation we defined a quantity F_i where i goes from 1 through 3 for Reactions (I-1), (I-2) and (I-3) respectively. It is given by

$$F_i = [(MM_i)^2 - (M_i)^2]/\Delta(MM_i)^2, \qquad \text{(III-1)}$$

where the MM_i are the measured missing masses defined by

$$K^-d \to p_s\pi^+\pi^-\pi^-(MM_i) \qquad \text{(III-2)}$$

for i = 1 and 2, while

$$K^-d \rightarrow p_s\pi^+\pi^-\pi^-\Lambda^\circ(MM_3) \qquad \text{(III-3)}$$

for i = 3. The M_i are the masses of the Λ°, Σ°, and π° respectively. The $\Delta(MM_i)^2$ are the errors in $(MM_i)^2$. The quantity F_i is the deviation of the missing mass squared from its expected value and its units are standard deviations. If there were no contamination, the distribution of F_i would be Gaussian.

An event was considered as unambiguously fitting Reaction (I-1) if the chi-squared probability for this main vertex fit was greater than one per cent, F_1 was less than 2.0, and either the probability of the two-constraint fit to Reaction (I-2) was less than one per cent or $|F_2|$ was greater than 2.0.

For purposes of distinguishing Reactions (I-1) and I-2) an event was designated as unambiguously fitting this second reaction if the probability for its two-constraint fit was greater than one per cent, $|F_2|$ was less than 2.0, the ratio of the probability of the two-constraint fit for Reaction (I-2) to the probability of the one-constraint fit to Reaction (I-3) was greater than 0.5 and either the probability of the fit for Reaction (I-1) was less than one per cent or F_1 was greater than 2.0. [This criterion for the ratio of the chi-squared probabilities for Reactions (I-2) and (I-3) is discussed at the end of this section.]

An event was designated as ambiguous between Reactions (I-1) and (I-2) if the probabilities for both fits were greater than one per cent, F_1 was less than 2.0, $|F_2|$ was less than 2.0, and the ratio of the probability of the fit for Reaction (I-2) to the probability of the fit for Reaction (I-3) was greater than 0.5. The distribution of the baryon

missing mass squared for these events is shown in Figure 5. There is no clean peak at either the lambda or sigma position. This implies that these ambiguous events are of both types.

To formulate a criterion for separating these events, we used the Σ° decay angular distribution. Parity conservation in the strong interaction guarantees that the sigma-zero can have no polarization along its direction of motion. If we take the axis of quantization of the spin of the sigma-zero to be its direction of motion, then half of the sigmas have a component of spin along this axis of +1/2 and the other half of the sigmas have a component of spin along this axis of -1/2. Thus the angular distribution for the sigmas is symmetric with respect to a plane perpendicular to the direction of motion. This means the angular distribution may be described by even powers of cos θ where θ is the angle between the momentum vector of one of the decay products, as seen in the Σ° rest system, and the direction of motion of the sigma in the laboratory. However, the highest power of cos θ which enters into the description of the angular distribution is 2J where J is the total angular momentum of the system.[11] For the sigma this means the highest power of cos θ is 1. Since only even powers of cos θ enter this angular distribution, the only contribution is from the zero-order term. Therefore the decay $\Sigma^\circ \rightarrow \Lambda^\circ\gamma$ has a flat distribution in cos θ. We transformed from the laboratory to the sigma-zero rest frame remembering the direction of travel of this sigma. We then calculated the cosine of the angle between the direction of travel of the lambda presumed to result from the decay, and the direction of travel of the sigma-zero. If the sample of events were purely due to Reaction (I-2), this cosine distribution should be flat as evidenced by Figure 6(A) where only events which were

Figure 5.--Distribution of baryon missing mass squared for events ambiguous between Reactions (I-1) and (I-2).

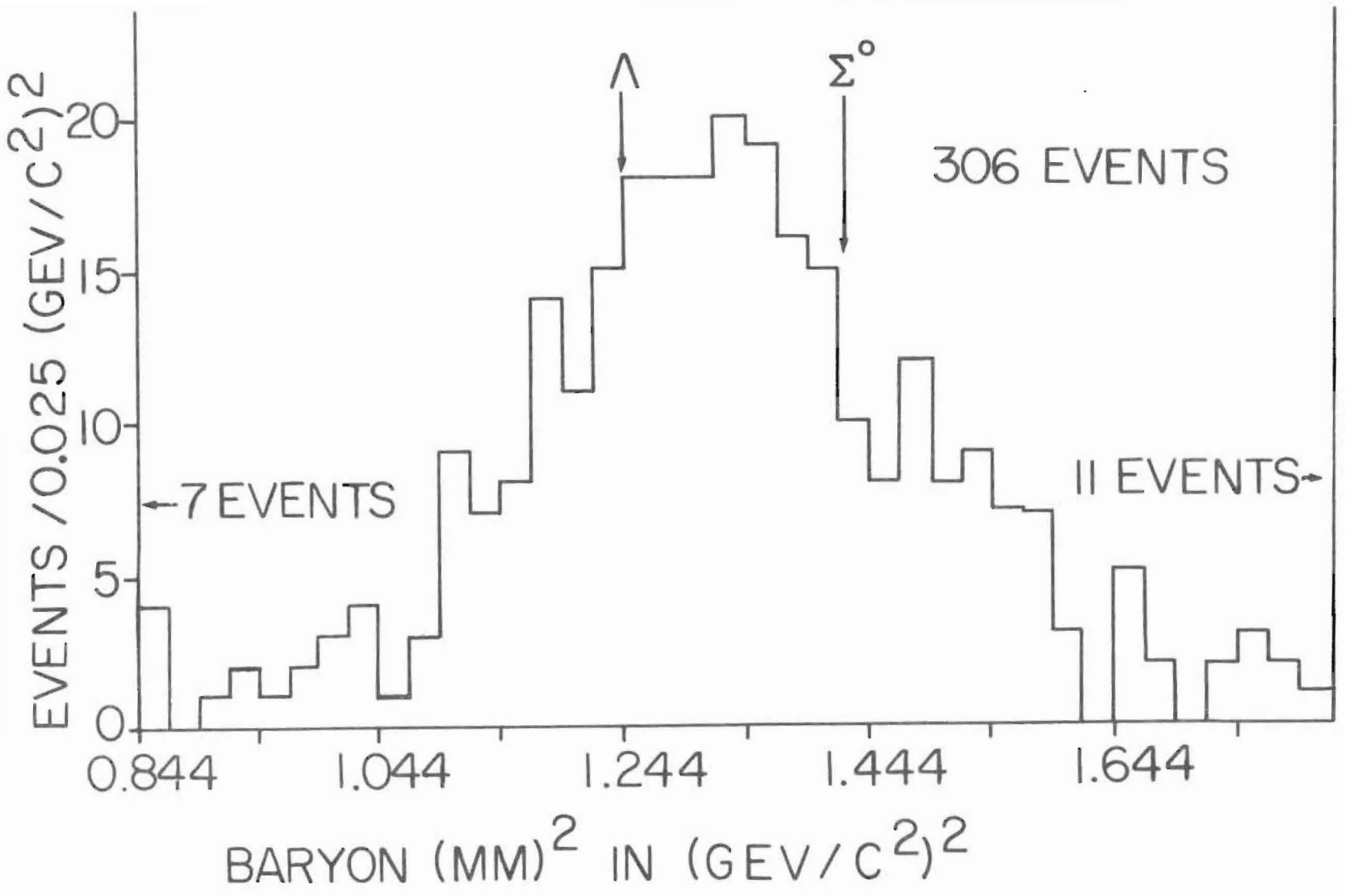
EVENTS /0.025 (GEV/C²)²
20
15
10
5
0
Λ
Σ°
306 EVENTS
7 EVENTS
11 EVENTS
0.844
1.044
1.244
1.444
1.644
BARYON (MM)² IN (GEV/C²)²

Figure 6.--Distribution of cosine of angle between Λ and Σ° direction in Σ° rest frame for (A) unambiguous Σ°, (B) ambiguous Λ/Σ° called Σ°, (C) ambiguous Λ/Σ° called Λ.

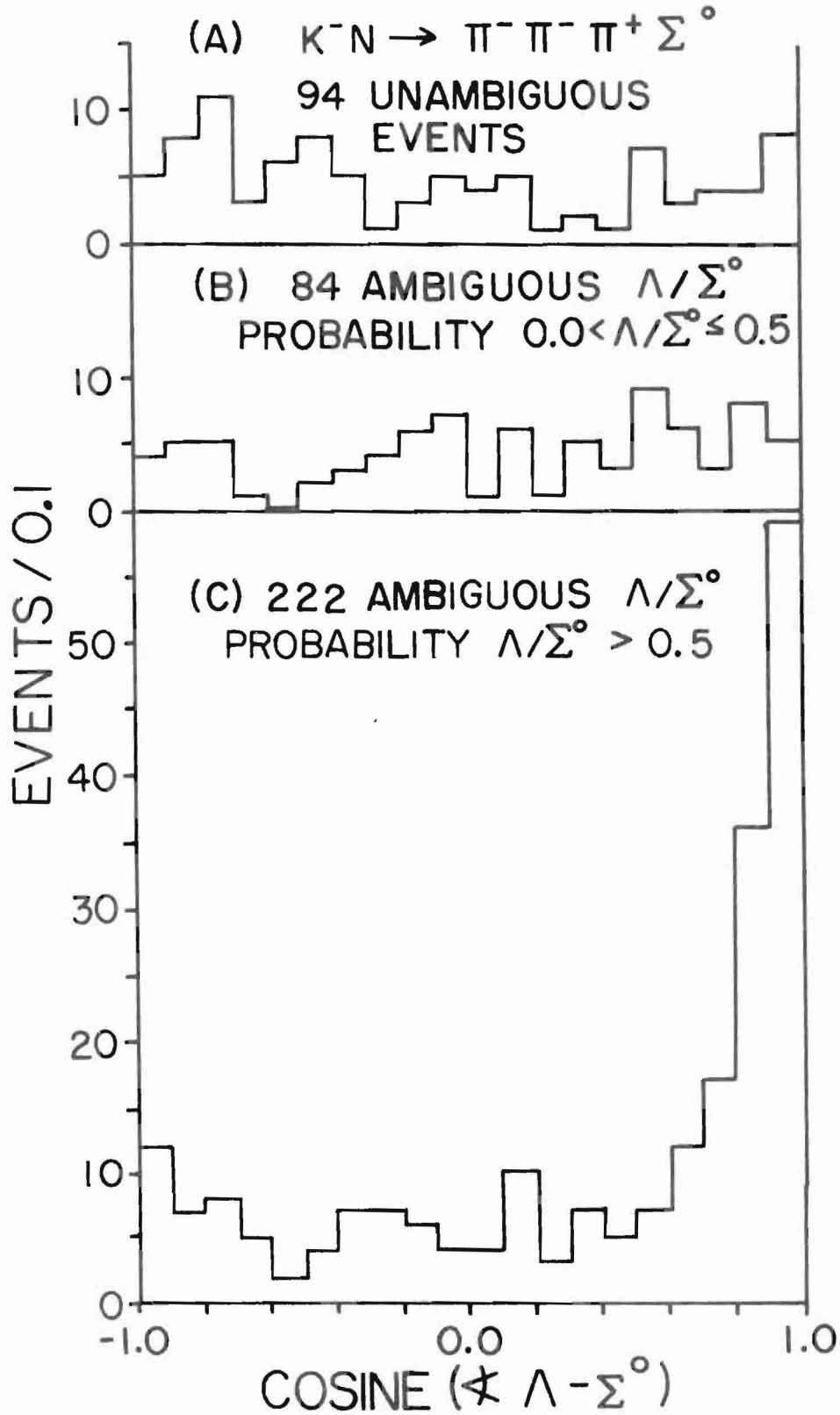
(A) $K^-N \rightarrow \pi^-\pi^-\pi^+\Sigma^0$
94 UNAMBIGUOUS EVENTS
(B) 84 AMBIGUOUS Λ/Σ^0
PROBABILITY $0.0 < \Lambda/\Sigma^0 \leq 0.5$
(C) 222 AMBIGUOUS Λ/Σ^0
PROBABILITY $\Lambda/\Sigma^0 > 0.5$
EVENTS / 0.1
0
10
0
10
0
50
40
30
20
10
0
-1.0
0.0
1.0
COSINE ($\measuredangle\ \Lambda-\Sigma^0$)

unambiguous fits to Reaction (I-2) were plotted. If the sample were purely due to Reaction (I-1) the distribution should be peaked in the direction of travel of the sigma-zero since we would expect a false sigma-zero momentum to be in the same direction as the true lambda momentum. Figure 6(B) shows this distribution for events ambiguous between Reactions (I-1) and (I-2) where the ratio of the probability of the fit of Reaction (I-1) to that of Reaction (I-2) lies between 0.0 and 0.5. This distribution is consistent with being flat and on this basis the events in Figure 6(B) were included in the sample for Reaction (I-2). Figure 6(C) shows this distribution for events ambiguous between Reactions (I-1) and (I-2) where this ratio of chi-squared probabilities is greater than 0.5. A definite forward peak is observed as would be expected if the sample of events were from the final state $\pi^-\pi^-\pi^+\Lambda^\circ$. On this basis we chose 0.5 as the dividing line between these reactions for the ambiguous events.

The distribution of the baryon missing mass squared for the 424 events used in subsequent analysis of the final state $\pi^-\pi^-\pi^+\Lambda^\circ$ is shown in Figure 7. It is approximately symmetric about the lambda position and peaks at this point. In fact, 201 of the events are below the lambda mass squared and 223 are above it. This is further justification of our criterion for distinguishing between these two reactions.

The distribution of F_2, the deviation of the missing mass squared, for the final state $\pi^-\pi^-\pi^+\Sigma^\circ$ measured in standard deviations, is shown in Figure 8(A) for the events of Reaction (I-2), except no cut on F_2 was taken. The smooth curve is a Gaussian normalized to the number of events in the interval from -0.9 to 0.9. When the problem of contamination from Reaction (I-3) to Reaction (I-2) was ignored, it

Figure 7.--Distribution of baryon missing mass squared for Reaction (I-1).

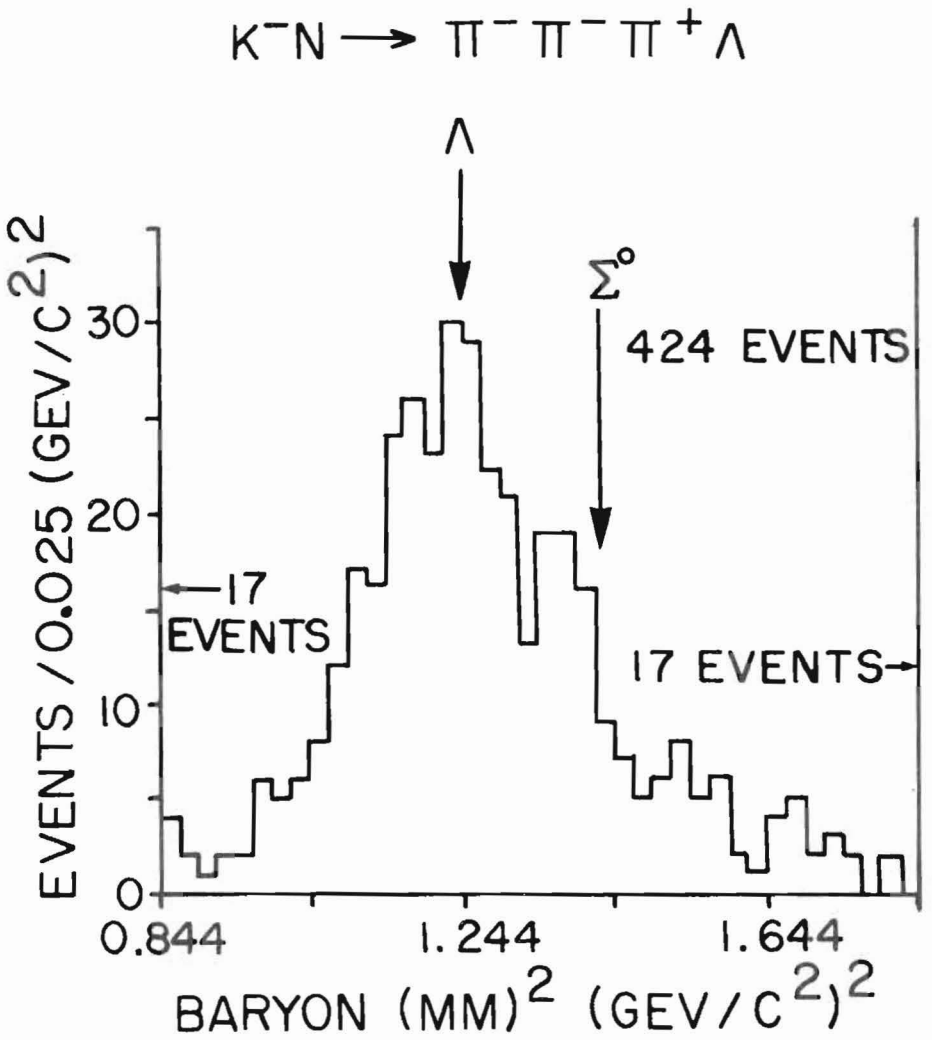
K⁻N → π⁻π⁻π⁺Λ
Λ
Σ°
424 EVENTS
17 EVENTS
17 EVENTS
EVENTS / 0.025 (GEV/C²)²
30
20
10
0
0.844
1.244
1.644
BARYON (MM)² (GEV/C²)²

Figure 8.--(A) Distribution of the deviation of the missing mass squared, F_2, for events having fit probabilities as follows:
Reaction (I-2) > one per cent,
[Reaction (I-2)/Reaction (I-3)] > 0.5, and
[Reaction (I-2)/Reaction (I-1)] > 2.0.
(B) Distribution of baryon $(MM)^2$ for events in (A) having $|F_2| < 2.0$.

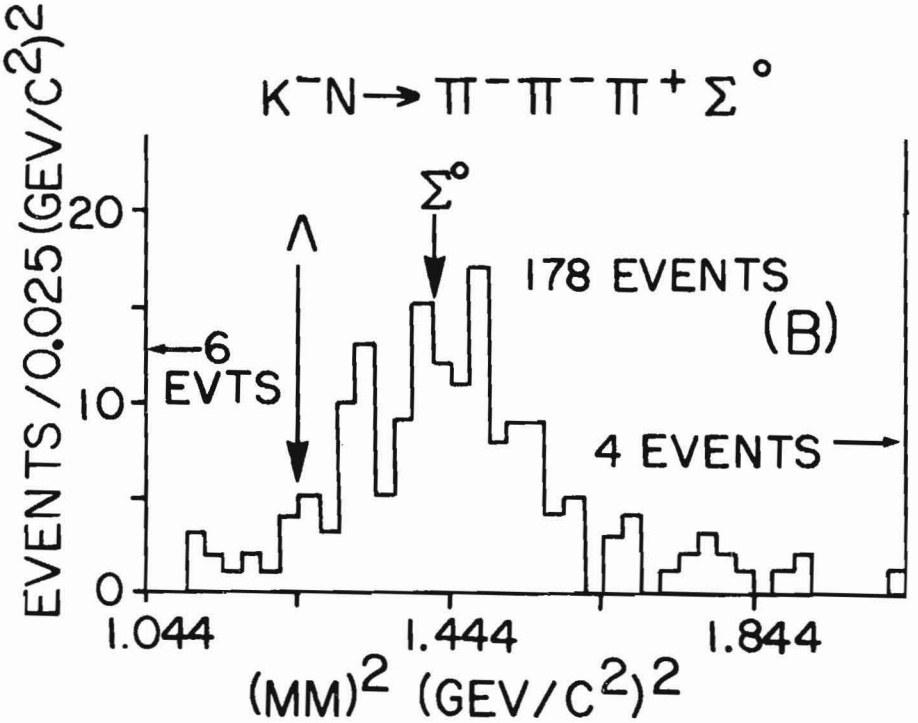
K⁻N → π⁻π⁻π⁺Σ°
EVENTS /0.025 (GEV/C²)²
Λ
Σ°
178 EVENTS
(B)
6 EVTS
4 EVENTS
0
10
20
1.044
1.444
1.844
(MM)² (GEV/C²)²

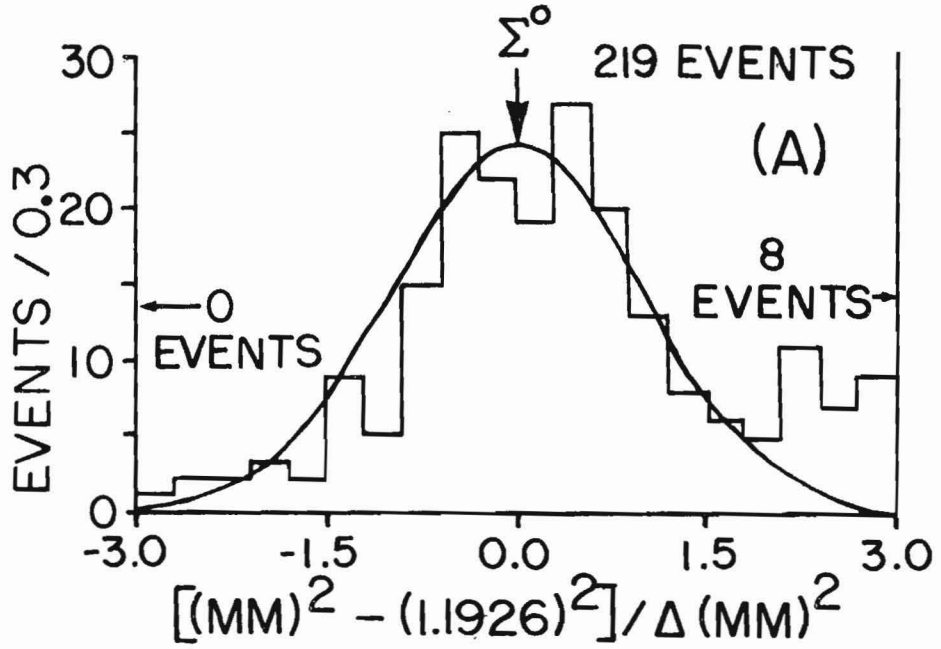
Σ°
219 EVENTS
(A)
EVENTS / 0.3
0 EVENTS
8 EVENTS
0
10
20
30
-3.0
-1.5
0.0
1.5
3.0
[(MM)² − (1.1926)²]/Δ(MM)²

was found that this distribution had an excess of events for $0.0 \leq F_2 \leq 2.0$. When we required the ratio of the probability for a two-constraint Reaction (I-2) fit to the probability for a one-constraint Reaction (I-3) fit to be greater than 0.5, this distribution became more nearly Gaussian. We demanded that $|F_2|$ be less than 2.0 to cut out the excess events in the tail. Figure 8(B) shows the distribution for the baryon missing mass squared that results. This distribution is approximately symmetric about the position of the sigma-zero. In fact there are 79 events on the low side and 99 on the high side. These 178 events were used for subsequent analysis of the final state $\pi^-\pi^-\pi^+\Sigma^\circ$.

3. The reaction $K^-N \rightarrow \pi^-\pi^-\pi^+\pi^\circ\Lambda^\circ$

An event was included in the sample for Reaction (I-3) if it was not included in the sample of Reaction (I-1) or (I-2), the probability of its one-constraint fit to Reaction (I-3) was greater than one per cent and F_3 was less than 1.25. Figure 9 shows the distribution of F_3 for events meeting these criteria except no restriction was imposed on F_3 itself. The smooth curve is a Gaussian normalized to the number of events having F_3 less than 0.0. The cut was taken at 1.25 to avoid the contamination contained in the upper tail. Figure 10 shows the distribution of the square of the missing boson mass minus the square of the pi-zero mass for all events not included in the sample of Reaction (I-1) and (I-2). A peak corresponding to Reaction (I-3) is clearly visible. The shaded portion corresponds to the 1,207 events with F_3 less than 1.25. These events were used for subsequent analysis of the final state $\pi^-\pi^-\pi^+\pi^\circ\Lambda^\circ$.

Figure 9.--Distribution of F_3 for all events not taken as Reaction (I-1) or (I-2) but having fit probability for Reaction (I-3) greater than one per cent. The smooth curve is a Gaussian normalized to the 644 events having $F_3 < 0.0$.

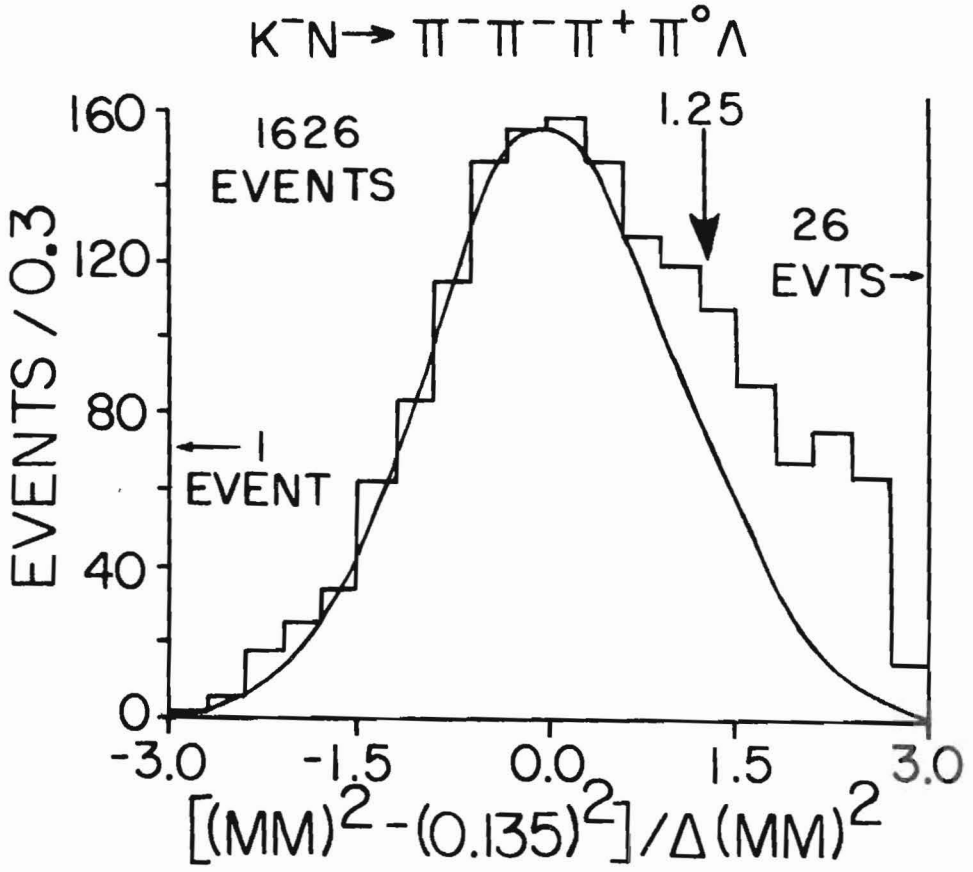
K⁻N → π⁻π⁻π⁺π°Λ
1626
EVENTS
1.25
26
EVTS
1
EVENT
EVENTS / 0.3
160
120
80
40
0
-3.0
-1.5
0.0
1.5
3.0
[(MM)² - (0.135)²] / Δ(MM)²

Figure 10.--Distribution of missing boson mass squared minus π° mass squared for all events not included in Reaction (I-1) or (I-2). Shaded portion corresponds to events included in Reaction (I-3). Cross-hatched portion corresponds to events having a fit probability to Reaction (I-3) of greater than one per cent and F_3 greater than 1.25.

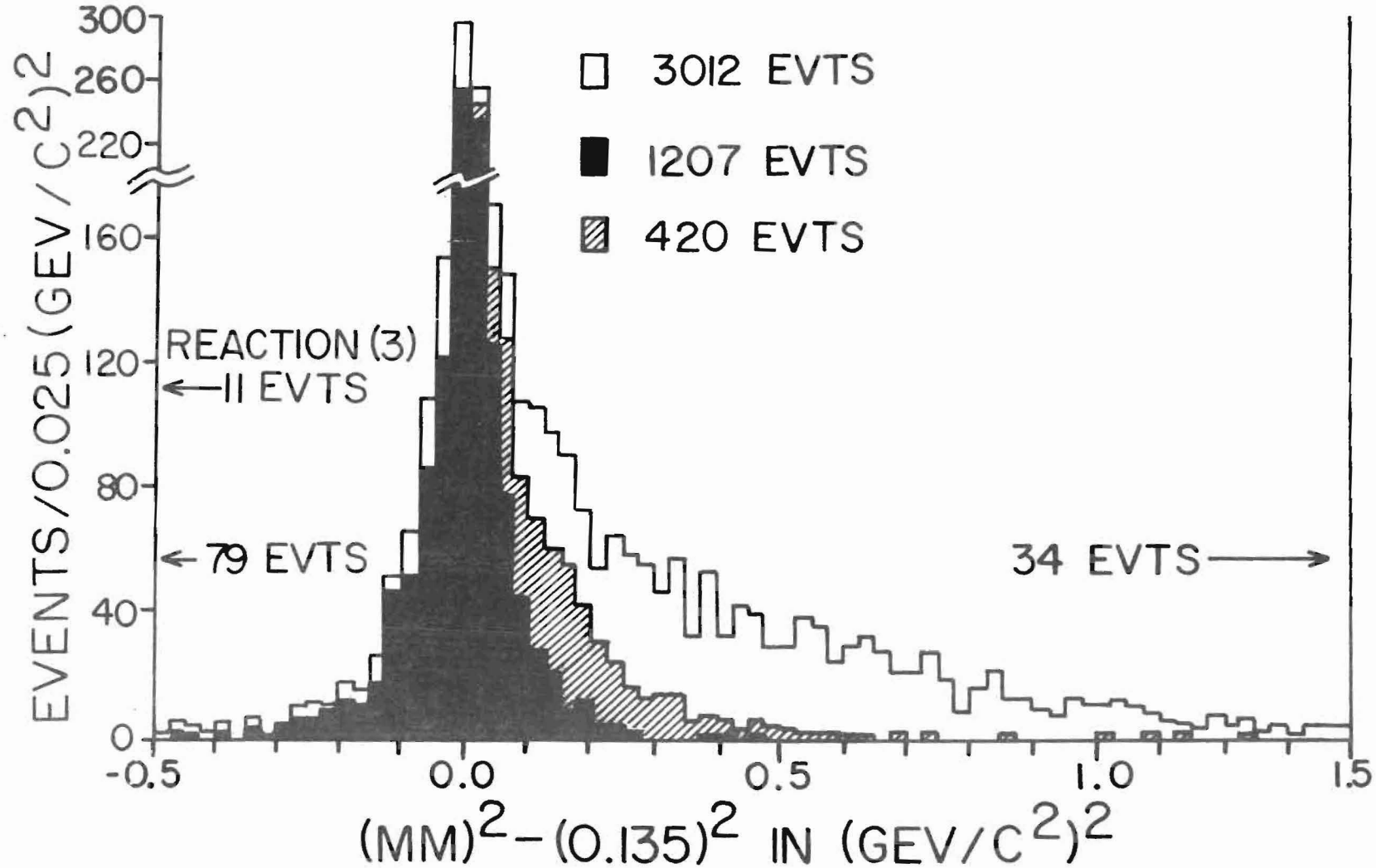
3012 EVTS
1207 EVTS
420 EVTS
REACTION (3)
← 11 EVTS
← 79 EVTS
34 EVTS →
EVENTS/0.025 (GEV/C²)²
300
260
220
160
120
80
40
0
-0.5
0.0
0.5
1.0
1.5
(MM)² − (0.135)² IN (GEV/C²)²

D. Small Corrections for Lost Vees

1. Vees lost out end of bubble chamber

Let P for a given event be the probability, averaged over the beam track's potential path, that the vee decays inside the fiducial volume.

To correct for vees which passed out the end of the fiducial volume before decaying and therefore were not in our sample, we gave each event a weight of 1/P. This probability is given by[12]

$$P = 1 - \frac{\exp\left[-\frac{(L+F)}{\ell \cos\theta}\right]\left[1 - \exp\left(-L\left(\frac{1}{G} - \frac{1}{\ell\cos\theta}\right)\right)\right]}{\left[1 - \frac{G}{\ell\cos\theta}\right]\left[1 - \exp\left(-\frac{L}{G}\right)\right]}, \qquad \text{(III-4)}$$

where

L = 146 cm is the length in the bubble chamber (along the x-direction) of the fiducial volume used for detecting both the main vertex of an event and the associated vee vertex,

G = 532 cm is the interaction mean free path for the K^- beam in deuterium,

F = 7.5 cm is an additional length along the x-direction in the bubble chamber immediately beyond L and used only for detecting vees,

$\cos\theta$ = x-component of momentum of vee divided by magnitude of its total momentum, and

ℓ = vee decay mean free path.

When this correction is included the number of events in Reactions (I-1), (I-2) and (I-3) are increased by 5.4, 4.5 and 4.6 per cent

respectively.

2. Vees lost due to slow pi-minus

We transformed from the laboratory system to the rest system of the lambda and computed the cosine of the angle between the momentum there of the pi-minus (resulting from the lambda decay) and the laboratory direction of travel of the lambda itself. For an unbiased sample of lambda's this distribution should be flat. The resulting distribution for the events[13] of Reaction (I-3) is shown in Figure 11 with various cuts taken on the lambda laboratory momentum. For the events having a lambda with momentum less than 1.0 GeV/c a depletion in this distribution is observed for the backward direction. The momentum distribution for the lambdas corresponding to Reaction (I-3) is shown in Figure 12. From this distribution we obtain a median value for the lambda momentum of approximately 0.74 GeV/c for those lambdas having a momentum less than 1.0 GeV/c. Then if the pi-minus from the decay comes off with a decay angle cosine of -0.9 it will have a median laboratory momentum of approximately 0.043 GeV/c and a corresponding range in deuterium of about 2 cm. These were not included in our sample because of the difficulty of measuring their momenta from the curvature of the tracks. To correct for this loss the weight given to an event was multiplied by a factor of 1.11 if the momentum was less than 0.8 GeV/c or by a factor of 1.04 if it was between 0.8 and 1.0 GeV/c. If it was greater than 1.0 GeV/c the weight was not changed. A similar study was made of this distribution for the events of Reactions (I-1) and (I-2) and similar results were obtained. Since the statistics are best for

Figure 11.--Distribution of the cosine of the angle between the π^- momentum and Λ direction in the Λ rest system for the events in Reaction (I-3) for various Λ momenta.

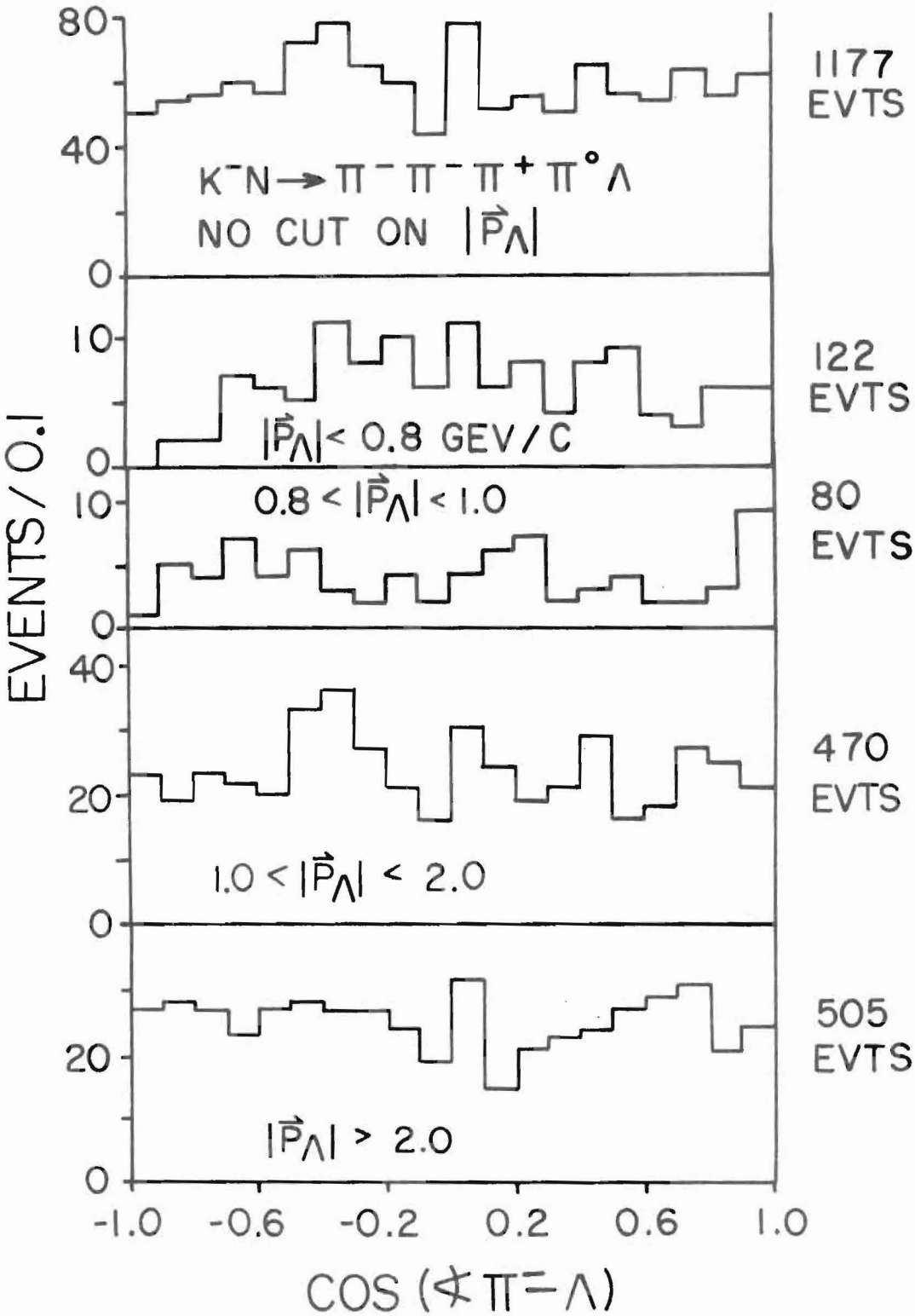
80
40
0
1177
EVTS
K⁻N → π⁻π⁻π⁺π°Λ
NO CUT ON |P⃗Λ|
10
0
122
EVTS
|P⃗Λ| < 0.8 GEV/C
10
0
0.8 < |P⃗Λ| < 1.0
80
EVTS
40
20
0
470
EVTS
1.0 < |P⃗Λ| < 2.0
20
0
505
EVTS
|P⃗Λ| > 2.0
EVENTS/0.1
-1.0
-0.6
-0.2
0.2
0.6
1.0
COS (∡ π⁻Λ)

Figure 12.--Distribution of lambda laboratory momentum for the events of Reaction (I-3).

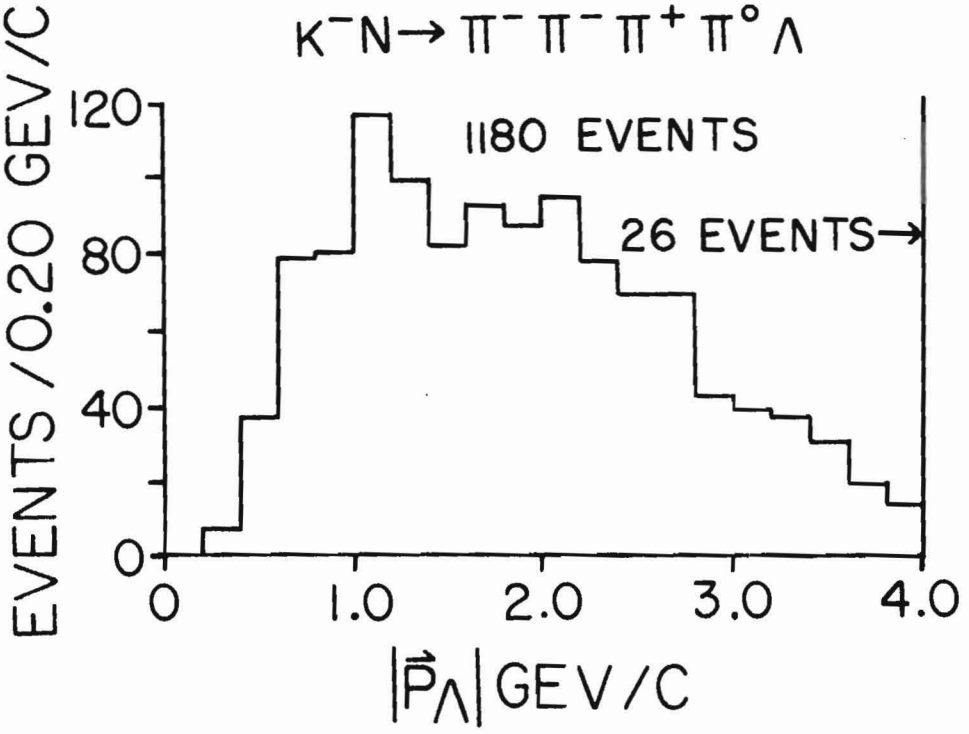
$K^-N \rightarrow \pi^- \pi^- \pi^+ \pi^0 \Lambda$
1180 EVENTS
26 EVENTS→
EVENTS /0.20 GEV/C
120
80
40
0
0
1.0
2.0
3.0
4.0
$|\vec{P}_\Lambda|$ GEV/C

Reaction (I-3) the correction factors obtained for it were also used for Reactions (I-1) and (I-2).

3. Vees lost near main vertex

The decay of the lambda follows an exponential function with a mean life τ of 2.51×10^{-10} seconds. For a lambda measured in the bubble chamber the time t (in seconds) it lived in its own rest frame before decaying is given by

$$t = (LM)/PC, \qquad \text{(III-5)}$$

where

L = distance traveled in the laboratory in cm,

P = laboratory momentum in GeV/c,

C = speed of light in cm/sec, and

M = rest mass of lambda in GeV/c^2.

For an unbiased sample of lambdas plotting frequency versus the exponential function $e^{-t/\tau}$ gives a flat distribution. This is easy to see. If N_I lambdas are present at time zero then the number of lambdas present at any later time t is given by

$$N_t = N_I\, e^{-t/\tau}. \qquad \text{(III-6)}$$

The number of lambdas N which decay in an interval between t_1 and t_2 is given by

$$N = N_I(e^{-t_1/\tau} - e^{-t_2/\tau}). \qquad \text{(III-7)}$$

We thus see that taking equal intervals in the difference of the

exponentials gives a flat distribution in frequency. Figures 13 and 14 show such distributions for the observed lambdas belonging to Reaction (I-3). Various cuts have been made on the momenta of the lambdas. A depletion is evident in the region near 1.0. This corresponds to vees decaying very close to the main vertex. Presumably the scanners have misinterpreted such events as 5- or 6-pronged events instead of correctly interpreting them as 3- or 4-pronged events with a vee. To correct for this loss the weight for each event was multiplied by a factor depending on the momentum of its lambda. If this momentum was

(1) Less than 1.2 GeV/c the weight was multiplied by 1.09;

(2) Between 1.2 and 1.6 GeV/c the weight was multiplied by 1.067;

(3) Between 1.6 and 2.2 GeV/c the weight was multiplied by 1.05; and

(4) Greater than 2.2 GeV/c the weight was multiplied by 1.025.

A similar study was made of this distribution for the events of Reactions (I-1) and (I-2) and similar results were obtained. Since the statistics are best for Reaction (I-3) the correction factors obtained for it were also used for Reactions (I-1) and (I-2).

The effect of making the corrections for the slow pi-minus in the lambda decay and the vees lost near the main vertex is to multiply the total number of events in Reactions (I-1), (I-2) and (I-3) by 1.07, 1.08 and 1.07 respectively. When these corrections and also the correction due to lambdas lost out the end of the bubble chamber are included, the number of events increases from 424 to 479 for Reaction (I-1), from 178 to 201 for Reaction (I-2) and from 1,207 to 1,350 for Reaction (I-3). The distributions displayed up to this point have all used a weight of

Figure 13.--Distribution of probability that lambda would go as far as it did or farther for Reaction (I-3) for various intervals of lambda laboratory momentum.

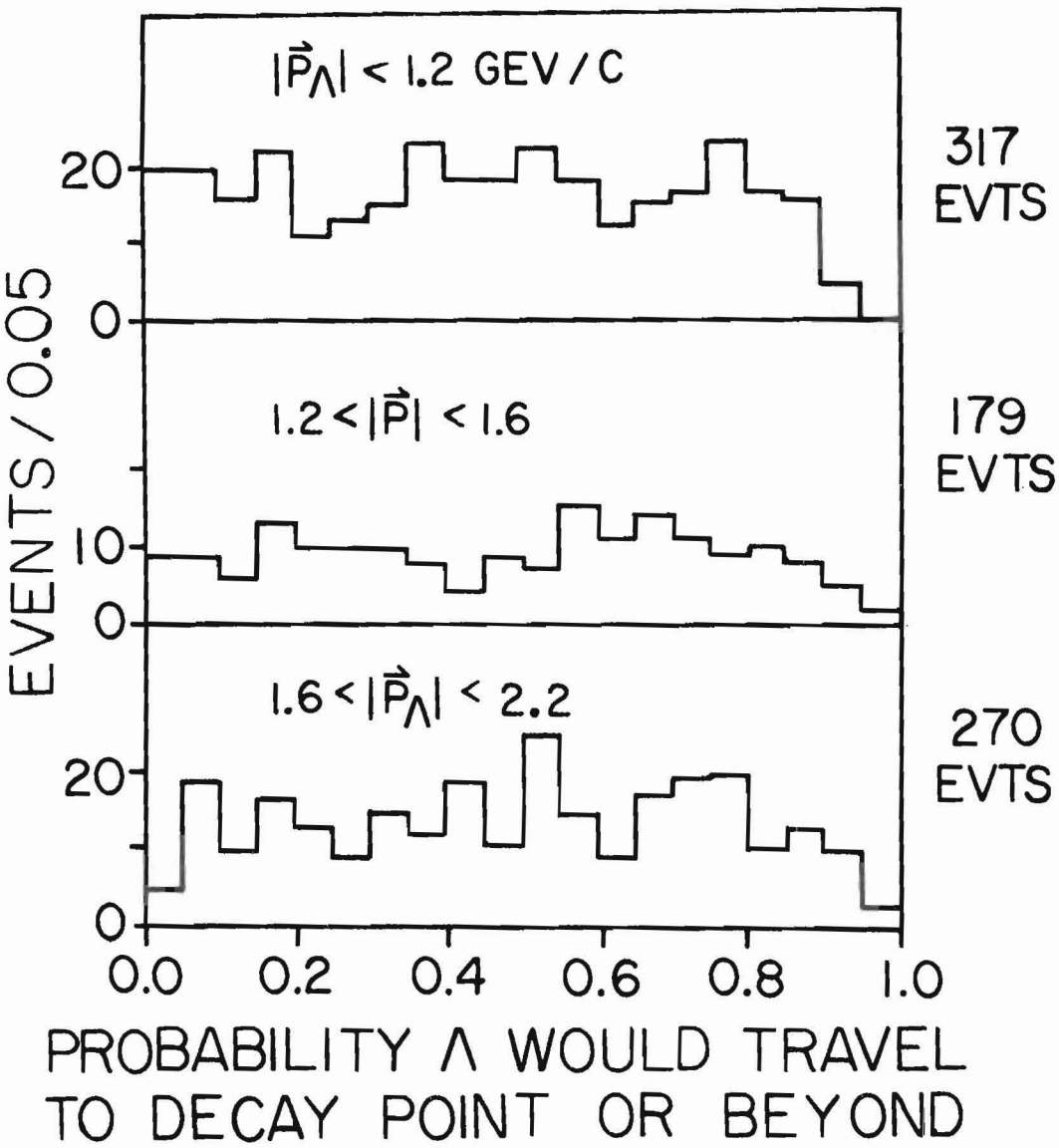
$|\vec{P}_\Lambda| < 1.2$ GEV/C
317 EVTS
$1.2 < |\vec{P}| < 1.6$
179 EVTS
$1.6 < |\vec{P}_\Lambda| < 2.2$
270 EVTS
EVENTS / 0.05
20
0
10
0
20
0
0.0
0.2
0.4
0.6
0.8
1.0
PROBABILITY Λ WOULD TRAVEL TO DECAY POINT OR BEYOND

Figure 14.--For Reaction (I-3) the distribution of probability that lambda would go as far as it did or farther for all values of lambda laboratory momentum and for values greater than 2.2 GeV/c.

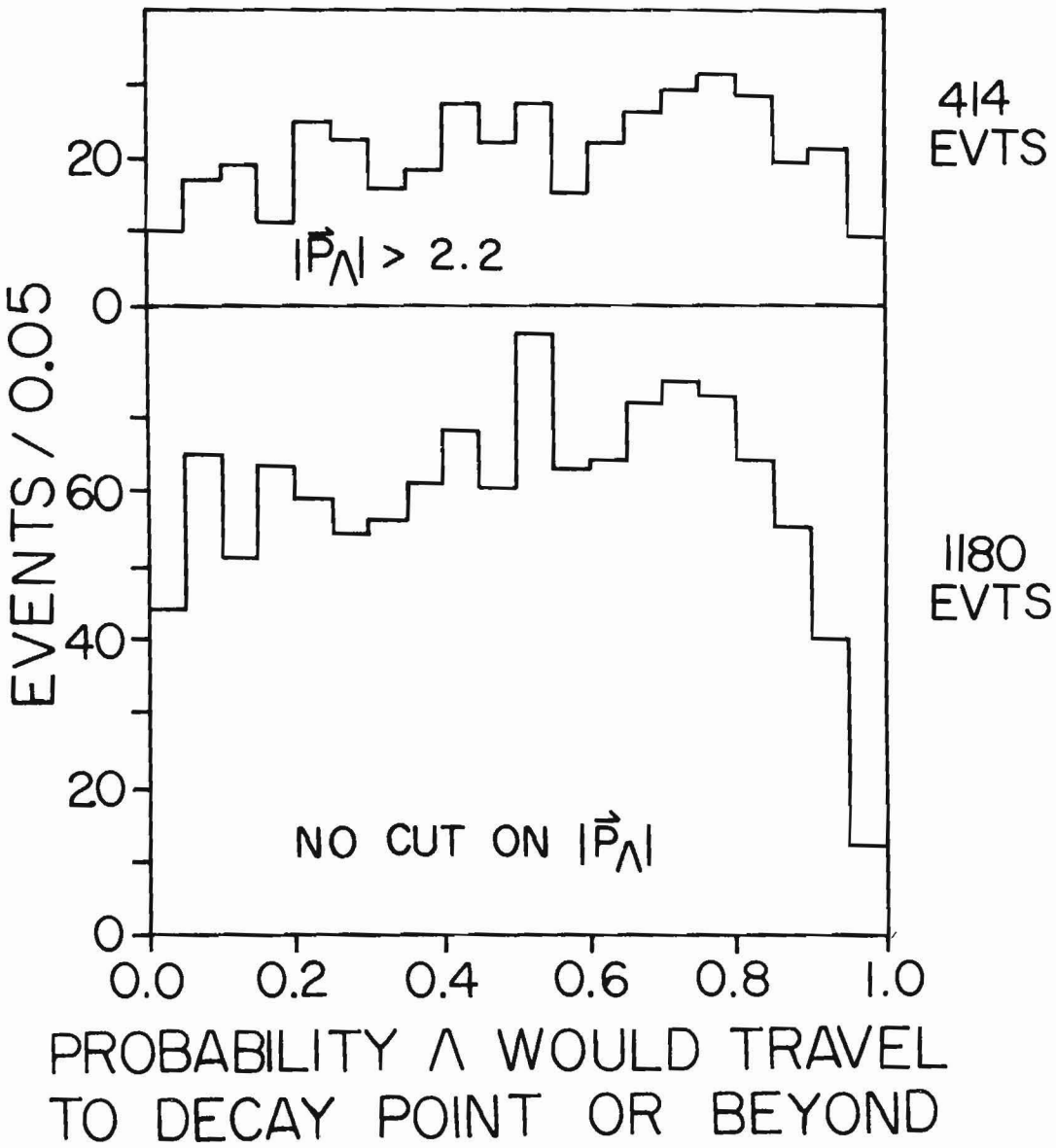
414
EVTS
$|\vec{P}_\Lambda| > 2.2$
1180
EVTS
NO CUT ON $|\vec{P}_\Lambda|$
EVENTS / 0.05
0
20
0
60
40
20
0
0.0
0.2
0.4
0.6
0.8
1.0
PROBABILITY Λ WOULD TRAVEL
TO DECAY POINT OR BEYOND

1.0 for each event. All subsequent distributions and analyses will include the corrections for lost events.

CHAPTER IV

MODELS

A. The Multiperipheral Model of Chan, Loskiewicz and Allison

Chan, Loskiewicz and Allison (hereafter referred to as CLA) have proposed a phenomenological Reggeized multiperipheral model for inelastic processes at high energy of the type

$$A + B \rightarrow 1 + 2 + 3 + \cdots + n. \qquad \text{(IV-1)}$$

A multiperipheral diagram for this process is given in Figure 15. In this model the square of the overall amplitude, $|A|^2$, is taken as an incoherent sum of the amplitudes, A_D, for the individual diagrams which describe the process. The amplitude, A_D, for a particular diagram is taken as a product of factors, A_i, where each A_i corresponds to a specific exchange and of course also depends on the vertices above and below it. The form prescribed by CLA for A_i is

$$A_i = \left(\frac{g_i S_i' + ca}{S_i' + a}\right)\left(\frac{S_i' + a}{a}\right)^{\alpha_i(0)}\left(\frac{S_i' + b_i}{b_i}\right)^{t_i} \qquad \text{(IV-2)}$$

where

$$S_i = (P_i + P_{i+1})^2, \qquad \text{(IV-3)}$$

$$S_i' = S_i - (m_i + m_{i+1})^2, \qquad \text{(IV-4)}$$

Figure 15.--The multiperipheral graph for the collision process $A + B \rightarrow 1 + 2 + 3 + \cdots + n$.

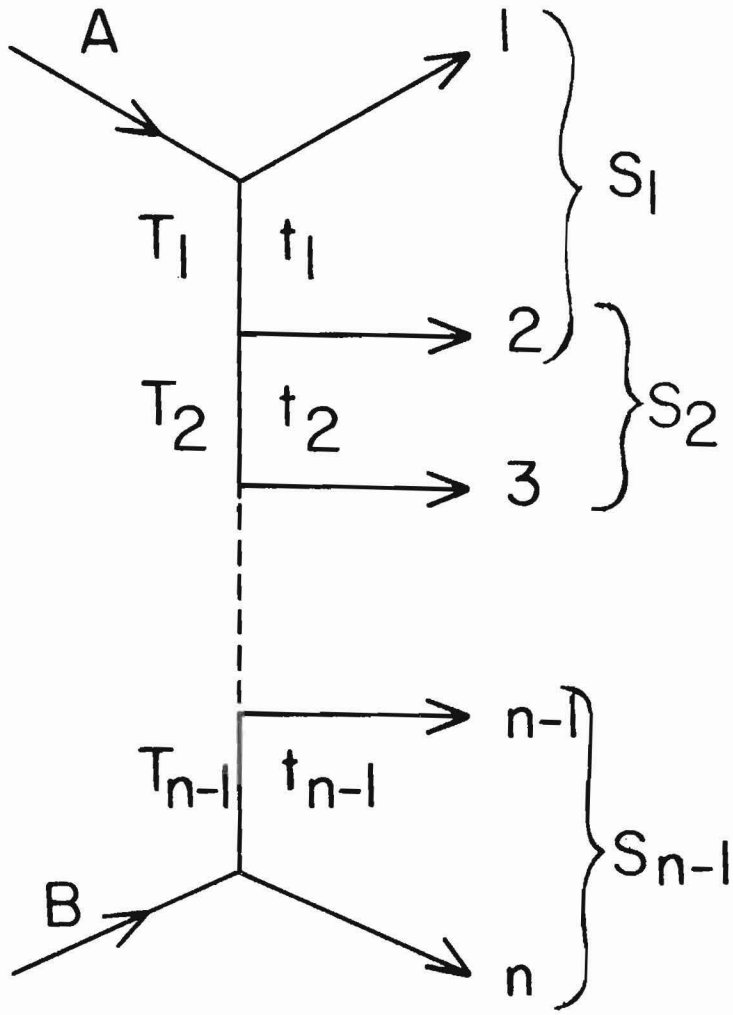
A
1
S_1
T_1
t_1
2
S_2
T_2
t_2
3
n-1
T_{n-1}
t_{n-1}
S_{n-1}
B
n

P_i is the four-momentum of the ith external particle,

m_i is the mass of ith external particle,

c is a constant giving the size of the contribution for small S_i', and

a is a constant setting the energy scale.

The b_i are parameters describing the exponential t-dependence of the vertices. They have three values. One is for an external vertex with the incident beam meson, one for an external vertex with the target nucleon, and one is for all internal vertices. The quantity g_i plays the role of a coupling constant, $\alpha_i(0)$ is the intercept of the Regge trajectory being exchanged, and t_i is the four-momentum transfer squared between the two adjacent external particles. For the parameters we have used the following values:

$c = 1.4$,

$a = 1.0\ \mathrm{GeV}^2$,

$b_i = 2.0\ \mathrm{GeV}^2$ for the external vertex with the beam meson,

$b_i = 1.0\ \mathrm{GeV}^2$ for the external vertex with the target nucleon,

$b_i = 2.4\ \mathrm{GeV}^2$ for all internal vertices,

$g_i = 1.3$ for the exchange of the nucleon Regge trajectory, and

$g_i = 1.0$ for the exchange of a meson Regge trajectory.

For the intercepts $\alpha_i(0)$ of the Regge trajectories we have used -0.35 and 0.30 for the nucleon and strange meson respectively. These are the values of the parameters used by CLA except we have doubled the values for the three b_i in order to get better agreement with our data. (This is discussed in Chapter V.)

Then

$$A_D = \prod_{i=1}^{n-1} A_i, \qquad \text{(IV-5)}$$

$$|A|^2 = \sum_D |A_D|^2. \qquad \text{(IV-6)}$$

The expression for A_i is designed to interpolate smoothly between pure phase space for small S_i' and a Reggeized form of the amplitude for large S_i'. Thus A_i is constructed such that as S_i' goes to zero, A_i goes to c, a constant, and as S_i' becomes large, A_i takes on a Reggeized form with exponential approximations to the vertices and linear approximations to the trajectories. All trajectories are assumed to have a slope of 1 $(\text{GeV}/c)^{-2}$. For

$$S_i' \to 0,\ A_i \to c \qquad \text{(IV-7)}$$

but for

$$S_i' \to \infty,\ A_i \to g_i\left(\frac{S_i}{a}\right)^{\alpha_i(0)+t_i} e^{(\ln \frac{a}{b_i})t_i} . \qquad \text{(IV-8)}$$

We observed single resonance production, but this form of the CLA amplitude does not describe resonance production. We included resonances by using the straightforward method of Bassompierre et al.[14] In this case one considers one of the external lines of the graph in Figure 15 to be the system of resonating particles when calculating the square of the diagram's amplitude. One also multiplies by the appropriate Breit-Wigner function[15] of the form

$$W_r(m_i) = (\Gamma_r/2\pi)/[(m_i - E_r)^2 + \Gamma_r^2/4], \qquad \text{(IV-9)}$$

where

Γ_r is the resonance width,

E_r is the central value of the resonance mass,

m_i is the particles' effective mass, and the subscript r labels the resonance, e.g. $Y^{*-}(1385)$.

The relative amount of each resonance observed in the data was reproduced by multiplying the amplitude squared for each diagram by an appropriate weight, f_r.

A Monte Carlo program[16] was used to generate events which were distributed according to pure phase space and the CLA model results were calculated using these events. To avoid calculating large numbers of Monte Carlo events which corresponded to sparsely populated regions of phase space, we constructed in an ad hoc fashion a density function that very crudely described the observed amounts of resonance production and the observed single particle momentum transfer distributions. This function was normalized such that its range of values was in the interval from zero to one. It was calculated for each Monte Carlo event. If the event was in a densely populated region, the function would have a value near 1.0. If the event was in a sparsely populated region, the function would have a value near 0.0. The value of the function was then compared with a random number whose value was in the interval from zero to one. If the random number was greater than the value of the function, the Monte Carlo event was given a weight of zero and was not used for computing with the CLA model. If the random number was less than the function, the Monte Carlo event was given a weight Q equal to the inverse of this density function and the event was used in the calculation. For a given Monte Carlo event of non-zero weight, the total weight P after being operated on by the CLA model was

$$P = Q\left[\sum_D |A_D|^2 + \sum_r f_r \sum_D |A_{Dr}|^2 W_r\right] \qquad \text{(IV-10)}$$

where the sums are over diagrams and resonances. The square brackets contain the CLA amplitude squared modified to include the amounts of observed resonance production. If it had been set equal to a constant, pure phase space would have been reproduced. We state this to emphasize that the factor Q is only used to save computer time and not to describe the dynamics. For ease of comparison with our data, the total weight of the Monte Carlo events was normalized to our number of physical events.

A sufficient number of Monte Carlo events was used so that the statistical error associated with a comparison of our data with the model was essentially set by our number of bubble chamber events. The factor by which the Monte Carlo calculation increased this error for the Kth reaction is given by

$$E_K = \frac{\sqrt{D_d^2 + D_m^2}}{D_d} \quad , \qquad \text{(IV-11)}$$

where D_d is the fractional error in the physical data and is taken as the inverse of the square root of the number of events. The quantity

$$D_m = \frac{\sqrt{\Sigma (P_i)^2}}{\Sigma P_i} \qquad \text{(IV-12)}$$

and is the fractional error in the Monte Carlo calculation where P_i is the weight for the ith Monte Carlo event as given by Equation (IV-10) and the sums are over the employed Monte Carlo events. For Reaction

(I-1) we generated 240,000 Monte Carlo events and about 9,100 of these had a non-zero weight. The quantity $D_m = 0.0267$ giving $E_1 = 1.14$. For Reaction (I-2) we began with 70,000 Monte Carlo events and about 8,800 of these were used in the CLA model calculation. This $D_m = 0.0181$ giving $E_2 = 1.03$. For Reaction (I-3) we generated 240,000 Monte Carlo events and about 7,200 of these had non-zero weight. We obtained $D_m = 0.0175$ giving $E_3 = 1.17$.

B. The Veneziano-Type Multiperipheral Model of Plahte and Roberts

Since the CLA model did not predict the amounts of two-particle resonance production or the phase of the amplitude, Plahte and Roberts suggested a modification to specify both of these.[2] They proposed that the A_i describing a specific exchange, its adjacent vertices, and adjacent external lines for the multiperipheral graph in Figure 15 have the form

$$A_i = g_i \left(\frac{S_i' + a}{a} \right)^{\alpha_i(0)} \left(\frac{S_i' + b_i}{b_i} \right)^{t_i} F_i \qquad \text{(IV-13)}$$

where g , S_i' , t_i, $\alpha_i(0)$, b_i, and a were defined previously. The factors multiplying F describe the t channel exchange and were adopted from the CLA model. Our calculations were carried out using the exchange of the K*(890), K*(1420), and nucleon trajectories. The factor

$$F_i = \left[\frac{1 + \cos \pi(\alpha_s - \sigma_s)}{\sin \pi(\alpha_s - \sigma_s)} \right] \left[\sin \pi(\alpha_t - \sigma_t) \right] + 1 + \cos \pi(\alpha_t - \sigma_t) \ , \qquad \text{(IV-14)}$$

where $\alpha_s \equiv \alpha(S_i)$ and $\alpha_t = \alpha(t_i)$ are the Regge trajectories for the S_i and t_i channels. Similarly σ_s is the spin for the lowest resonance on the Regge trajectory corresponding to the S channel and σ_t is the spin for the lowest resonance on the Regge trajectory corresponding to the t channel.

This factor F describes resonance production and was adopted by Plahte and Roberts from a factor contained in Veneziano's amplitude for $\pi\pi \to \pi\omega$. As the Regge trajectory α_s passes through a narrow resonance F becomes very large and the corresponding amplitude is large for the resonance region. If the imaginary part of α_s is an increasing function of S_i, then as S_i becomes large the expression for F becomes the Regge phase factor $1 + \mathrm{EXP}[-i\pi(\alpha_t - \sigma_t)]$. For the imaginary part of $\pi\alpha_s$ Plahte and Roberts suggest

$$\mathrm{IM}(\pi\alpha_s) = H \ln(1 + \frac{S_i'}{a}) \qquad \text{(IV-15)}$$

where the parameter H is chosen so that the correct width is obtained for the lowest resonance of the trajectory. Our calculations were carried out using the $\rho(765)$ and f(1260) trajectories in the S channel for Reactions (I-1), (I-2), and (I-3). For Reactions (I-1) and (I-3) we also used the Y*(1385) trajectory in the S channel. For Reaction (I-2) we replaced the factor F by $1 + \mathrm{EXP}[-i\pi(\alpha_t - \sigma_t)]$ for the baryon S channel cases because the Y*(1385) branching ratio to $\Sigma\pi$ is only about ten per cent and we in fact detected no hyperon resonance production in the $\pi^-\pi^-\pi^+\Sigma^\circ$ final state. These trajectories were taken to be linear. For the $\rho(765)$, f(1260), and Y*(1385) respectively, we used 0.50, 0.50,

and -.2417 for the intercepts; .854, .939, and .908 $(GeV)^{-2}$ for the slopes; and .619, .560, and .500 for H. The slopes for these meson trajectories were determined from the standard intercept of 0.50 and the mass squared of the lowest resonance. The slope and intercept of the Y*(1385) trajectory was determined from the square of the masses of the Y*(1385) and its first Regge recurrence, the Y*(2030).

Since we wanted to see if the Plahte and Roberts model would correctly predict the relative amounts of resonance production, we included the effect of isospin Clebsch-Gordan coefficients. Figure 16(A) shows a typical diagram. Figure 16(B) illustrates our method and each vertex there is labeled by its Clebsch-Gordan coefficient. We took isospin into account in an approximate manner by multiplying the Plahte and Roberts amplitude by the factor

$$C_D \equiv C_{a1}C_{b1}C_{a2}C_{b2}C_{a3}C_{b3}. \qquad \text{(IV-16)}$$

As in the case of the CLA model, the Monte Carlo events of nonzero weight Q were used when calculating with this model. The weight P for a given Monte Carlo event was

$$P = Q\left|\sum_D C_D A_D\right|^2 \qquad \text{(IV-17)}$$

where $A_D = \prod_i A_i$. The sum is over the diagrams and the product is over the exchanges of a given diagram. The total weight of all the Monte Carlo events was normalized to our number of physical events.

The Plahte and Roberts model can only describe the production of two particle resonances. We observe in Reaction (I-3) the $\omega^\circ(784)$

Figure 16.--(A) A typical diagram. (B) Method of including Clebsch-Gordan coefficients.

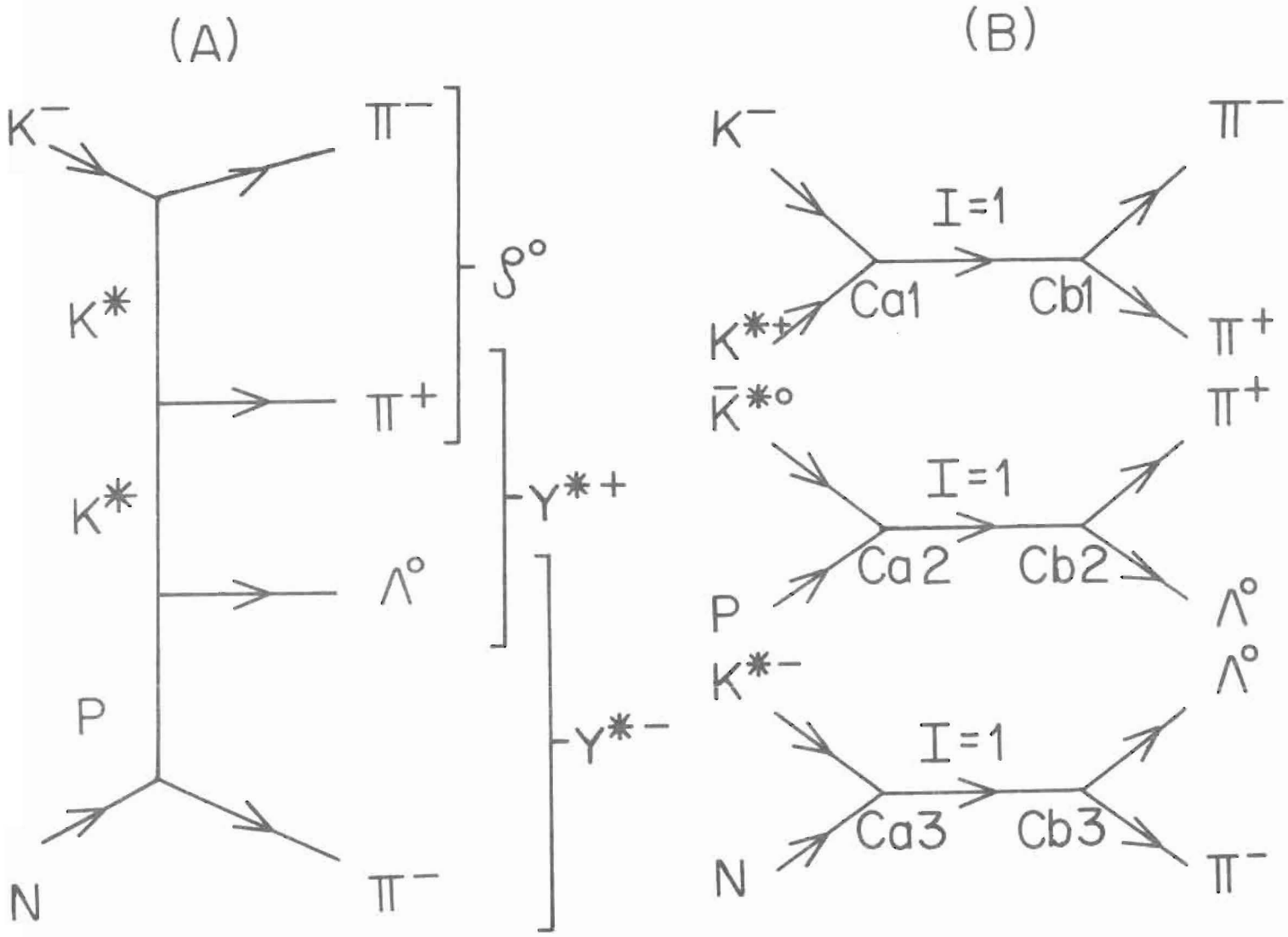
(A)
K⁻
π⁻
ρ°
K*
π⁺
Y*⁺
K*
Λ°
P
Y*⁻
N
π⁻
(B)
K⁻
π⁻
I=1
Ca1
Cb1
K*⁺
π⁺
K̄*°
π⁺
I=1
Ca2
Cb2
P
Λ°
K*⁻
Λ°
I=1
Ca3
Cb3
N
π⁻

resonance which decays into three particles. We took the $\omega^{\circ}(784)$ into account by adding the CLA amplitude for its production incoherently to the Plahte and Roberts amplitude. As in the case of the CLA model, we calculated E_K as defined by Equation (IV-11) for our work with this model of Plahte and Roberts. For this model and using the same Monte Carlo events of non-zero weight as for the CLA model, we obtained for Reaction (I-1) $D_m = 0.045$, giving $E_1 = 1.32$. For Reaction (I-2) we obtained $D_m = 0.026$, giving $E_2 = 1.06$. For Reaction (I-3) we obtained $D_m = 0.084$, giving $E_3 = 3.09$. The disagreement between this model and the data of this third reaction was so great that there was no point in doing a statistically better calculation. (See Chapter V.)

CHAPTER V

DATA AND RESULTS OF THE CLA CALCULATIONS

Resonances were included in the CLA calculations for two reasons. When we determined the amount of production of a given resonance by using the appropriate mass plot, we wanted the CLA model to include the effect of other resonances in its description of the background. We wished to take into account the fact that the presence of low mass resonances effectively reduces the multiplicity of a reaction and thus causes it to be more peripheral.[1]

As an example of how the CLA model calculations were carried out we show in Figure 17 the 13 diagrams which were used for Reaction (I-1). Four of them are non-resonant and the remaining nine correspond to resonances observed in the data. Ten diagrams were calculated for Reaction (I-2). They can be obtained from those of Reaction (I-1) by replacing the Λ by a Σ° and discarding those with $Y^{*}(1385)$. Seventy-eight diagrams were calculated for Reaction (I-3). These included all the possible combinations with a π° appearing at any outgoing position on the diagrams and also all the single resonance diagrams containing $Y^{*\pm 0}(1385)$, $\rho^{\pm 0}(765)$, and $\omega^{\circ}(784)$ production. The production of $f^{\circ}(1260)$ in Reaction (I-1) and $B^{-}(1235)$ and $\Sigma^{\circ}(1750)$ in Reaction (I-3) were not included, but they accounted for only 14, 5, and 6 per cent of the events respectively. The amount of $\omega^{\circ}(784)$ was adjusted to include both direct production and that resulting from $B^{-}(1235)$ decay.

Figure 17.--The thirteen diagrams which were calculated for Reaction (I-1) using the CLA model.

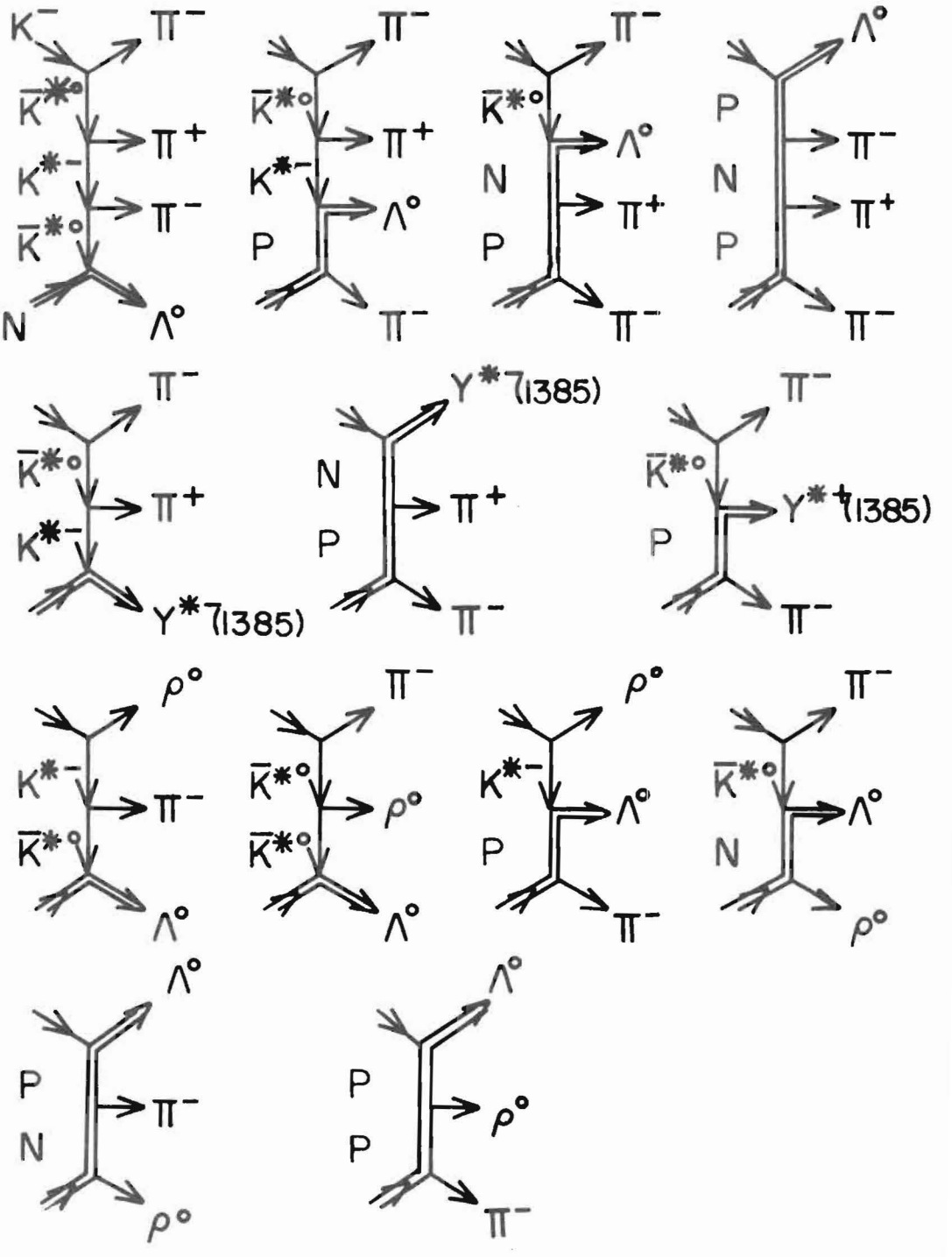
K⁻
π⁻
K̄*°
π⁺
K*⁻
π⁻
K̄*°
N
Λ°
π⁻
K̄*°
π⁺
K*⁻
P
Λ°
π⁻
π⁻
K̄*°
Λ°
N
π⁺
P
π⁻
Λ°
P
π⁻
N
π⁺
P
π⁻
π⁻
K̄*°
π⁺
K*⁻
Y*⁻(1385)
Y*⁻(1385)
N
π⁺
P
π⁻
π⁻
K̄*°
Y*⁺(1385)
P
π⁻
ρ°
K*⁻
π⁻
K̄*°
Λ°
π⁻
K̄*°
ρ°
K̄*°
Λ°
ρ°
K*⁻
Λ°
P
π⁻
π⁻
K̄*°
Λ°
N
ρ°
Λ°
P
π⁻
N
ρ°
Λ°
P
ρ°
P
π⁻

For Reactions (I-1) to (I-3) the outgoing signed charges must alternate in sign as we go down a diagram, i.e. the top and bottom outgoing signed charge must be negative. This is a consequence of only allowing isospin 1/2 strange meson and nucleon trajectory exchanges. Strange mesons with isospin ≥ 1 have not been observed. We ignore possible $\Delta(1236)$ trajectory exchange because its coupling is known to be weaker than the nucleon's.[17]

A. Resonance Production

The first step in determining the amount of each resonance present in the data was to compare the effective mass distributions with the prediction of pure Lorentz invariant phase space in the resonance region. The estimates thus obtained were first approximations and were used as input to the CLA model. The weighting factor for each resonance included in the CLA model was then adjusted until it gave the final value of the amount of observed resonance to within about one standard deviation. Final adjustments were carried out by hand. If the background on either side of the resonance region disagreed with the model prediction by between about two and three standard deviations, we took an average between the model and an adjusted curve to obtain the background, and increased the error estimate. In the case of the ω° the background was estimated from a straight line connecting the mass distributions above and below the resonance region because the CLA model disagreed with the data by about 3.5 standard deviations on the high mass side.

Each resonance region was approximately centered on the resonant mass. In all but two cases our mass resolution was much smaller than

the natural line width and thus the resonance region was taken as about 2Γ wide. (The quantity Γ is the full width at half height.) For the ω°, Γ is only 12 MeV/c^2, but our mass resolution is ±33 MeV/c^2. In this case we used a band 100 MeV/c^2 wide. For the $Y^{*\circ}(1385)$, Γ = 36 MeV/c^2, our mass resolution is also ±36 MeV/c^2, and we used a band 150 MeV/c^2 wide.

These cross-sections for resonance production will be presented in Tables 1 and 2.

In examining the effective mass distributions for all the possible particle combinations of Reaction (I-1) two of the most prominent features are the peaks due to the well known resonance Y*(1385) appearing in the $\Lambda\pi^-$ and $\Lambda\pi^+$ mass distributions. These distributions are given in Figure 18. The distributions of the cosines of the production angles of the $\Lambda^\circ\pi^-$ and $\Lambda^\circ\pi^+$ as seen in the K^-N center of mass (CM) system are given in Figure 19. We measured all production angles with respect to the K^-. The cross-hatched portion represents those events in the region of the Y*(1385). Qualitatively the CLA model agrees with the data.

The existence of a hyperon resonance whose mass is in the region from about 1620 to 1640 MeV/c^2 is a question of interest associated with the $\Lambda\pi^\pm$ mass spectra of Reaction (I-1). Evidence supporting such a resonance was first reported by a Brookhaven National Laboratory (BNL) group[18] in the reaction

$$K^-N \rightarrow \underset{\hookrightarrow\ \Lambda\pi^\pm}{Y^{*\pm}(1619)}\pi^\mp\pi^- \qquad \text{(V-1)}$$

Figure 18.--For the reaction $K^-N \rightarrow \pi^-\pi^-\pi^+\Lambda$ [Reaction (I-1)] with 479 events (A) gives the effective mass distributions for the particle combinations $\Lambda^o\pi^-$ [hereafter denoted as the distribution of $M(\Lambda\pi^-)$], and (B) distribution of $M(\Lambda\pi^+)$. The smooth curves on these and all subsequent graphs (unless otherwise indicated) are the results of the CLA model normalized to the data.

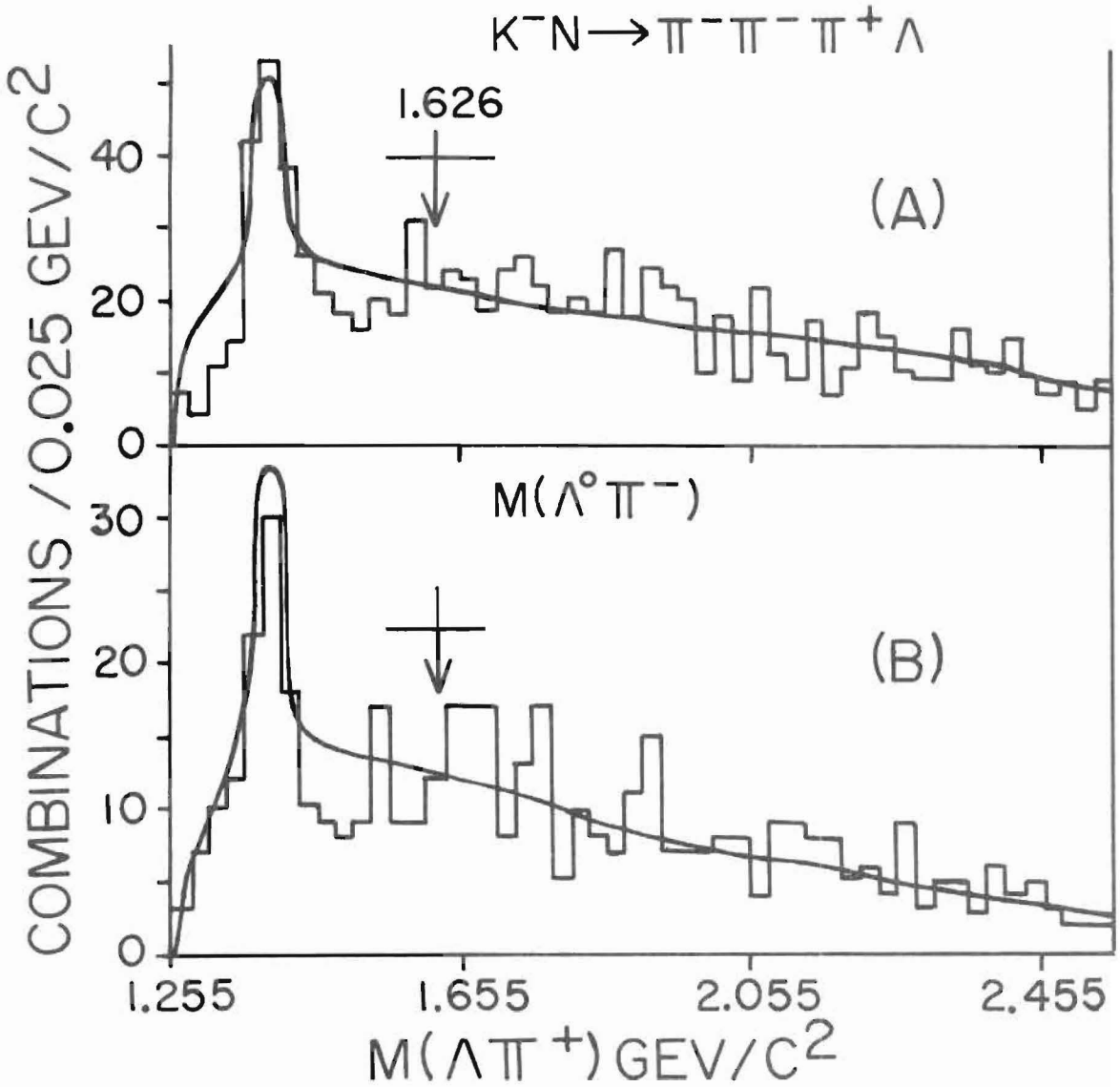
K⁻N → π⁻π⁻π⁺Λ
1.626
(A)
M(Λ°π⁻)
(B)
COMBINATIONS /0.025 GEV/C²
0
20
40
0
10
20
30
1.255
1.655
2.055
2.455
M(Λπ⁺) GEV/C²

Figure 19.--Center of mass production cosine distribution of Reaction (I-1) for the particle combinations (A) $\Lambda\pi^-$ where cross-hatched portion corresponds to 137 combinations obtained by demanding $M(\Lambda\pi^-)$ in the mass interval [1.342, 1.442] GeV/c^2. If both possible combinations had masses in the interval of interest we plotted only the combination having the mass closer to the resonance of interest [in this case the $Y^{*-}(1385)$]. Unless otherwise indicated this procedure will be adhered to in subsequent graphs where mass cuts are made and an ambiguity exists between π^- combinations. (B) $\Lambda\pi^+$ where cross-hatched portion corresponds to 78 combinations obtained by demanding $M(\Lambda\pi^+)$ in the mass interval [1.342, 1.442] GeV/c^2.

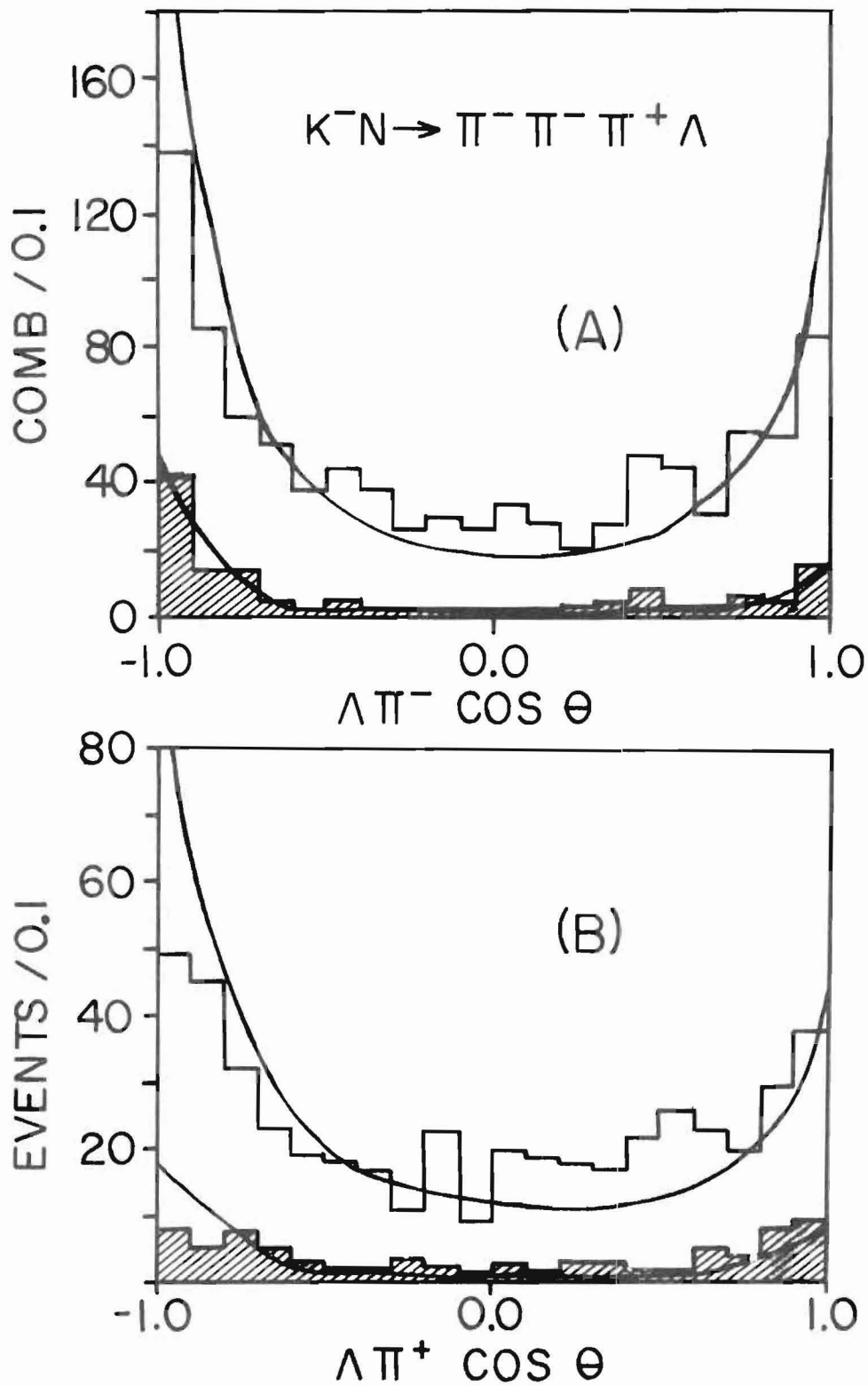
$K^-N \rightarrow \pi^-\pi^-\pi^+\Lambda$
(A)
COMB /0.1
160
120
80
40
0
-1.0
0.0
1.0
$\Lambda\pi^-$ COS θ
(B)
EVENTS /0.1
80
60
40
20
-1.0
0.0
1.0
$\Lambda\pi^+$ COS θ

at a laboratory beam momentum of 3.9 GeV/c. At the Lund Conference[19] more evidence in support of its existence was presented by the same group based on the same reaction but with approximately four times as much data. Their final sensitivity was 16 events per μbarn. They reported a mass of (1619 ± 8) MeV/c^2 and a width of $(72 \begin{smallmatrix} +22 \\ -15 \end{smallmatrix})$ MeV/c^2. At the same conference the results of the SABRE[20] collaboration were presented on the same reaction at 3.0 GeV/c in which no evidence for the existence of this resonance was observed. Recently a Purdue group has presented confirmatory evidence for this resonance based on the same reaction at an incident laboratory momentum of 4.5 GeV/c.[21] They reported a mass of (1642 ± 12) MeV/c^2 and a width of (55 ± 24) MeV/c^2. In addition they reported that it is observed to be produced with a cross-section of (18 ± 3) μbarns. Their exposure sensitivity is five events per μbarn. The weighted average of the two reports of this possible resonance gives a mass of (1.626 ± .007) GeV/c^2 and a width of (0.066 ± 0.014) GeV/c^2. In subsequent discussion we shall refer to this possible resonance as $Y^{*\pm}(1626)$.

To obtain an estimate of how the cross-section for $Y^{*\pm}(1626)$ production might possibly change as the beam momentum changes, we have made use of the CLA model to compute the unnormalized average squared matrix element, $\overline{|T_{if}|^2}$. Then the unnormalized cross-section σ_p is given by[22]

$$\sigma_p = \frac{1}{4\ PM} \int |T_{if}|^2 d(ps) \qquad \text{(V-2)}$$

where

P = the beam laboratory momentum,

M = mass of the target neutron and

d(ps) = an infinitesimal element of Lorentz-invariant phase space.

The expression

$$\int |T_{if}|^2 d(ps) \qquad \text{(V-3)}$$

may be rewritten as

$$\overline{|T_{if}|^2} \int d(ps) \qquad \text{(V-4)}$$

and then the integral represents the phase space available for the reaction. We have computed σ_p for the reactions $K^-N \rightarrow Y^{*\mp}(1385)\pi^{\pm}\pi^-$ and $K^-N \rightarrow Y^{*\mp}(1626)\pi^{\pm}\pi^-$ for incident beam momenta of 3.9, 4.5, 4.9 and 5.5 GeV/c. We normalized the results to the measured values at 4.5 GeV/c and have plotted the results in Figure 20 as a hand-drawn smooth curve through each set of four points. We have also plotted in Figure 20 the cross-sections based on the experimental data. We obtained the values at 3.9 GeV/c by counting the $\Lambda^o\pi^{\pm}$ mass combinations in the regions of interest as shown in the BNL paper[19] and using a hand-drawn smooth curve as background. The value at 4.5 GeV/c for the $Y^{*\pm}(1626)$ was taken as quoted by Purdue.[21] The value at 4.5 GeV/c for the $Y^{*\pm}(1385)$ was obtained from the Purdue paper[21] by counting the $\Lambda^o\pi^{\pm}$ mass combinations in the region of interest and using as background the phase space curves which were published on the plots. The value of the cross-section for $Y^{*\pm}(1385)$ at our beam momentum was obtained by the method described at the beginning of this section. To estimate the cross-section for the

Figure 20.--Cross-section versus beam momentum as predicted by CLA model for $Y^{*\pm}(1385)$ and $Y^{*\pm}(1626)$. Curves are normalized to the Purdue data at 4.5 GeV/c.

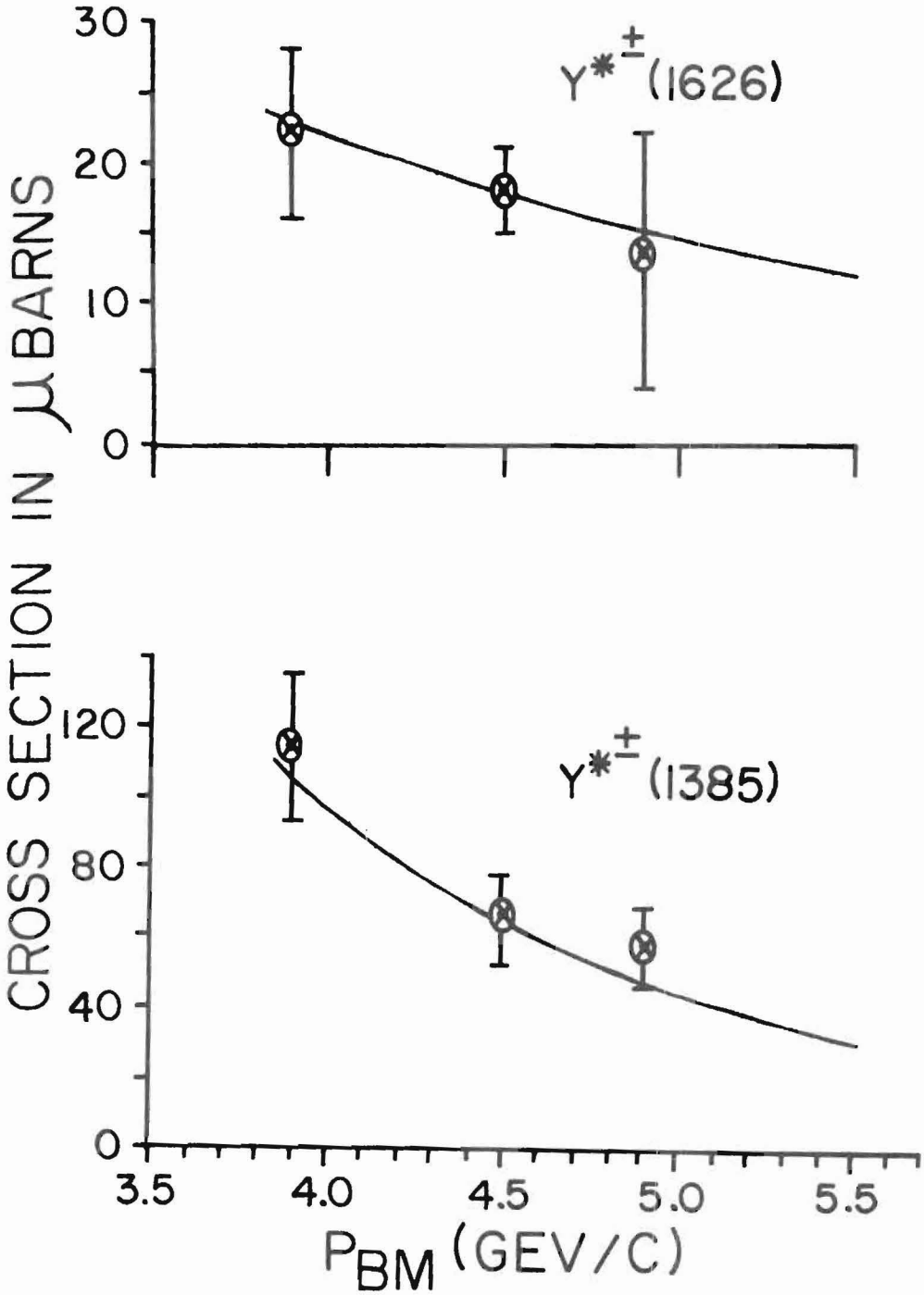
30
20
10
0
Y*±(1626)
CROSS SECTION IN μBARNS
120
80
40
0
Y*±(1385)
3.5
4.0
4.5
5.0
5.5
PBM (GEV/C)

possible $Y^{*\pm}(1626)$ present in our data we tried two different methods of estimating the background in the region of interest. If we use the CLA model for the background in the mass region [1.555, 1.705] GeV/c^2 we expect 199 $\Lambda^\circ\pi^\pm$ mass combinations. In the experimental data we find 217 combinations in this mass region thus giving a 1.3 standard deviation excess. We have also used the data on either side of the mass region of interest as an estimate of the background. Using the number of $\Lambda^\circ\pi^\pm$ mass combinations in the intervals [1.455, 1.555] and [1.705, 1.805] GeV/c^2 and a linear interpolation we expect (188 ± 18) mass combinations in the interval [1.555, 1.705] GeV/c^2. Thus the data gives a 1.5 standard deviation excess. Based on these results we can not confirm the existence of this resonance. We used the number of excess events as determined by this second method to obtain the cross-section (14 ± 9) μbarns for $Y^{*\pm}(1626)$ at our beam momentum as shown in Figure 20. This figure shows that the CLA model gives the correct energy dependence for $Y^{*\pm}(1385)$ production. It also shows that this model for $Y^*(1626)$ and the results of BNL, Purdue, and ourselves are consistent. Therefore, although we can not confirm its existence, our data are consistent with the results of workers reporting this resonance.

We have also looked for this resonance in our data in a slightly different manner by using the BNL criteria for including events in the sample for Reaction (I-1). When the $\Lambda\pi$ mass distribution was examined for the sample thus obtained we saw no increase in the significance of a possible signal in the region of the $Y^{*\pm}(1626)$.

We used a method of the BNL group to try to reduce the background due to $Y^{*\pm}(1385)$ and $\rho^\circ(765)$. The resulting $\Lambda\pi^\pm$ mass distributions

are shown in Figure 21. The BNL criteria are:

"(a) If one $\Lambda\pi$ combination is in the $Y_1^*(1385)$ region (1390 ± 40 MeV) we plot only that particular combination and no other. If more than one is in this Y_1^* region we weight them appropriately.

(b) If the $\pi^-_{a(b)}\ \pi^+$ system forms a peripheral ρ (with mass 760 ± 60 MeV and $\Delta^2_{K^- \to \rho^\circ} < 1.2\ GeV^2$), we do not plot the $\Lambda\pi^+$ or $\Lambda\pi^-_{a(b)}$ combination."

When plotted in this manner we still cannot detect the presence of $Y^{*\pm}(1626)$ in our data.

Figure 22(B) shows the $\pi^-\pi^+$ mass distribution for Reaction (I-1). A strong $\rho^\circ(765)$ resonance signal is evident. Figure 22(A) shows the corresponding CM production angular distribution with the cross-hatched region corresponding to a cut on the $\rho^\circ(765)$ mass region.

In addition to the $\rho^\circ(765)$, when one examines the $\pi^-\pi^+$ mass distribution versus the CLA model, there is an indication of some $f^\circ(1260)$. This resonance was not included in the model. The amount of $f^\circ(1260)$ present was found by using the CLA model as an estimate of the background. To make sure that leaving the $f^\circ(1260)$ out of the CLA model did not affect our conclusions, we removed the events in its mass region from our mass plots and found that this made no significant changes in our conclusions.

In the reaction $K^-N \to \pi^-\pi^-\pi^+\Sigma^\circ$, Reaction (I-2), we have detected only one resonance, the $\rho^\circ(765)$. It appears in the distribution of the invariant mass $M(\pi^-\pi^+)$ given in Figure 23(B). The corresponding CM production angular distribution is given in Figure 23(A). The cross

Figure 21.--Mass distributions for Reaction (I-1) when we attempted to reduce background by using BNL criteria[18] for (A) $M(\Lambda\pi^{\pm})$, (B) $M(\Lambda\pi^{-})$ with 518 combinations, and (C) $M(\Lambda\pi^{+})$ with 246 combinations.

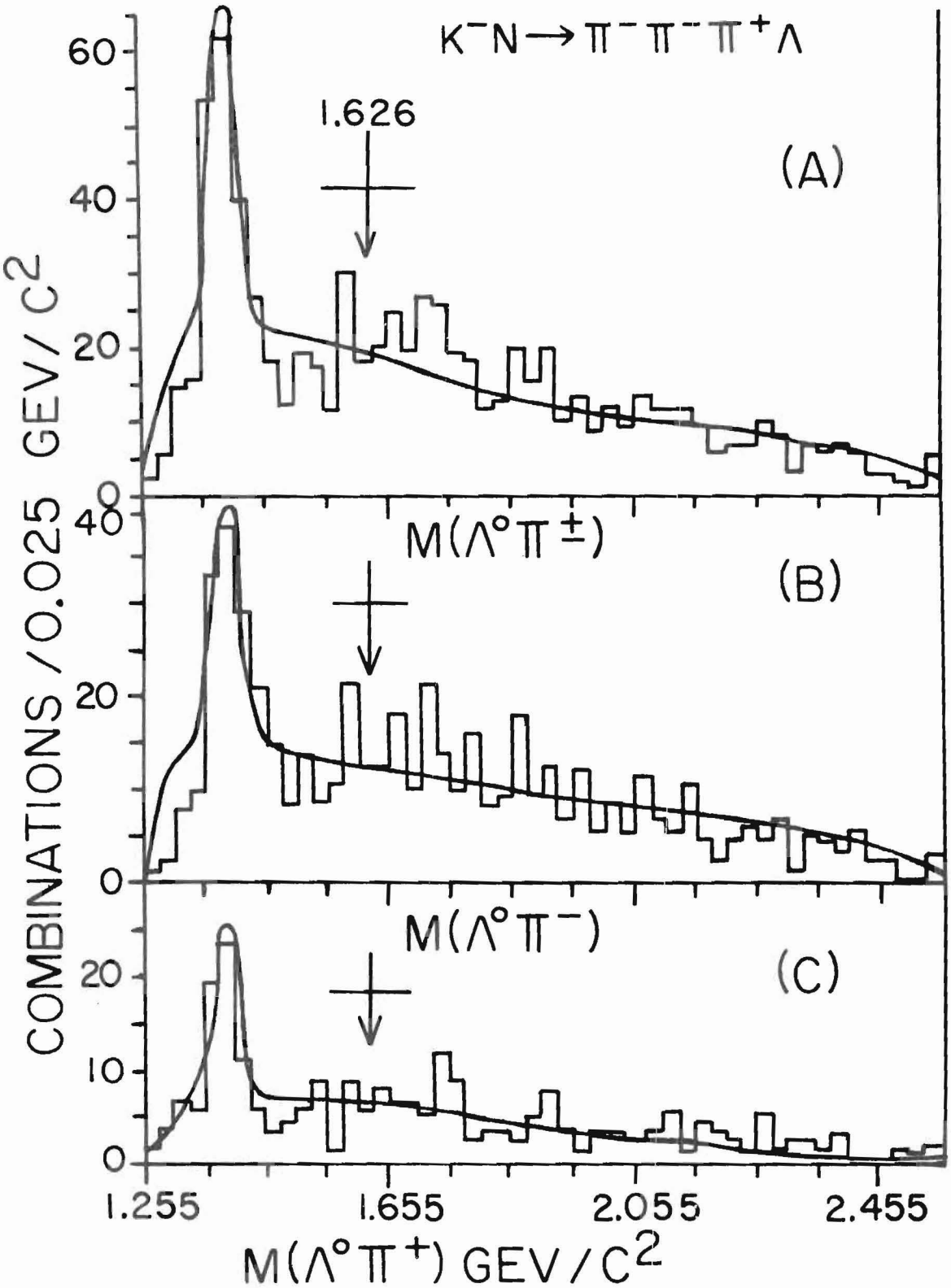
K⁻N → π⁻π⁻π⁺Λ
1.626
(A)
(B)
(C)
M(Λ°π±)
M(Λ°π⁻)
COMBINATIONS /0.025 GEV/C²
M(Λ°π⁺) GEV/C²
1.255
1.655
2.055
2.455
60
40
20
0
40
20
0
20
10
0

Figure 22.--For Reaction (I-1) (A) $\pi^-\pi^+$ center of mass production angular distribution where cross-hatched region corresponds to 245 combinations having $M(\pi^-\pi^+)$ in the mass interval [0.667, 0.867] GeV/c^2. (B) $M(\pi^-\pi^+)$ distribution.

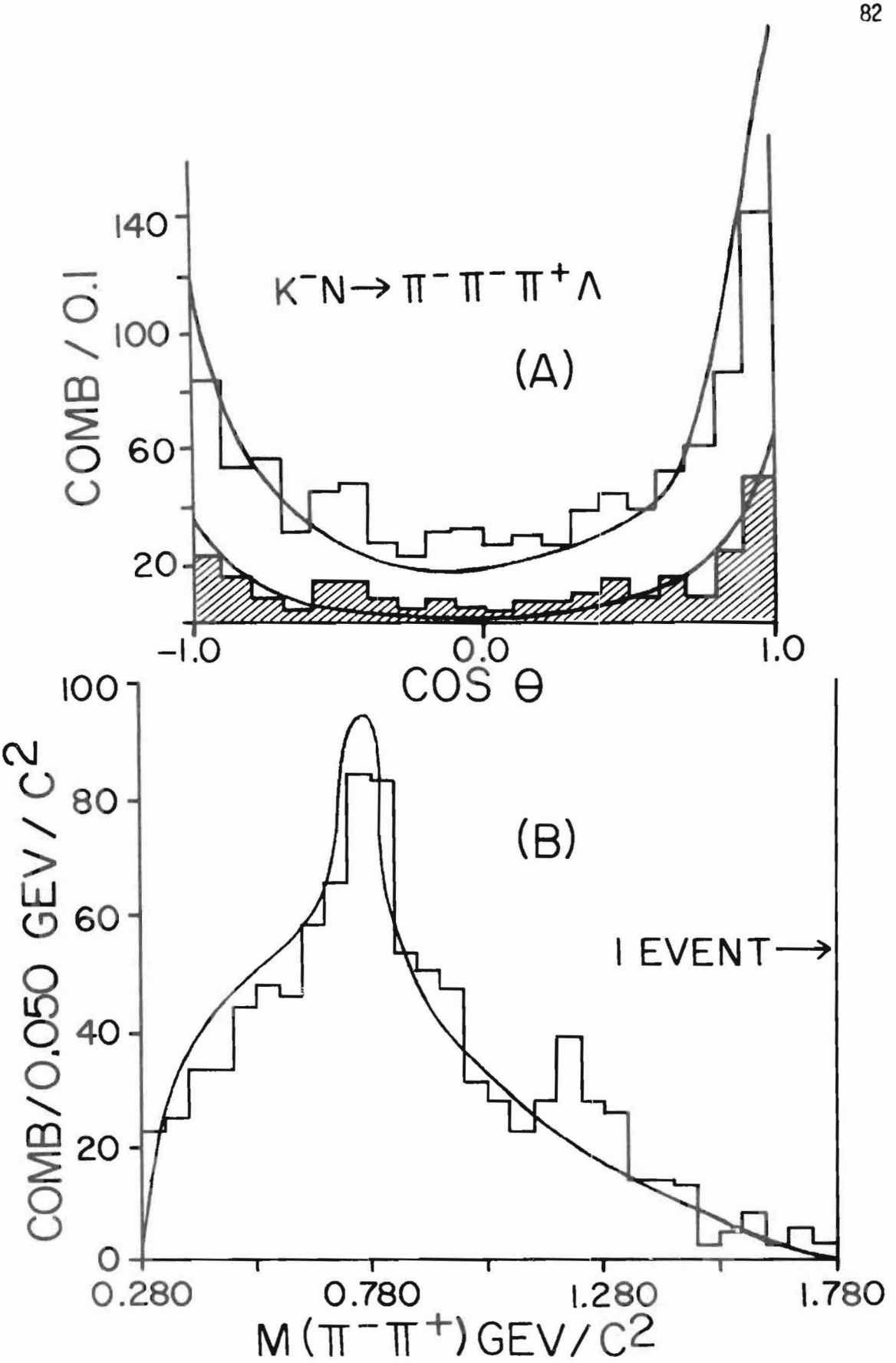
K⁻N→π⁻π⁻π⁺Λ
(A)
COMB / 0.1
140
100
60
20
-1.0
0.0
1.0
COS θ
(B)
I EVENT→
COMB/0.050 GEV / C²
100
80
60
40
20
0
0.280
0.780
1.280
1.780
M(π⁻π⁺) GEV/C²

Figure 23.--$K^-N \rightarrow \pi^-\pi^-\pi^+\Sigma^\circ$ [Reaction (I-2)] with 201 events (A) is the center of mass production angular distribution for the $\pi^-\pi^+$ combinations where the cross-hatched area corresponds to the 107 events obtained by demanding $M(\pi^-\pi^+)$ in the mass interval [0.667, 0.867] GeV/c^2, and (B) the $M(\pi^-\pi^+)$ distribution.

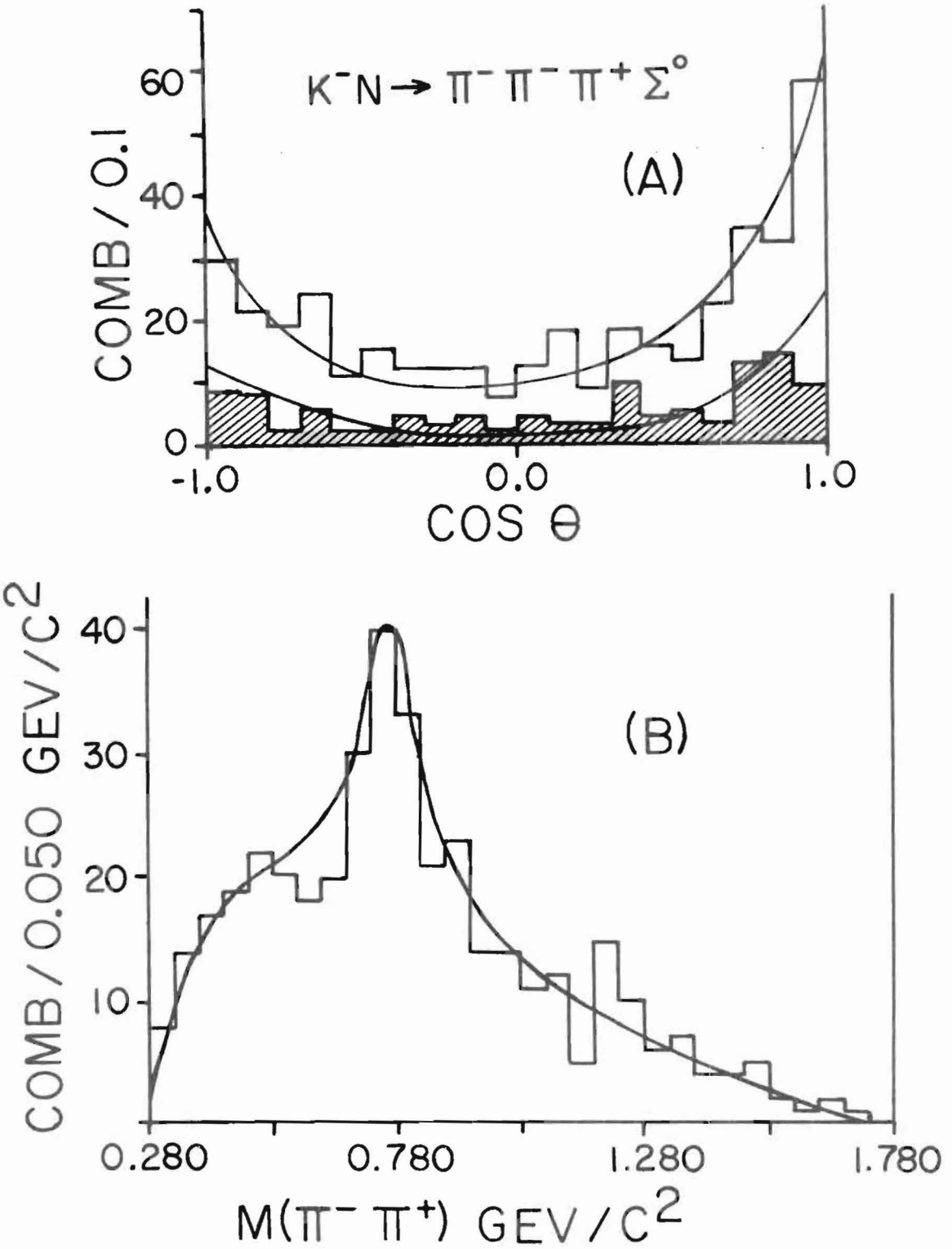
K⁻N → π⁻ π⁻ π⁺ Σ°
(A)
COMB / 0.1
60
40
20
0
-1.0
0.0
1.0
COS θ
(B)
COMB / 0.050 GEV/C²
40
30
20
10
0.280
0.780
1.280
1.780
M(π⁻ π⁺) GEV/C²

hatched region corresponds to events in the $\rho^\circ(765)$ region. The distributions given by the model and the data have the same shapes.

A question of interest for both Reactions (I-1) and (I-2) is the possible presence in the data of A_2^- meson decaying to $\pi^-\pi^-\pi^+$. The existence of this resonance was first reported in 1964[23] but has only recently been reported for K^-N reactions. The Purdue group[24] report a fitted mass of (1.330 ± 0.015) GeV/c² and a fitted width of (0.054 ± 0.030) GeV/c² for the A_2^- as observed in the reactions $K^-N \rightarrow \pi^-\pi^-\pi^+\Lambda$ and $K^-N \rightarrow \pi^-\pi^-\pi^+\Sigma^\circ$ for an incident beam laboratory momentum of 4.48 GeV/c. Their data show no compelling evidence for the $\rho^\circ(765)\pi^-$ decay mode of the A_2, whereas the Brookhaven group[25] does see the $\rho^\circ(765)\pi^-$ decay mode for the A_2 produced in the reaction $K^-N \rightarrow \Lambda^\circ\pi^-\pi^-\pi^+$ at an incident beam momentum of 3.9 GeV/c. The sensitivity of the experiment at 4.48 GeV/c is five events per μbarn. The sensitivity of our experiment (as computed in the Appendix) is (4.5 ± 0.7) events per μbarn. Figures 24(A) and 24(B) show our observed 3π mass distributions versus the CLA model for Reactions (I-1) and (I-2) respectively. The region that extends 0.054 GeV/c² on both sides of 1.330 GeV/c² is designated by the arrow and cross bar. Figures 25(A) and 25(B) show our 3π mass distributions versus the CLA model for Reactions (I-1) and (I-2) respectively where we have demanded that at least one $\pi^-\pi^+$ combination have an invariant mass between 0.666 and 0.866 GeV/c². When examining these distributions we find no compelling evidence for the presence of A_2 meson in our data.

There is Y*(1385) production in Reaction (I-3) as evidenced by the $\Lambda\pi$ mass distributions shown in Figures 26(B), 27(B), and 28(B).

Figure 24.--The 3π mass distribution for (A) Reaction (I-1) and (B) Reaction (I-2).

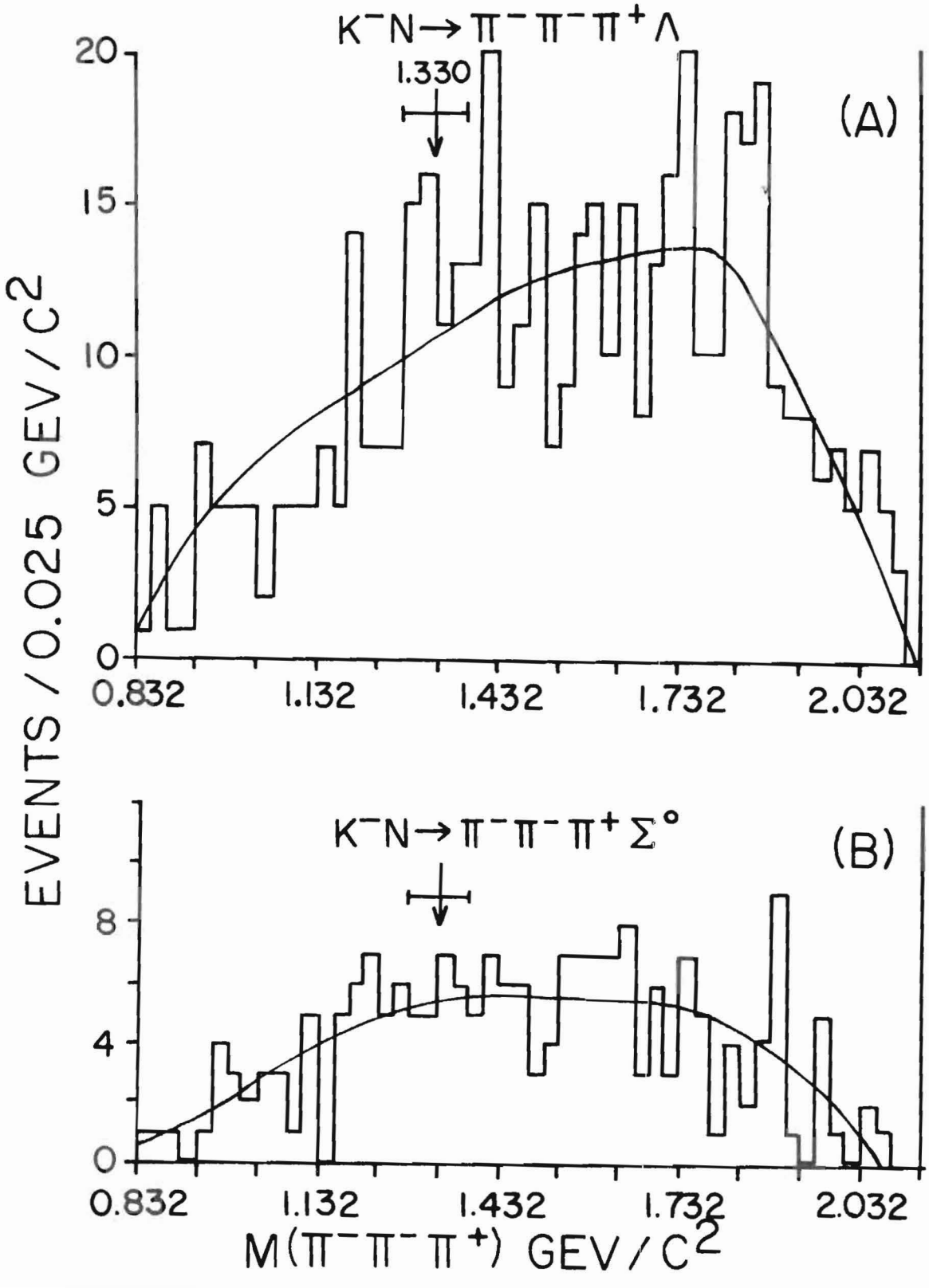
K⁻N → π⁻π⁻π⁺Λ
1.330
(A)
20
15
10
5
0
0.832
1.132
1.432
1.732
2.032
EVENTS / 0.025 GEV / C²
K⁻N → π⁻π⁻π⁺Σ°
(B)
8
4
0
0.832
1.132
1.432
1.732
2.032
M(π⁻π⁻π⁺) GEV / C²

Figure 25.--The 3π mass distribution where we have demanded that at least one $\pi^-\pi^+$ mass combination be in the mass interval from 0.666 to 0.866 GeV/c^2 for (A) Reaction (I-1) giving 248 events and (B) Reaction (I-2) giving 107 events.

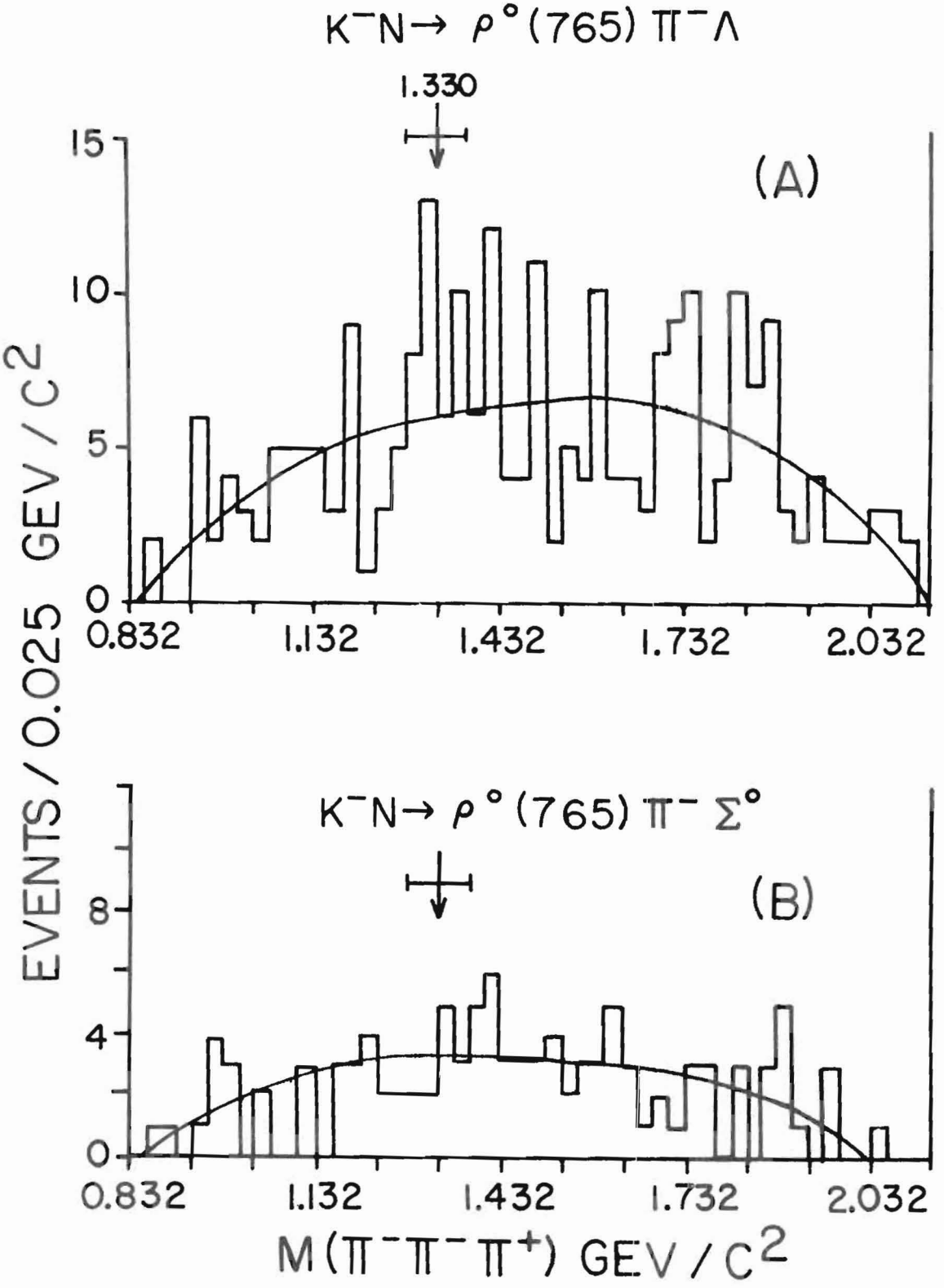
K⁻N→ ρ°(765) π⁻Λ
1.330
(A)
15
10
5
0
0.832
1.132
1.432
1.732
2.032
EVENTS / 0.025 GEV / C²
K⁻N→ ρ°(765) π⁻ Σ°
(B)
8
4
0
0.832
1.132
1.432
1.732
2.032
M(π⁻π⁻π⁺) GEV / C²

Figure 26.--For the reaction $K^-N \rightarrow \pi^-\pi^-\pi^+\pi^0\Lambda$ [Reaction (I-3)] with 1347 events (A) the center of mass production angular distribution for the $\Lambda\pi^-$ combinations where the cross-hatched area corresponds to the 495 events obtained by demanding a $\Lambda\pi^-$ mass combination in the mass interval from 1.342 to 1.442 GeV/c^2. (B) Distribution in $M(\Lambda\pi^-)$.

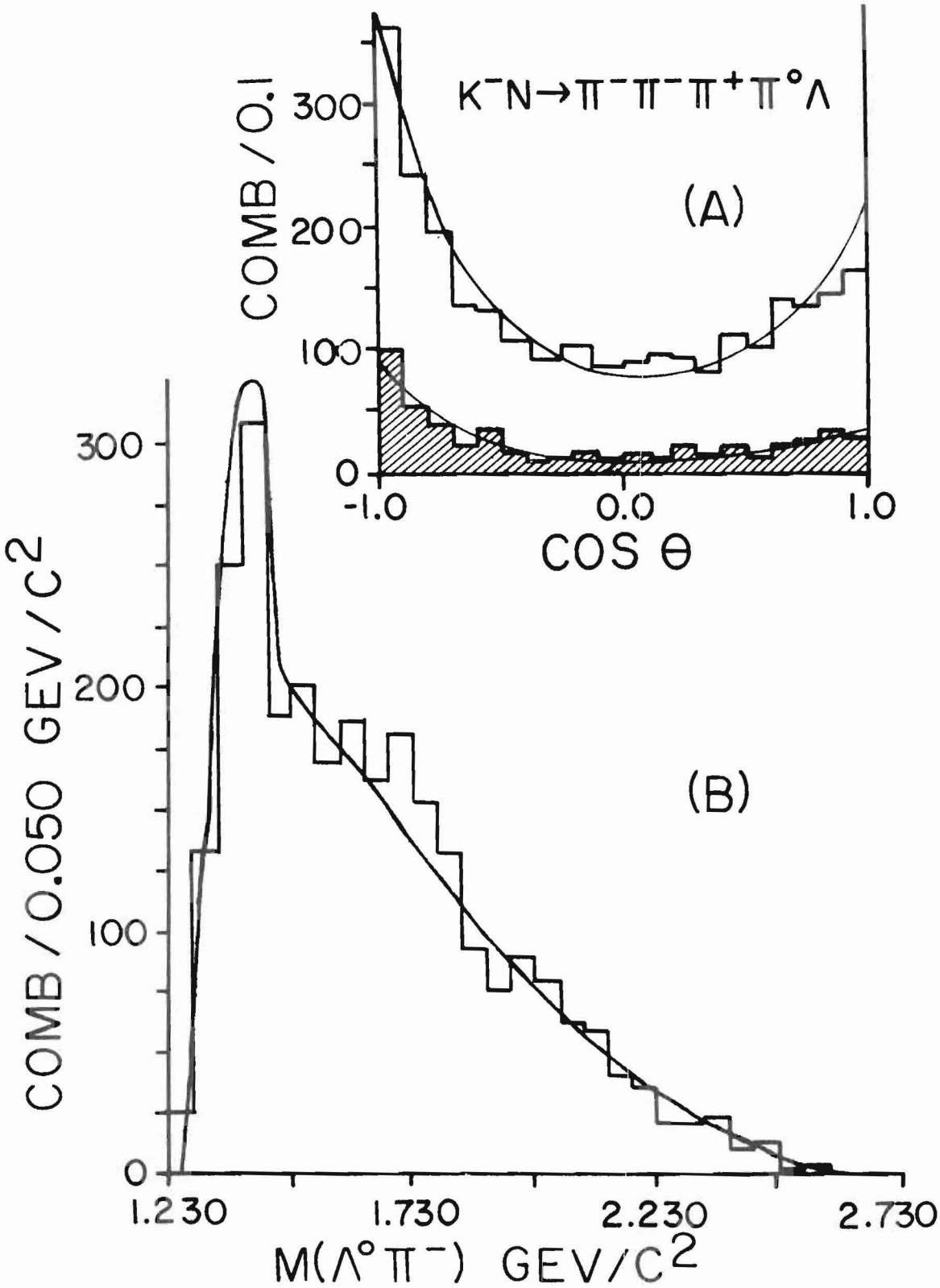
K⁻N→π⁻π⁻π⁺π°Λ
(A)
COMB / 0.1
300
200
100
0
-1.0
0.0
1.0
COS θ
(B)
COMB / 0.050 GEV / C²
300
200
100
0
1.230
1.730
2.230
2.730
M(Λ°π⁻) GEV/C²

Figure 27.--For the particle combination $\Lambda\pi^+$ of Reaction (I-3) (A) gives the center of mass production angular distribution where the cross-hatched area corresponds to the 238 events obtained by demanding $M(\Lambda\pi^+)$ be in the mass interval [1.342, 1.442] GeV/c^2. (B) The distribution of $M(\Lambda\pi^+)$.

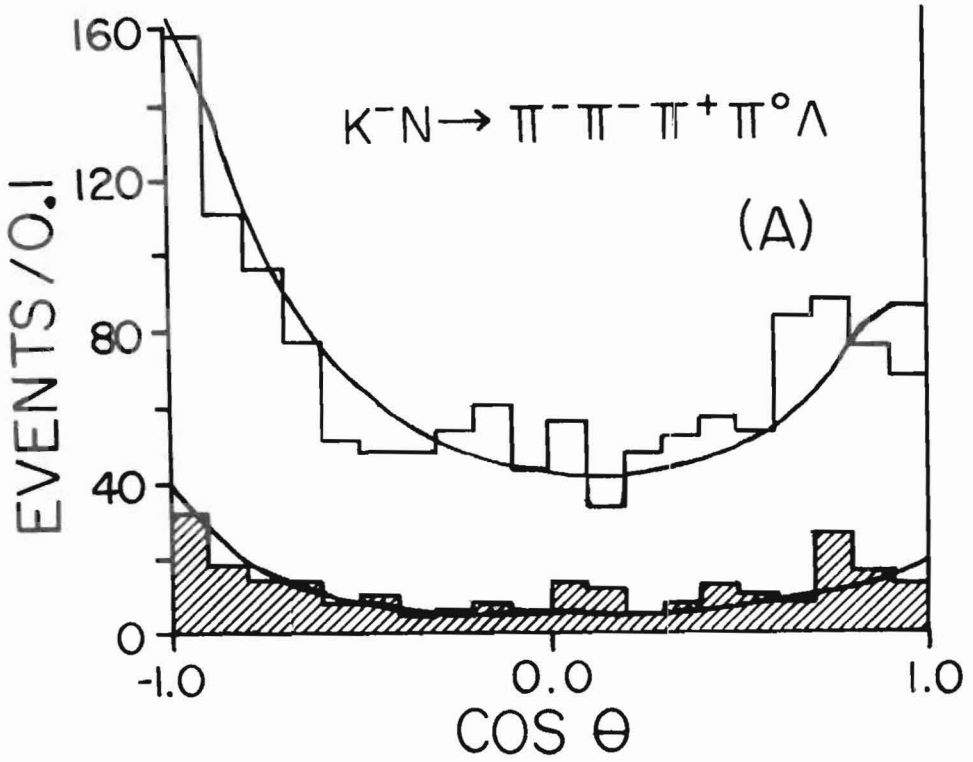
160
120
80
40
0
EVENTS/0.1
$K^-N \rightarrow \pi^-\pi^-\pi^+\pi^0\Lambda$
(A)
-1.0
0.0
1.0
COS θ

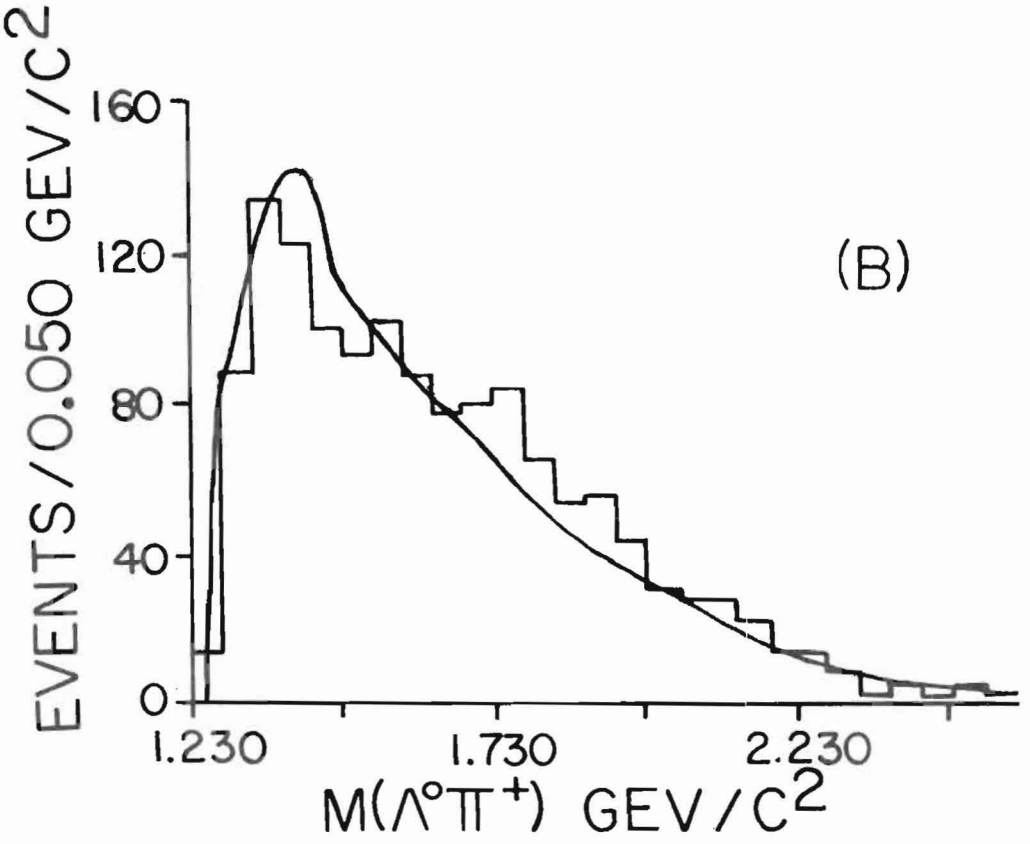
EVENTS/0.050 GEV/C^2
160
120
80
40
0
(B)
1.230
1.730
2.230
$M(\Lambda^0\pi^+)$ GEV/C^2

Figure 28.--For the particle combination $\Lambda\pi^\circ$ of Reaction (I-3) (A) gives the center of mass production angular distribution where the cross-hatched area corresponds to the 281 events obtained by requiring $M(\Lambda\pi^\circ)$ be in the mass interval [1.300, 1.450] GeV/c^2. (B) The distribution of $M(\Lambda\pi^\circ)$.

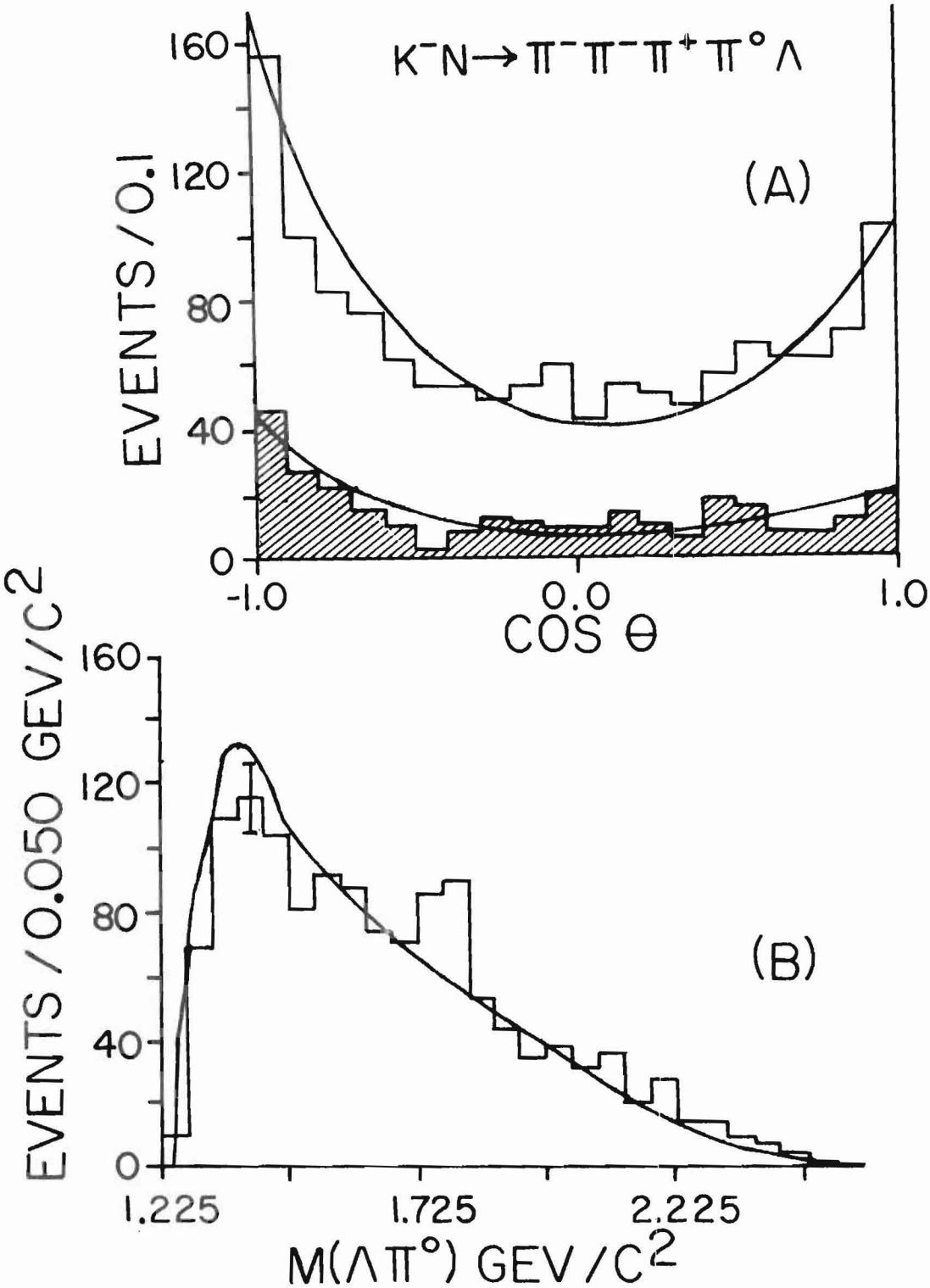
K⁻N → π⁻π⁻π⁺π°Λ
(A)
EVENTS / 0.1
160
120
80
40
0
-1.0
0.0
1.0
COS θ
(B)
EVENTS / 0.050 GEV/C²
160
120
80
40
0
1.225
1.725
2.225
M(Λπ°) GEV/C²

The corresponding center of mass production angular distributions are given in Figures 26(A), 27(A), and 28(A).

In the interval from 1.725 to 1.825 GeV/c^2 the $\Lambda\pi^\circ$ mass spectrum shows an excess of 55 events above a background of (123 ± 11) events. The reported branching ratios[26] imply we should see a signal of about 43 events in the $\overline{K}^\circ N$ mass spectrum of the reaction

$$K^- N \rightarrow \pi^+\pi^-\pi^-\overline{K}^\circ N \qquad \text{(V-5)}$$

if this $\Lambda\pi^\circ$ effect is due to the $\Sigma(1765)$ hyperon resonance and if interference effects are not important. On the other hand, if it is due to the $\Sigma(1750)$ there should only be about three such events. This measured $\overline{K}^\circ N$ mass spectrum[5] shows a two standard deviation depletion from the estimated background of 77 events. Because of this we conclude that the $\Lambda\pi^\circ$ excess is probably due to the decay of the $\Sigma(1750)$. Our data imply a mass of (1.762 ± .018) GeV/c^2 for this enhancement. When we take our mass resolution of ±40 MeV/c^2 into account we find that Γ is less than 30 MeV/c^2 at the 90 per cent confidence level. There are also excess events at the same mass interval in the $\Lambda\pi^-$ and $\Lambda^\circ\pi^+$ mass spectra for this reaction, but these are less statistically significant and have smaller signal-to-noise ratios. To examine the possibility that this enhancement may be due to events which have a Σ° or an additional π° in the final state, we have plotted the $\Lambda\pi^\circ$ mass distribution in three separate parts. To do this we made use of F_3, the number of standard deviations by which the missing boson mass squared exceeded the π° mass squared. We have discussed the distribution of F_3 earlier. One $\Lambda^\circ\pi^\circ$ mass distribution comprised only those events having $F_3 \leq 0.0$;

the second corresponded to those events with $0.0 < F_3 < 1.25$; the third corresponded to those events with $F_3 \geq 1.25$. The first and second of these had a three standard deviation excess, while the third only had a one standard deviation excess and thus we concluded that the events in this enhancement show no sign of coming from contaminating reactions. We have also looked to see if this bump results from the decay of a parent resonance or is produced preferentially with another mass enhancement by plotting all the possible mass combinations for Reaction (I-3) with the restriction that the $\Lambda^\circ\pi^\circ$ mass be in the interval from 1.725 to 1.825 GeV/c^2. We used the CLA model as an estimate for the background and found no evidence for either of these effects.

When the CLA model was first compared with the $\pi^-\pi^+$, $\pi^-\pi^\circ$, and $\pi^+\pi^\circ$ mass distributions of Reaction (I-3) the model was observed to be overpredicting in the low mass regions. Normalizing the model to the data in the mass intervals [0.480 to 0.680] and [0.880 to 1.580] GeV/c^2 for the $\pi^-\pi^+$ mass distribution gave the dashed line shown in the $\rho^\circ(765)$ mass region on Figure 29(B). Normalizing the model to the data in the mass intervals [0.475 to 0.675] and [0.875 to 1.575] GeV/c^2 for the $\pi^-\pi^\circ$ and $\pi^+\pi^\circ$ mass distributions gave the dashed lines in the region of the $\rho^\pm(765)$ shown in Figures 30(B) and 31(B). Using this renormalized CLA model result as an indication of the background we obtained an estimate of the amounts of these resonances present in the data. The CLA model was then recalculated taking into account the presence of these additional resonances. The resulting CLA model calculations are the smooth curves shown in Figures 29(B), 30(B), and 31(B) and we see better agreement when the presence of the $\rho(765)$ is taken into account. Requiring

Figure 29.--For the particle combination $\pi^-\pi^+$ of Reaction (I-3) (A) gives the center of mass production angular distribution where the cross-hatched area corresponds to the 599 events obtained by requiring $M(\pi^-\pi^+)$ be in the interval from 0.680 to 0.880 GeV/c^2. (B) Distribution of $M(\pi^-\pi^+)$ where the dashed line shows the result of the CLA model computed without including any diagrams for $\rho(765)$ production and normalized to the number of observed combinations in the mass intervals [0.480 to 0.680] and [0.880 to 1.580] GeV/c^2. The solid line gives the CLA result where all diagrams for ρ production are included.

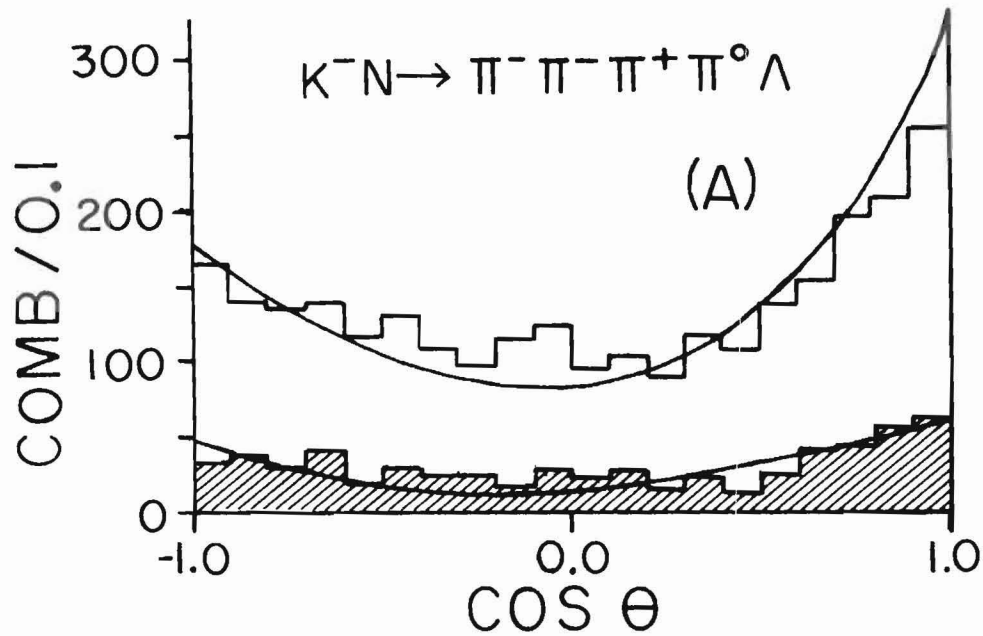
K⁻N→ π⁻π⁻π⁺π°Λ
(A)
COMB/0.1
300
200
100
0
-1.0
0.0
1.0
COS θ

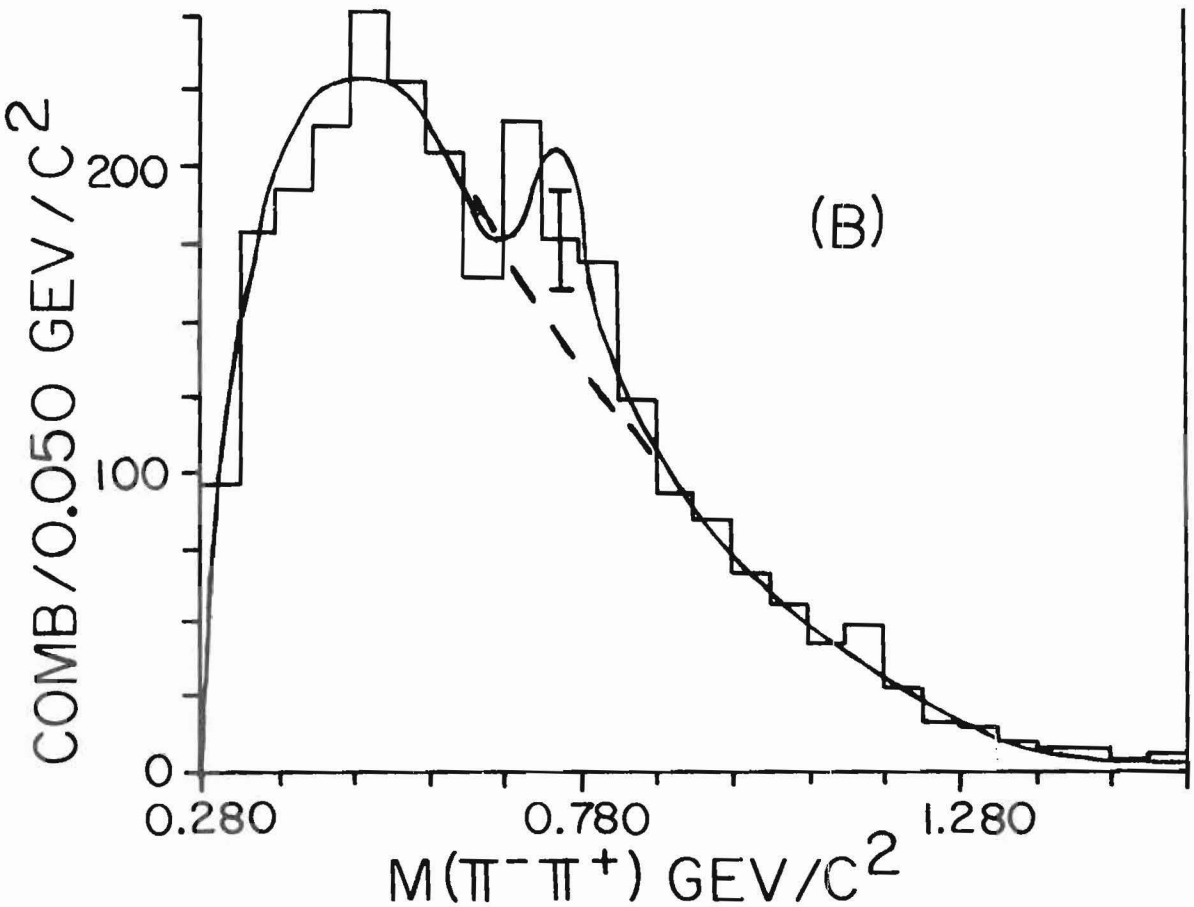
(B)
COMB/0.050 GEV/C²
200
100
0
0.280
0.780
1.280
M(π⁻π⁺) GEV/C²

Figure 30.--For the particle combinations $\pi^-\pi^\circ$ for Reaction (I-3) (A) gives the center of mass production angular distribution where the cross-hatched area corresponds to the 607 events obtained by requiring $M(\pi^-\pi^\circ)$ to be in the interval 0.675 to 0.875 GeV/c^2. (B) Distribution of $M(\pi^-\pi^\circ)$ where the dashed line shows the result of the CLA model computed without including diagrams for $\rho(765)$ and normalized to the number of events in the mass intervals [0.475 to 0.675] and [0.875 to 1.575] GeV/c^2.

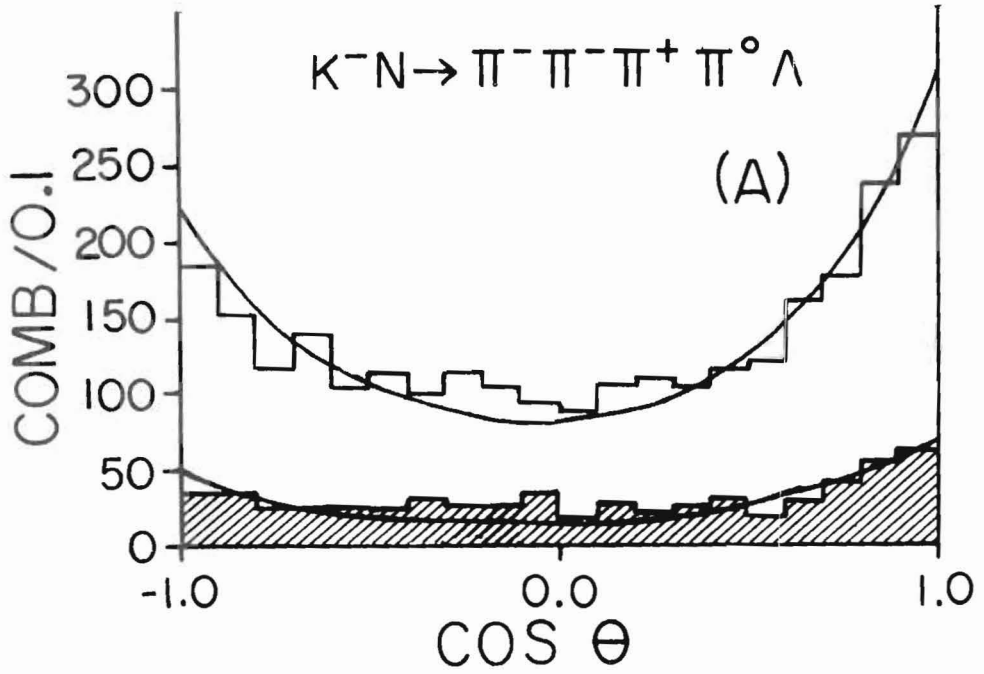
K⁻N→π⁻π⁻π⁺π°Λ
(A)
COMB/0.1
300
250
200
150
100
50
0
-1.0
0.0
1.0
COS θ

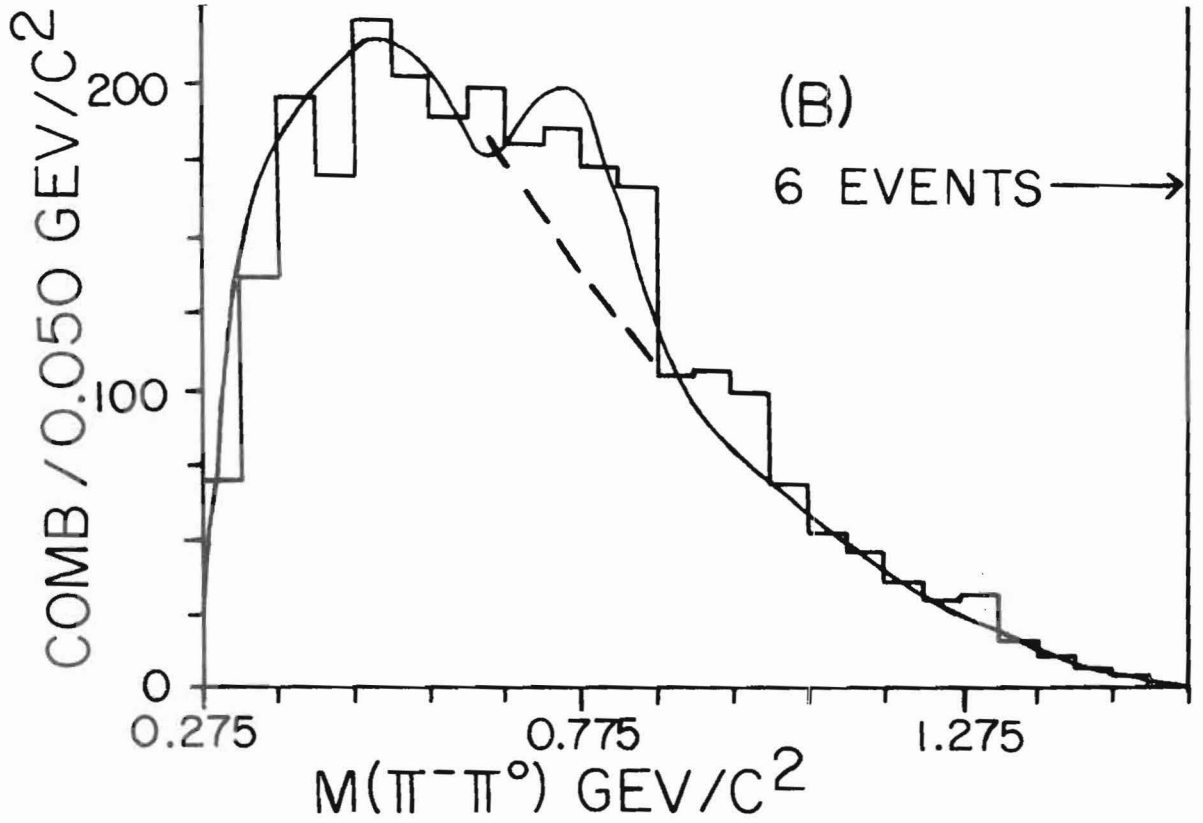
(B)
6 EVENTS
COMB/0.050 GEV/C²
200
100
0
0.275
0.775
1.275
M(π⁻π°) GEV/C²

Figure 31.--For Reaction (I-3) the mass distributions of the particle combinations (A) $\pi^-\pi^-$ and (B) $\pi^+\pi^\circ$ where dashed line shows the distribution given by the CLA model computed without including diagrams for $\rho(765)$ and normalized to the number of events in the mass intervals [0.475 to 0.675] and [0.875 to 1.575] GeV/c^2.

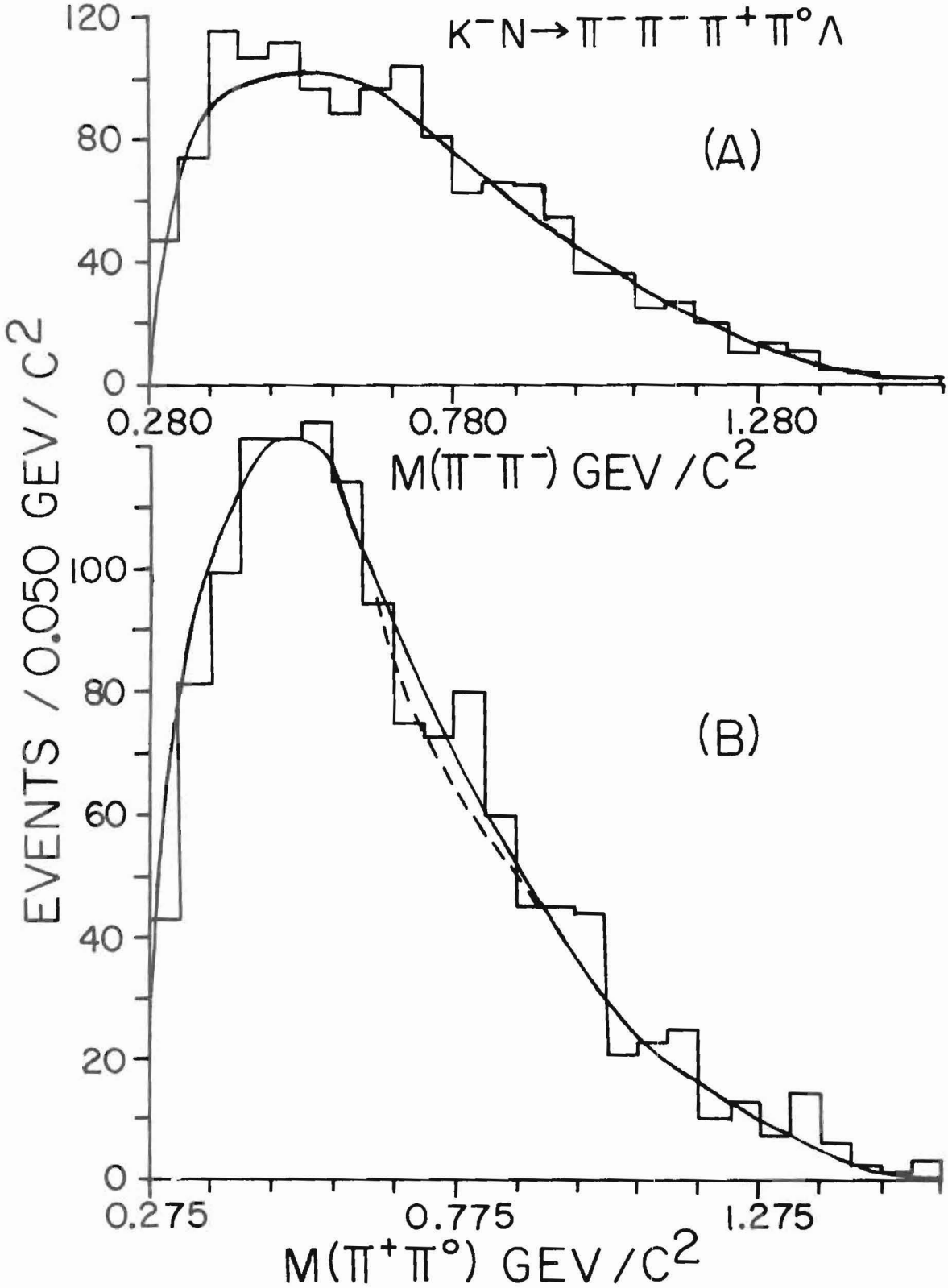
K⁻N→π⁻π⁻π⁺π°Λ
(A)
120
80
40
0
0.280
0.780
1.280
M(π⁻π⁻) GEV/C²
EVENTS / 0.050 GEV/C²
(B)
100
80
60
40
20
0
0.275
0.775
1.275
M(π⁺π°) GEV/C²

$M(\pi^-\pi^+)$ in the $\rho^\circ(765)$ region and $M(\pi^-\pi^\circ)$ in the $\rho^-(765)$ region gives the cross-hatched areas of the CM production angular distributions shown in Figure 29(A) and Figure 30(A) respectively. The CLA model gives qualitative agreement with these distributions. As a check (since the isospin one ρ cannot decay to $\pi^-\pi^-$) we show the $M(\pi^-\pi^-)$ distribution in Figure 31(A) versus the CLA model which was calculated including the presence of neutral and singly charged $\rho(765)$. The CLA model shows good agreement with the data in the mass region of the ρ.

The chi-squared probability that the observed $M(\pi^+\pi^-)$ distribution and the one given by the CLA model have the same shape in the region from .680 to .880 GeV/c^2 is only about one per cent. Since the model did not contain $B^-(1235)$ production, we studied the effect of removing those events with a $M(\pi^+\pi^-\pi^\circ)$ in the interval from .740 to .840 GeV/c^2. This removed the ω° and therefore also the B^- events. This left the number of excess events and their shapes in the region of the ρ mass in all four $\pi\pi$ mass distributions essentially unchanged. In fact, it produced no significant changes in our conclusion about any mass enhancement of this reaction. We also found that removing events with $M(\Lambda\pi^\circ)$ from 1.725 to 1.825 GeV/c^2 left our conclusions unchanged. Because of the shape of this $\pi^+\pi^-$ enhancement, we feel that the amount of ρ° production in Reaction (I-3) that is quoted in Table 2 should be viewed with a certain amount of caution.

The mass distribution for the particle combination $\pi^-\pi^+\pi^\circ$ is shown in Figure 32(B). Because of the disagreement between the CLA model and the data on the high side of the $\omega^\circ(784)$ resonance a background estimate was made by linearly interpolating the number of combinations

Figure 32.--For the particle combination $\pi^-\pi^+\pi^\circ$ of Reaction (I-3) (A) gives the center of mass production angular distribution where the cross-hatched area corresponds to the 239 events obtained by requiring $M(\pi^-\pi^+\pi^\circ)$ in the mass interval [0.740 to 0.840] GeV/c^2. (B) The $M(\pi^-\pi^+\pi^\circ)$ distribution where the dashed curve in the region of the $\omega^\circ(784)$ is a linear estimate of the background.

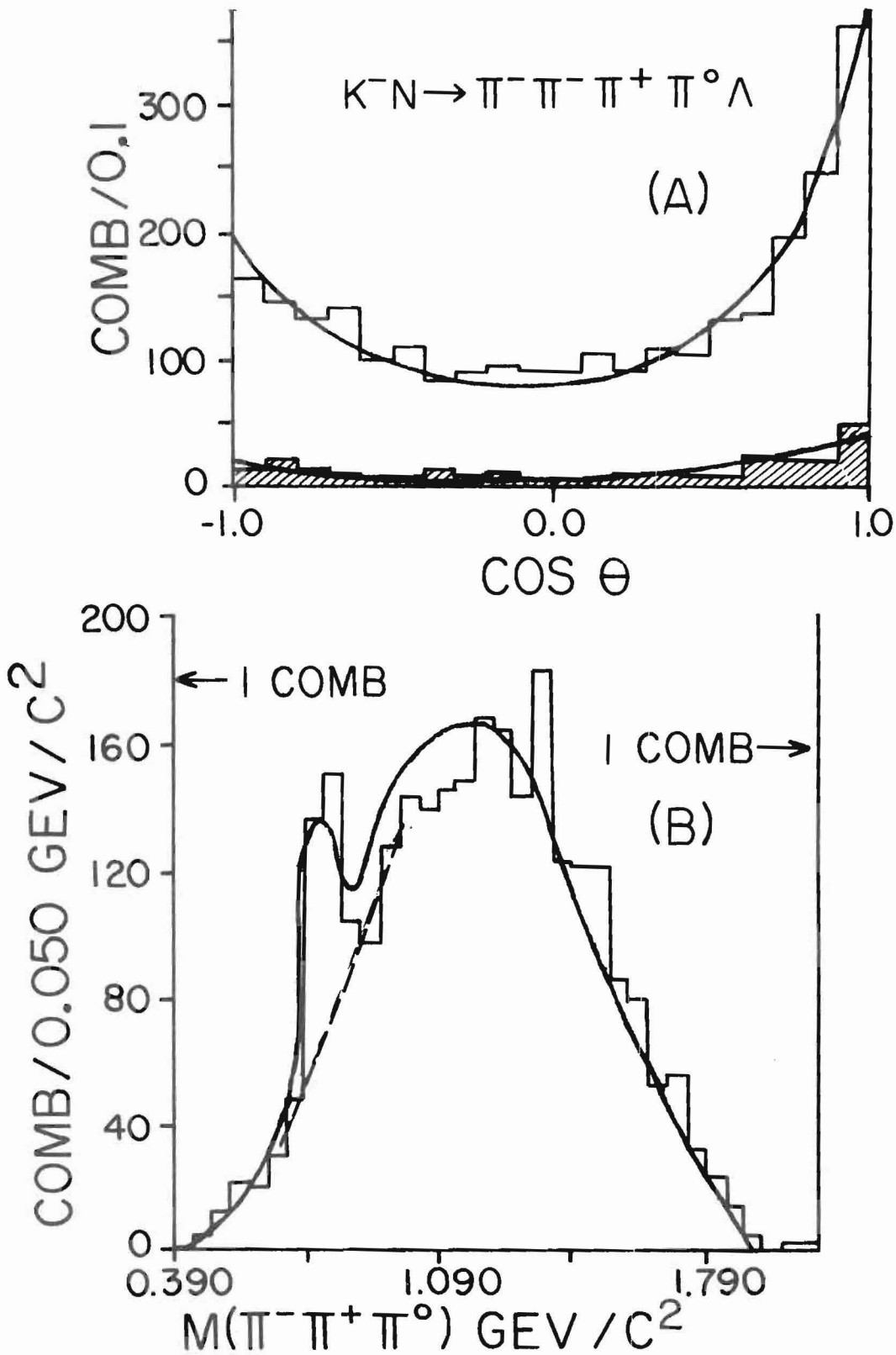
K⁻N → π⁻π⁻π⁺π°Λ
(A)
COMB/0.1
300
200
100
0
-1.0
0.0
1.0
COS θ
200
160
120
80
40
0
← 1 COMB
1 COMB →
(B)
COMB/0.050 GEV/C²
0.390
1.090
1.790
M(π⁻π⁺π°) GEV/C²

per unit mass between the Regions from [.615 to .715] and [.915 to 1.065] GeV/c^2. Figure 32(A) shows the center of mass production angular distribution for the $\pi^-\pi^+\pi^\circ$ combinations. The cross-hatched portion represents those events in the region of the $\omega^\circ(784)$. The CLA model shows qualitative agreement with the data for the mass and angular distributions.

Figure 33 shows the 4π uncut mass distribution for Reaction (I-3). There is an indication of some $B^-(1235)$ resonance here. This resonance was not included in the model. Essentially 100 per cent[26] of any $B^-(1235)$ produced would decay to $\omega^\circ(784)\pi^-$. Therefore, if any $B^-(1235)$ resonance was produced in Reaction (I-3) the background under it should be reduced by demanding the presence of $\omega^\circ(784)$. This was done by plotting only 4π mass combinations which had a $\pi^-\pi^+\pi^\circ$ mass combination in the interval from 0.740 to 0.840 GeV/c^2. The resulting mass distribution is shown in Figure 34(B) and the $B^-(1235)$ is clearly evident. To estimate the amount of $B^-(1235)$ resonance which was present the CLA model was used to give the shape of the background since it does so correctly on both sides of the resonance. The $B^-(1235)$ is an established resonance but has only recently been observed in a K^- nucleon interaction for the first time.[27] This was Reaction (I-3) at 3 GeV/c.

We have searched the data of all three reactions for final states containing more than one resonance by cutting in turn on each resonance given in Tables 1 and 2 and plotting all the possible particle mass distributions. The CLA model was used to estimate the background. We found no compelling evidence for the simultaneous production of two or more resonances either with or without the sharing of particles nor for the production of resonances that decayed to daughter resonances

Figure 33.--The mass distribution of the particle combination $\pi^-\pi^-\pi^+\pi^\circ$ for Reaction (I-3).

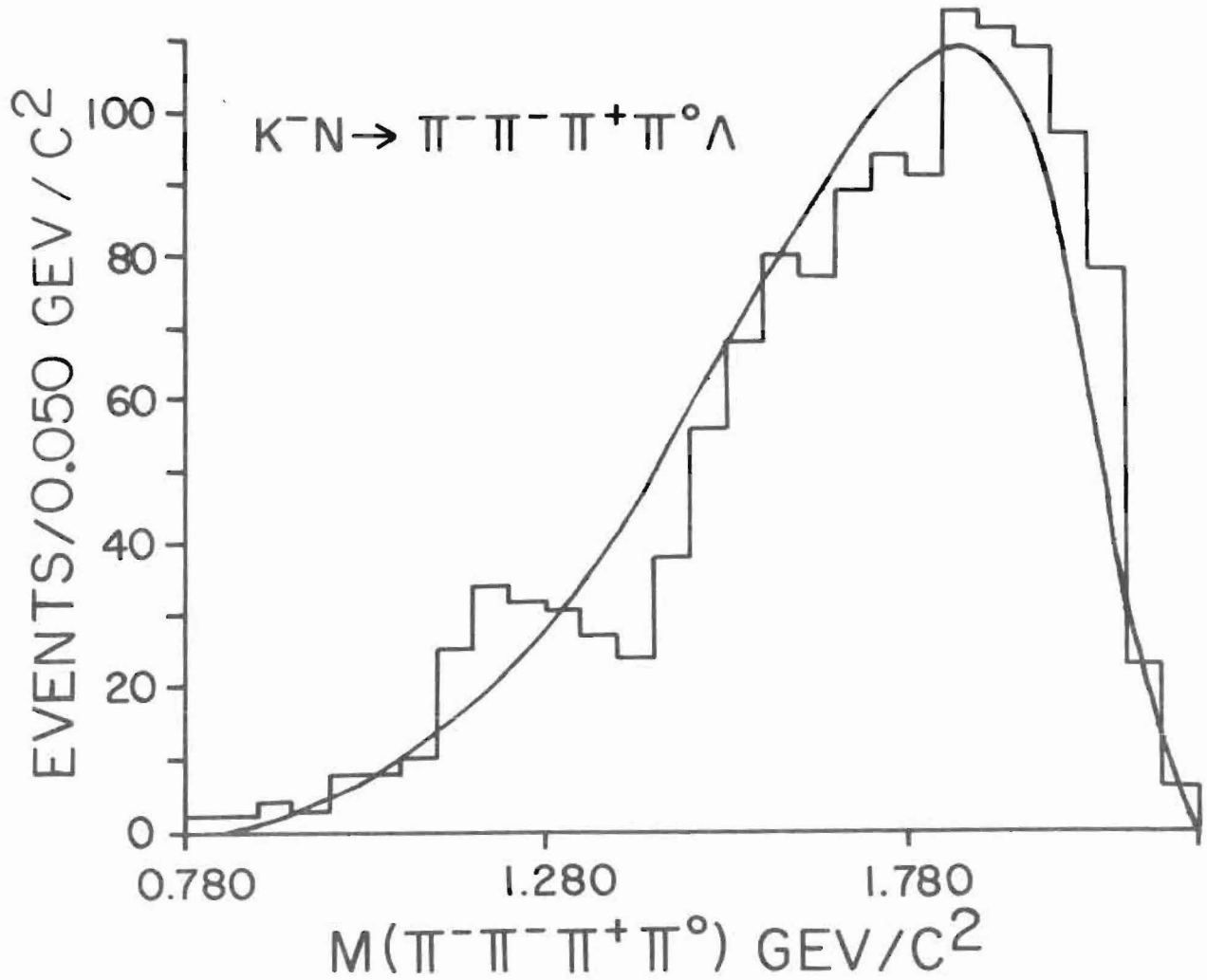
$K^-N \rightarrow \pi^-\pi^-\pi^+\pi^\circ\Lambda$
EVENTS/0.050 GEV / C^2
0
20
40
60
80
100
0.780
1.280
1.780
$M(\pi^-\pi^-\pi^+\pi^\circ)$ GEV/C^2

Figure 34.--For the 267 events obtained for the reaction $K^-N \rightarrow \omega^\circ(784)\pi^-\Lambda$ by requiring $M(\pi^-\pi^+\pi^\circ)$ to be in the interval [0.740 to 0.840] GeV/c^2 (A) gives the center of mass production angular distribution where the cross-hatched area corresponds to 76 events obtained by requiring $M(\pi^-\pi^-\pi^+\pi^\circ)$ to be in the interval [1.130, 1.330] GeV/c^2. (B) gives the distribution in $M(\pi^-\pi^-\pi^+\pi^\circ)$.

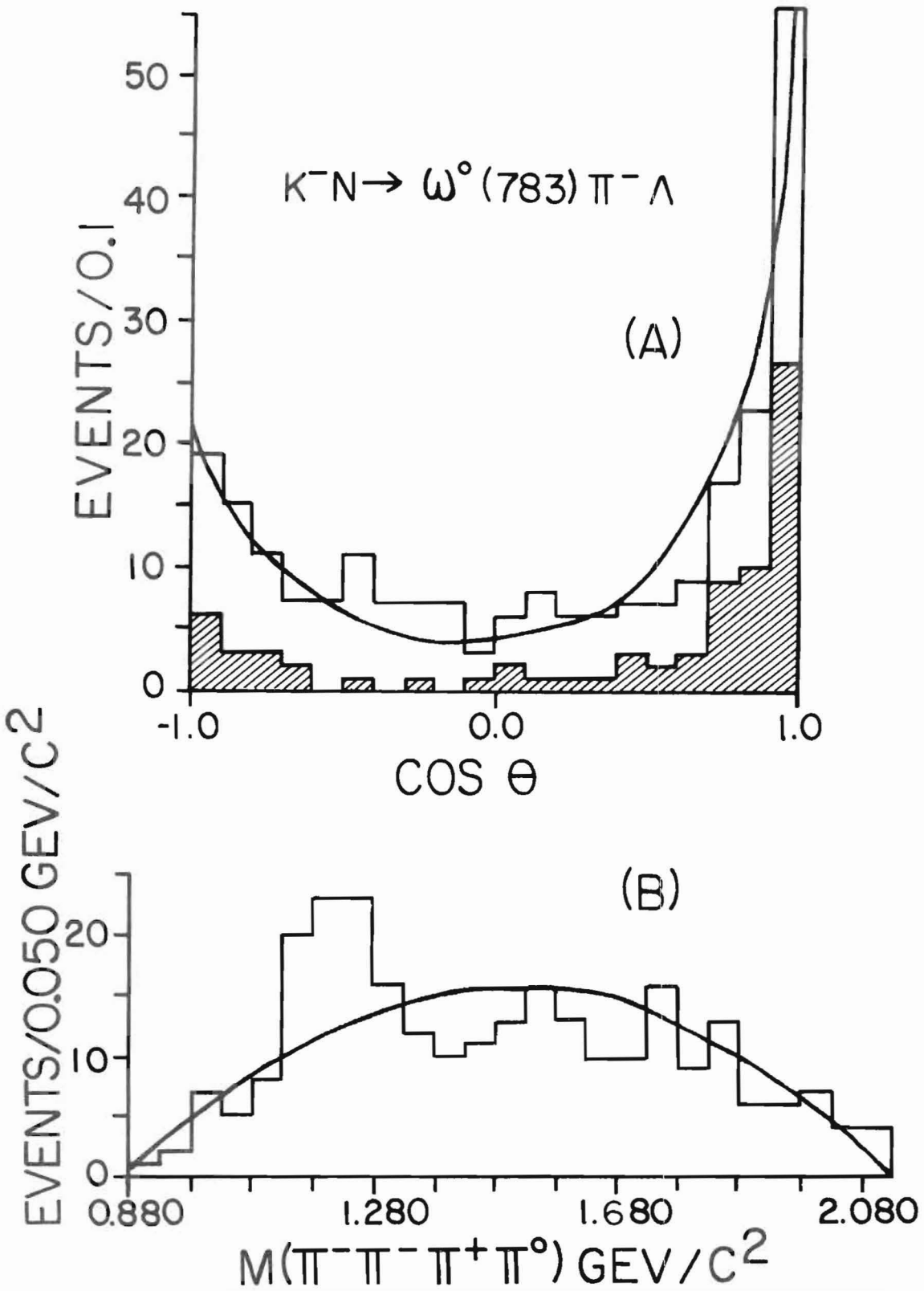
K⁻N→ ω°(783) π⁻ Λ
(A)
EVENTS/0.1
50
40
30
20
10
0
-1.0
0.0
1.0
COS θ
(B)
EVENTS/0.050 GEV/C²
20
10
0
0.880
1.280
1.680
2.080
M(π⁻π⁻π⁺π°) GEV/C²

except for the $B^-(1235)$.

For each resonance produced in each reaction Tables 1 and 2 show the number of events, the percentage contribution to the reaction, and the cross-section. We have already stated our method for obtaining the number of events for each resonance. In computing the cross-sections use was made of our cross-section per event, which is (0.220 ± 0.033) μbarns per event. Our method of obtaining this number is given in the Appendix. We applied a correction factor of 1.057 to take into account the fact that we discarded events having stopping protons with momenta larger than .275 GeV/c. An additional correction factor of 1.089 was used to take into account hiding in the deuteron.[6,7] The cross-sections shown do not include corrections for the other decay modes of the resonances. However, they are corrected by the factor 1.53 to take into account the neutral decay mode of the lambda. They are also corrected for the chi-squared probability cuts at one per cent. The cross-sections for Reaction (I-1) were found by normalizing to the number of events having a baryon missing mass less than the lambda mass. For Reaction (I-2) the cross-sections were found by normalizing to the number of events having $F_2 \leq |0.90|$. For Reaction (I-3) the cross-sections were found by normalizing to the number of events having $F_3 < 0.0$.

Figure 35 shows the production angular distributions for the $Y^{*\pm}(1385)$ and $\rho^\circ(765)$ produced in Reaction (I-1) and Figure 36 shows them for the $Y^{*-0}(1385)$ and $\rho^\circ(765)$ produced in Reaction (I-3). This distribution for the $B^-(1235)$ and for those $\omega^\circ(784)$ not resulting from B^- decay are shown in Figure 37. The background under each resonance was subtracted in order to obtain these.

TABLE 1

NUMBER OF EVENTS, PERCENTAGE CONTRIBUTIONS AND CROSS-SECTIONS FOR RESONANT AND NON-RESONANT EVENTS OBSERVED IN REACTIONS (I-1) AND (I-2)

Reaction	Events	%	Cross-Section (μbarns)
$K^-N \to Y^{*-}(1385)\pi^+\pi^-$, $Y^{*-} \to \pi^-\Lambda$	92 ± 24	19	34 ± 10
$\to Y^{*+}(1385)\pi^-\pi^-$, $Y^{*+} \to \pi^+\Lambda$	61 ± 15	13	23 ± 7
$\to \rho^\circ(765)\pi^-\Lambda$, $\rho^\circ \to \pi^-\pi^+$	197 ± 24	41	74 ± 14
$\to f^\circ(1260)\pi^-\Lambda$, $f^\circ \to \pi^-\pi^+$	69 ± 16	14	26 ± 7
$\to \pi^-\pi^-\pi^+\Lambda$	61 ± 46	13	23 ± 18
TOTALS	480 ± 22	100	180 ± 30
$K^-N \to \rho^\circ(765)\pi^-\Sigma^\circ$, $\rho^\circ \to \pi^-\pi^+$	78 ± 16	39	35 ± 9
$\to \pi^-\pi^-\pi^+\Sigma^\circ$	122 ± 17	61	55 ± 11
TOTALS	200 ± 14	100	90 ± 16

TABLE 2

NUMBER OF EVENTS, PERCENTAGE CONTRIBUTIONS, AND CROSS-SECTIONS FOR RESONANT AND NON-RESONANT EVENTS OBSERVED IN REACTION (I-3)

Reaction	Events	%	Cross-Section (μbarns)
$K^-N \rightarrow Y^{*-}(1385)\pi^-\pi^+\pi^\circ$ $\hookrightarrow \pi^-\Lambda$	273 ± 29	20	115 ± 21
$\rightarrow Y^{*+}(1385)\pi^-\pi^-\pi^\circ$ $\hookrightarrow \pi^+\Lambda$	22 ± 19	1.6	9 ± 8
$\rightarrow Y^{*\circ}(1385)\pi^-\pi^-\pi^+$ $\hookrightarrow \pi^\circ\Lambda$	77 ± 22	5.7	32 ± 10
$\rightarrow \Sigma^\circ(1750)\pi^-\pi^-\pi^+$ $\hookrightarrow \Lambda^\circ\pi^\circ$	81 ± 17	6.0	34 ± 9
$\rightarrow \rho^\circ(765)\pi^-\pi^\circ\Lambda$ $\hookrightarrow \pi^-\pi^+$	237 ± 37	18	100 ± 22
$\rightarrow \rho^-(765)\pi^-\pi^+\Lambda$ $\hookrightarrow \pi^-\pi^\circ$	204 ± 37	15	86 ± 20
$\rightarrow \rho^+(765)\pi^-\pi^-\Lambda$ $\hookrightarrow \pi^+\pi^\circ$	20 ± 24	1.5	9 ± 11
$\rightarrow \omega^\circ(784)\pi^-\Lambda$ $\hookrightarrow \pi^-\pi^+\pi^\circ$	89 ± 21	6.6	37 ± 10 *
$\rightarrow B^-(1235)\Lambda$ $\hookrightarrow \omega^\circ(784)\pi^-$ $\hookrightarrow \pi^-\pi^+\pi^\circ$	62 ± 15	4.6	26 ± 7
$\rightarrow \pi^-\pi^-\pi^+\pi^\circ\Lambda$	282 ± 84	21	119 ± 40
TOTALS	1347 ± 37	100	567 ± 88

* These values do not include $\omega^\circ(784)$ resulting from $B^-(1235)$ decay.

Figure 35.--For Reaction (I-1) the center of mass production angular distributions where background has been subtracted for (A) $Y^{*-}(1385)$ with 71 events, (B) $Y^{*+}(1385)$ with 44 events and (C) $\rho^{\circ}(765)$ with 101 events.

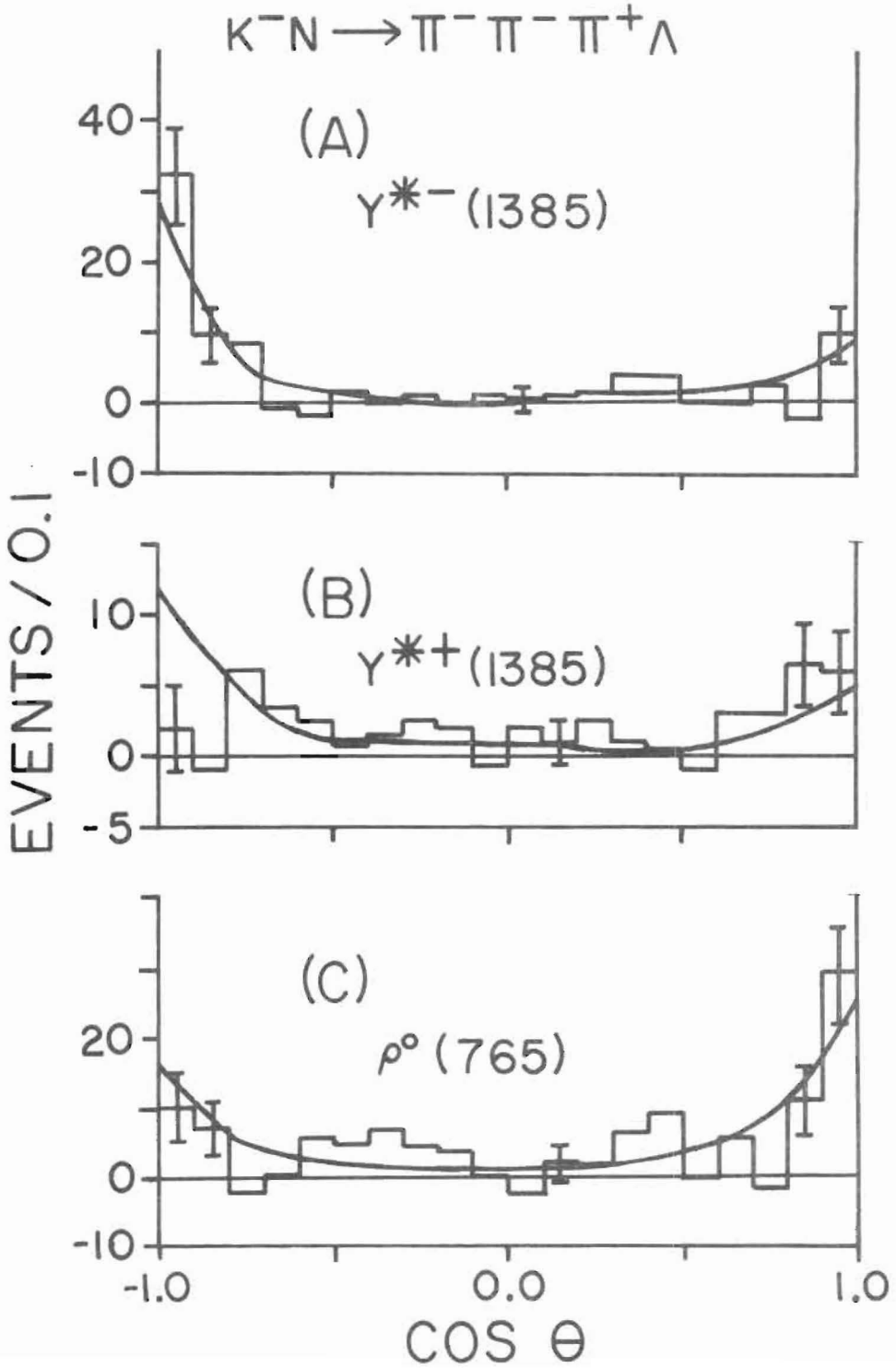
K⁻N → π⁻π⁻π⁺Λ
(A)
Y*⁻(1385)
(B)
Y*⁺(1385)
(C)
ρ°(765)
EVENTS / 0.1
40
20
0
-10
10
0
-5
20
0
-10
-1.0
0.0
1.0
COS θ

Figure 36.--For Reaction (I-3) the center of mass production angular distributions where background has been subtracted for (A) $Y^{*-}(1385)$ with 188 events, (B) $Y^{*\circ}(1385)$ with 50 events, and (C) $\rho^{\circ}(765)$ with 128 events.

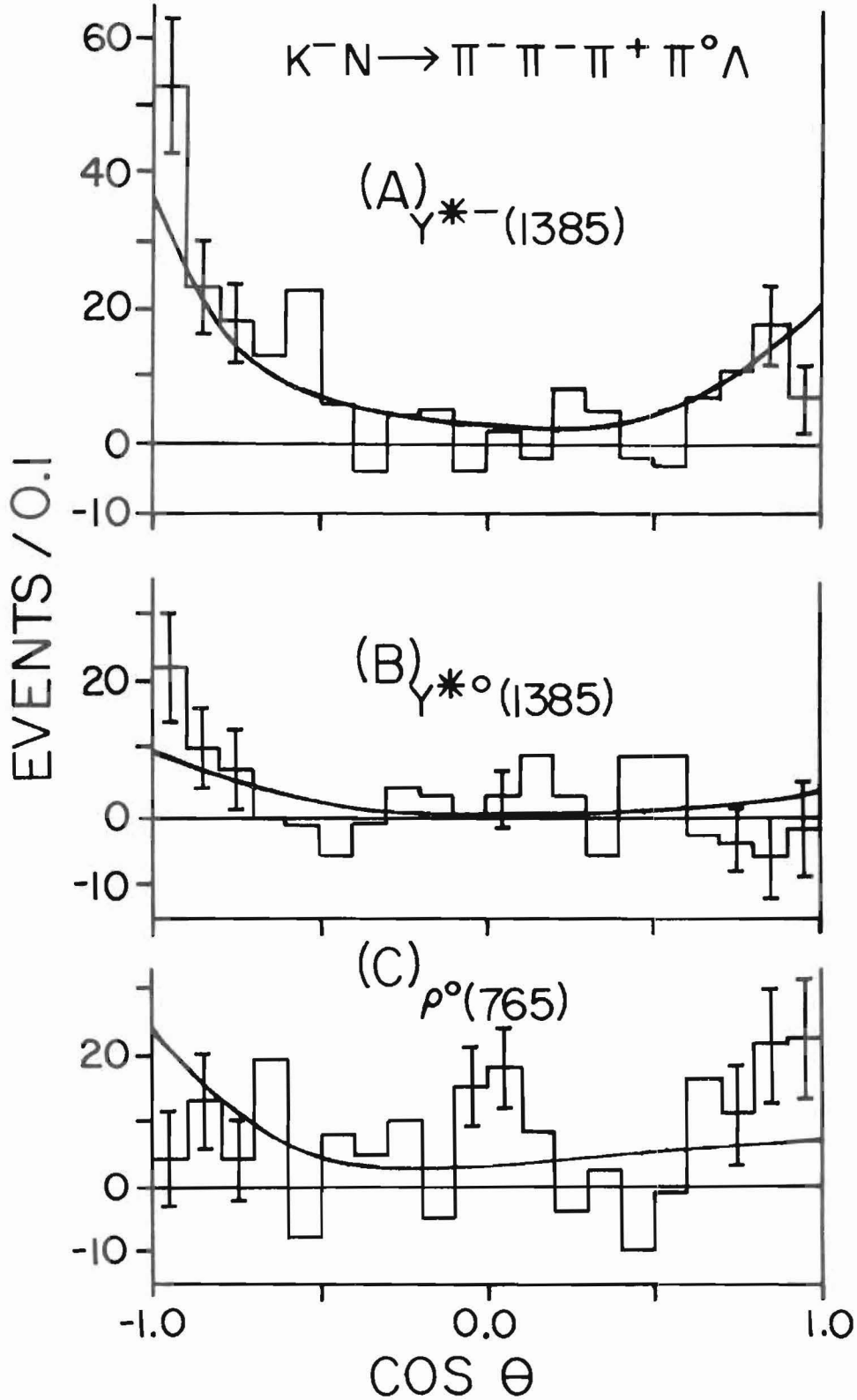
K⁻N → π⁻π⁻π⁺π°Λ
(A) Y*⁻(1385)
(B) Y*°(1385)
(C) ρ°(765)
EVENTS / 0.1
60
40
20
0
-10
20
0
-10
20
0
-10
-1.0
0.0
1.0
COS θ

Figure 37.--For Reaction (I-3) the center of mass production angular distributions where background has been subtracted for (A) $B^-(1235)$ with 40 events and (B) $\omega^\circ(784)$ with 62 events.

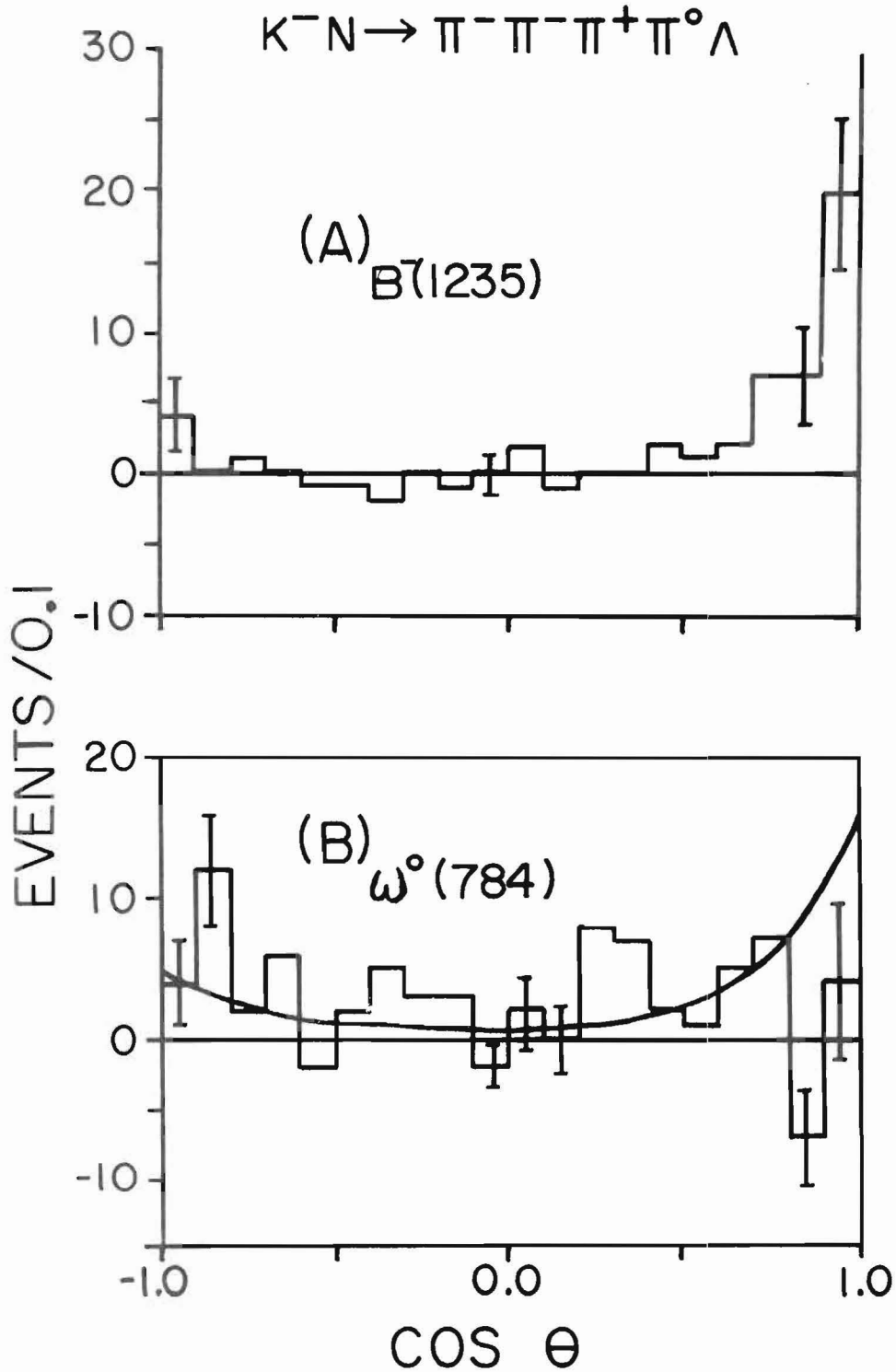
K⁻N → π⁻π⁻π⁺π°Λ
(A) B(1235)
(B) ω°(784)
EVENTS /0.1
30
20
10
0
-10
20
10
0
-10
-1.0
0.0
1.0
COS θ

The production angular distribution for the events of Reaction (I-1) in the mass region of the $f^{\circ}(1260)$ is shown in Figure 38, for $\rho^{\circ}(765)$ of Reaction (I-2) in Figure 23(A), for $\rho^{-}(765)$ in Figure 30(A), and for $\Sigma^{\circ}(1750)$ in Figure 39. For each of these four cases, the angular distribution has the same shape for the events of the resonance and control regions. In fact the chi-squared probabilities obtained when comparing them were never smaller than 50 per cent. Therefore these are presented without a background subtraction.

We have looked for peaking in the production angular distributions of our resonances. The results are summarized in Table 3. Even in those cases where the background and control regions had the same angular distributions, we carried out a background subtraction before drawing conclusions. This is why the events in the mass region of the ρ^{-} show a forward peak, but we cannot detect a peak for the resonance itself. The signal-to-background ratio in this case is only 0.3. In those cases where peaking was detected the $Y^{*}(1385)$ peak in the backward direction and the meson resonances peak in the forward direction.

We searched for alignment in the Jackson[28] and helicity frames for those resonances produced with yields greater than 100 events in a given reaction. The helicity frame is defined in analogy to the Jackson frame, but with its polar axis parallel to the direction of motion of the resonance. We found no compelling evidence for alignment.

We looked for polarization of the Λ° along the normal to its production plane for Reactions (I-1) and (I-3). We found no compelling evidence for such polarization at any Λ° production angle or in the average over production angle. We also cut on the invariant mass regions

Figure 38.--For Reaction (I-1) the center of mass production angular distribution for the 141 events obtained by demanding $M(\pi^-\pi^+)$ in the mass interval [1.092, 1.417] GeV/c^2.

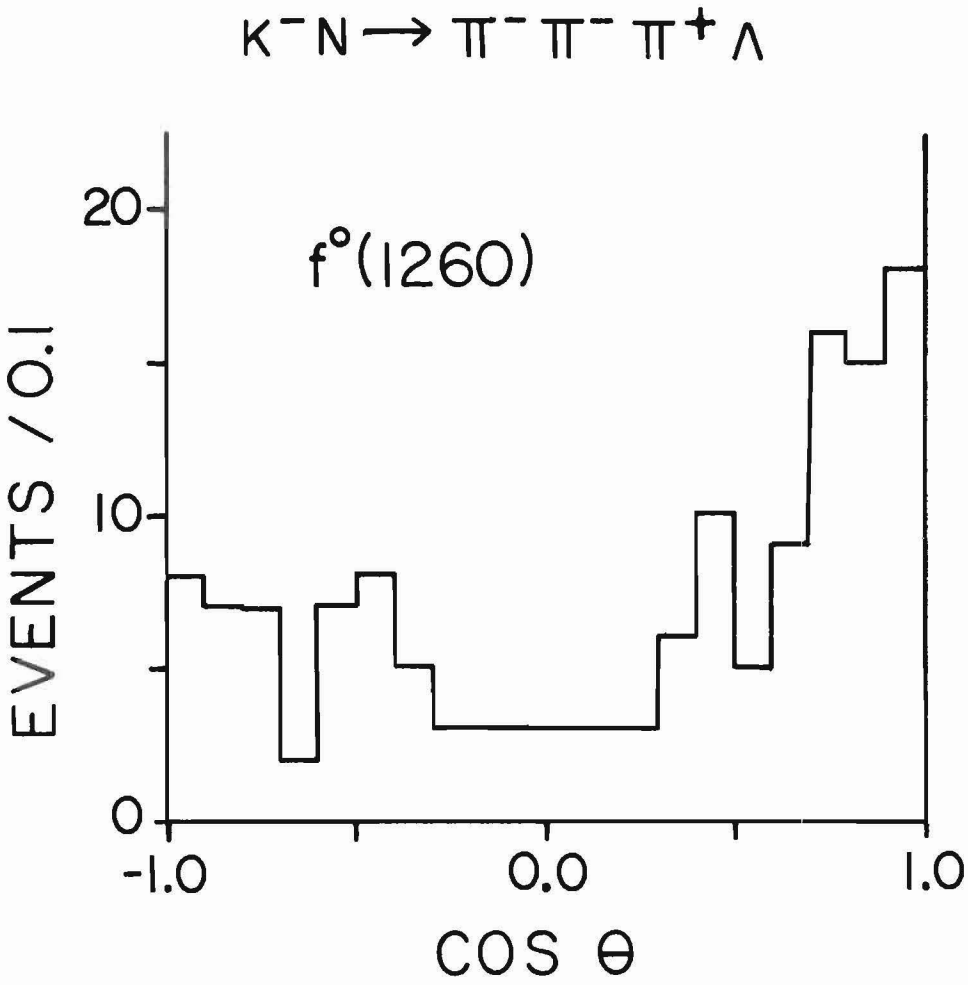
$K^- N \rightarrow \pi^- \pi^- \pi^+ \Lambda$
$f^0(1260)$
EVENTS / 0.1
20
10
0
-1.0
0.0
1.0
COS θ

Figure 39.--For Reaction (I-3) the center of mass production angular distribution for the 178 events obtained by demanding $M(\Lambda\pi^{\circ})$ in the mass interval [1.725, 1.825] GeV/c^2.

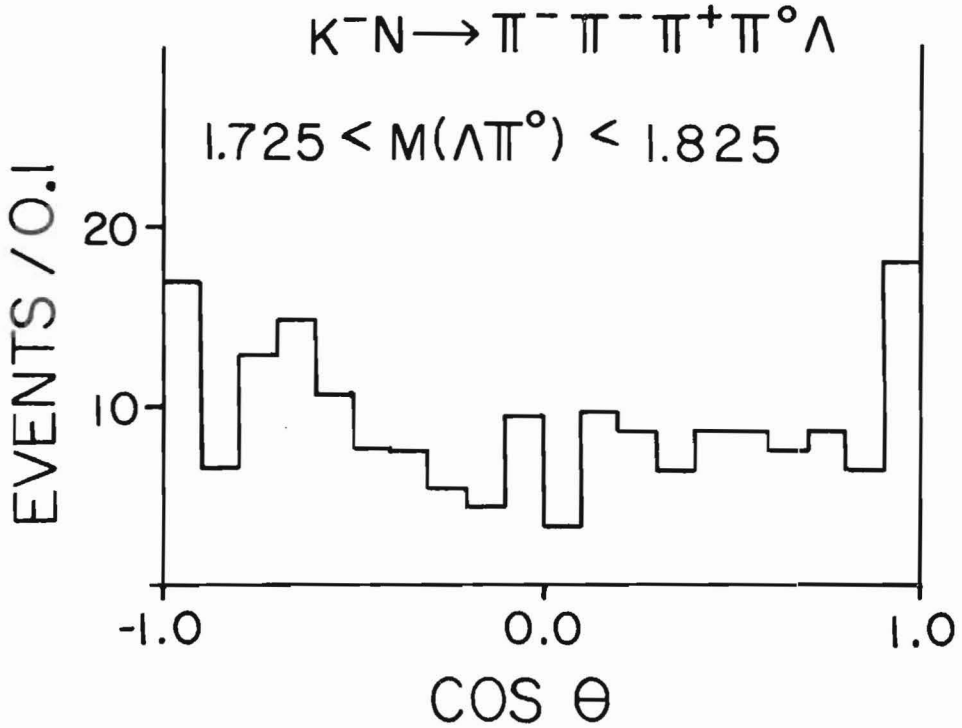
$K^-N \longrightarrow \pi^-\pi^-\pi^+\pi^0\Lambda$
$1.725 < M(\Lambda\pi^0) < 1.825$
EVENTS /0.1
20
10
-1.0
0.0
1.0
COS θ

TABLE 3

DESCRIPTION OF PEAKING IN RESONANCE PRODUCTION ANGULAR DISTRIBUTIONS, SIGNAL TO BACKGROUND RATIOS, AND MASS CUTS FOR RESONANCES AND CONTROL REGIONS

Reaction	Resonance	Mass Regions (GeV/c^2) Resonance Cut	Control Cuts	Signal/Background	Peaking
(I-1)	Y^{*-}(1385)	(1.342,1.442)	(1.255,1.315) (1.455,1.605)	1.2	Backward
(I-1)	Y^{*+}(1385)	(1.342,1.442)	(1.255,1.315) (1.455,1.605)	1.5	None Discernable
(I-1)	ρ°(765)	(.667,.867)	(.430,.630) (.900,1.100)	0.9	Forward
(I-1)	f°(1260)	(1.092,1.417)	(.890,1.092) (1.417,1.617)	0.5	Forward
(I-2)	ρ°(765)	(.667,.867)	(.430,.630) (.900,1.100)	0.8	Forward
(I-3)	Y^{*-}(1385)	(1.342,1.442)	(1.255,1.315) (1.455,1.605)	0.7	Backward
(I-3)	$Y^{*\circ}$(1385)	(1.300,1.450)	(1.250,1.287) (1.500,1.650)	0.2	Perhaps Backward
(I-3)	Σ°(1750)	(1.725,1.825)	(1.475,1.675) (1.875,2.075)	.4	None Discernable

TABLE 3--Continued

Reaction	Resonance	Mass Regions (GeV/c^2) Resonance Cut	Control Cuts	Signal/Background	Peaking
(I-3)	$\rho^\circ(765)$	(.680,.880)	(.430,.630) (.900,1.100)	0.3	Perhaps Forward
(I-3)	$\rho^-(765)$	(.675,.875)	(.430,.630) (.900,1.100)	0.3	None Discernable
(I-3)	$B^-(1235)$	(1.130,1.330)	(.880,1.055) (1.405,1.705)	1.3	Forward
(I-3)	$\omega^\circ(784)$	(.740,.840)	(.615,.715) (.890,1.015)	.8	None Discernable

of those resonances with yields greater than 100 events and in each case looked for Λ° polarization averaged over production angle. None was found.

B. Single Particle Distributions

We use the single particle distributions in the K^- neutron center of mass for the variables cos θ, P_T and P_L to test the CLA model. The quantity θ is the angle of production of the single particle with respect to the incident K^- direction. The quantity P_T is its component of momentum perpendicular to the beam direction and is called the transverse momentum. The quantity P_L is called the longitudinal momentum and is the component in the K^- direction. Of course cos θ is not independent of P_T and P_L. The distributions in these variables for the single particles of the three reactions are shown in Figures 40 to 48. The smooth curves are the results of the CLA model normalized to the data. Figures 42, 45, and 48 give the production angular distributions. The dashed curve represents the results of the CLA model using values of b_i which were the same as originally used by Chan et al.[1] These values gave results that are more peripheral than our data. They also gave results that are more peripheral than the data for $K^-N \rightarrow \pi^-\pi^-P\overline{K}^\circ$, $K^-N \rightarrow \pi^-\pi^-\pi^+N\overline{K}^\circ$, and $K^-N \rightarrow \pi^-\pi^-P\pi^\circ\overline{K}^\circ$ obtained from the same bubble chamber film.[5] We found that multiplying the b_i by 2.0 gave better agreement with the data for the six reactions. We therefore compare our data with the CLA model using the larger b_i.

Table 4 gives the average values and statistical errors for P_T and P_L obtained from both the data and CLA model. The shapes of the distributions show qualitative agreement between the model and data.

Figure 40.--The single particle center of mass longitudinal momentum (P_L) distributions of Reaction (I-1) for (A) Λ, (B) π^-, and (C) π^+.

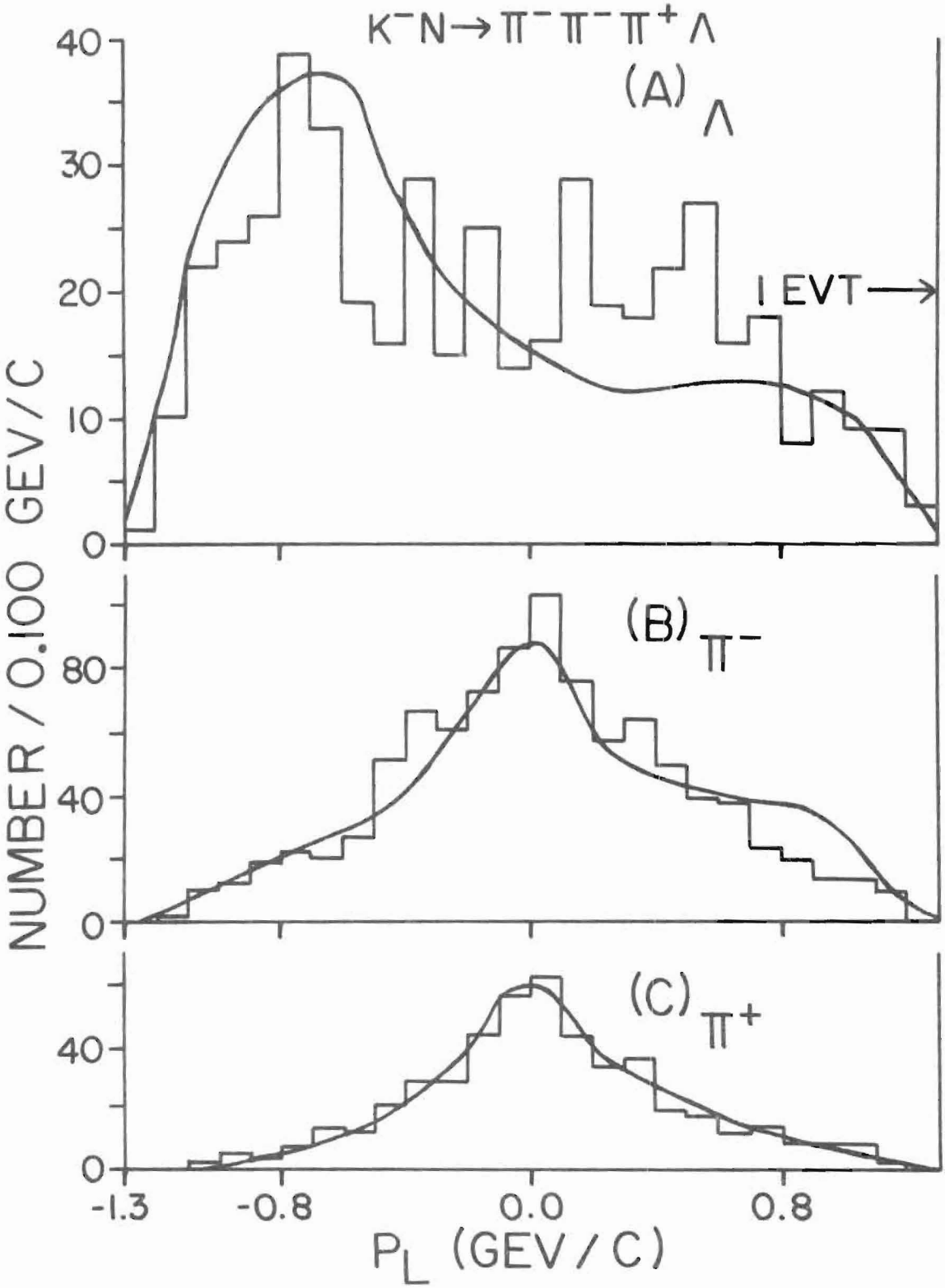
K⁻N→π⁻π⁻π⁺Λ
(A) Λ
1 EVT
(B) π⁻
(C) π⁺
NUMBER / 0.100 GEV/C
40
30
20
10
0
80
40
0
40
0
-1.3
-0.8
0.0
0.8
P_L (GEV/C)

Figure 41.--The single particle center of mass transverse momentum (P_T) distributions of Reaction (I-1) for (A) Λ, (B) π^- and (C) π^+.

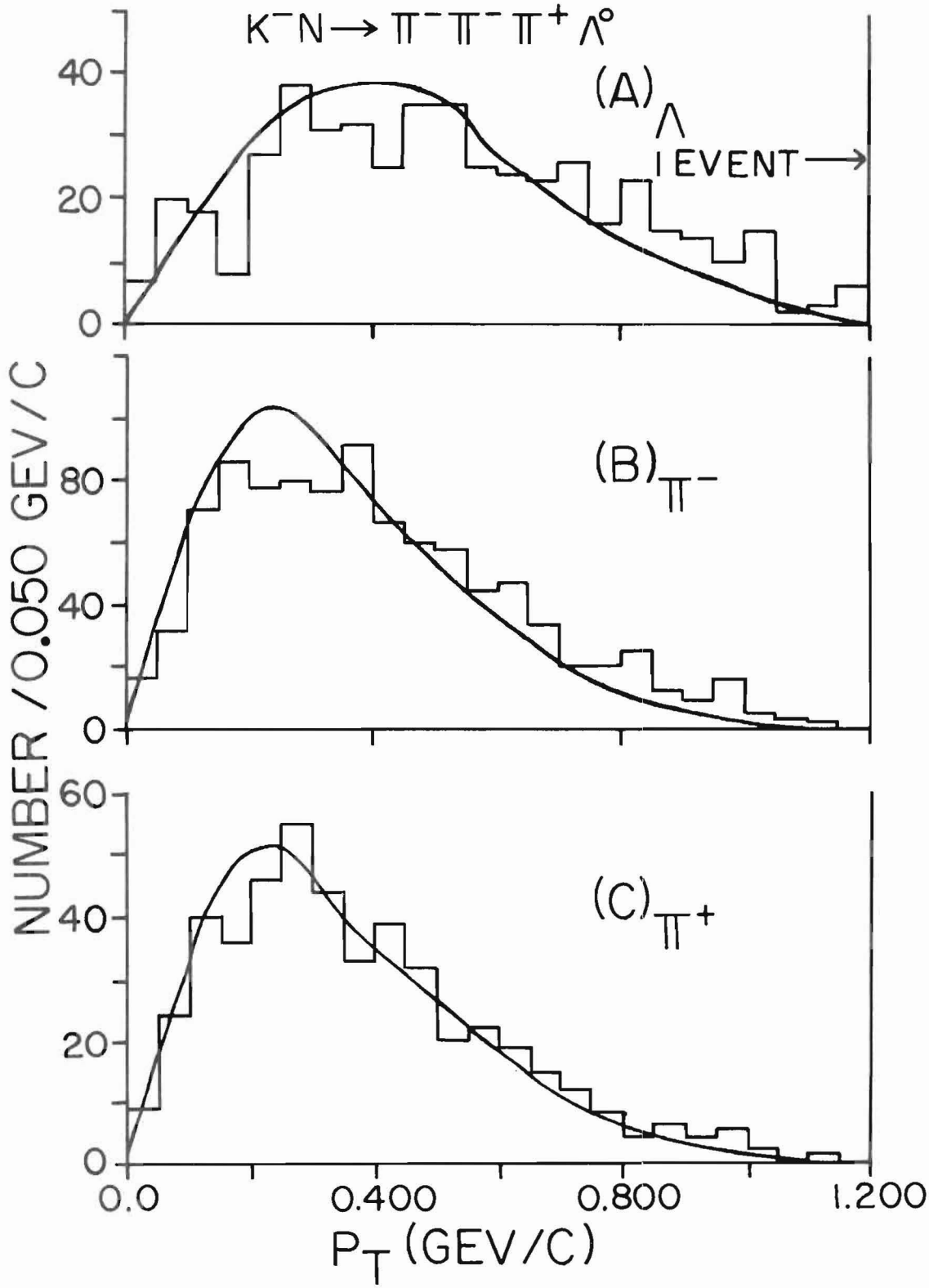
K⁻N → π⁻π⁻π⁺Λ°
(A)
1 EVENT
(B) π⁻
(C) π⁺
NUMBER /0.050 GEV/C
0
20
40
60
80
0.0
0.400
0.800
1.200
P_T (GEV/C)

Figure 42.--The single particle center of mass production angular distributions of Reaction (I-1) for (A) Λ, (B) π^-, and (C) π^+, where dashed lines give the CLA model results when we use values for b_i that are 0.5 times the ones we regularly used.

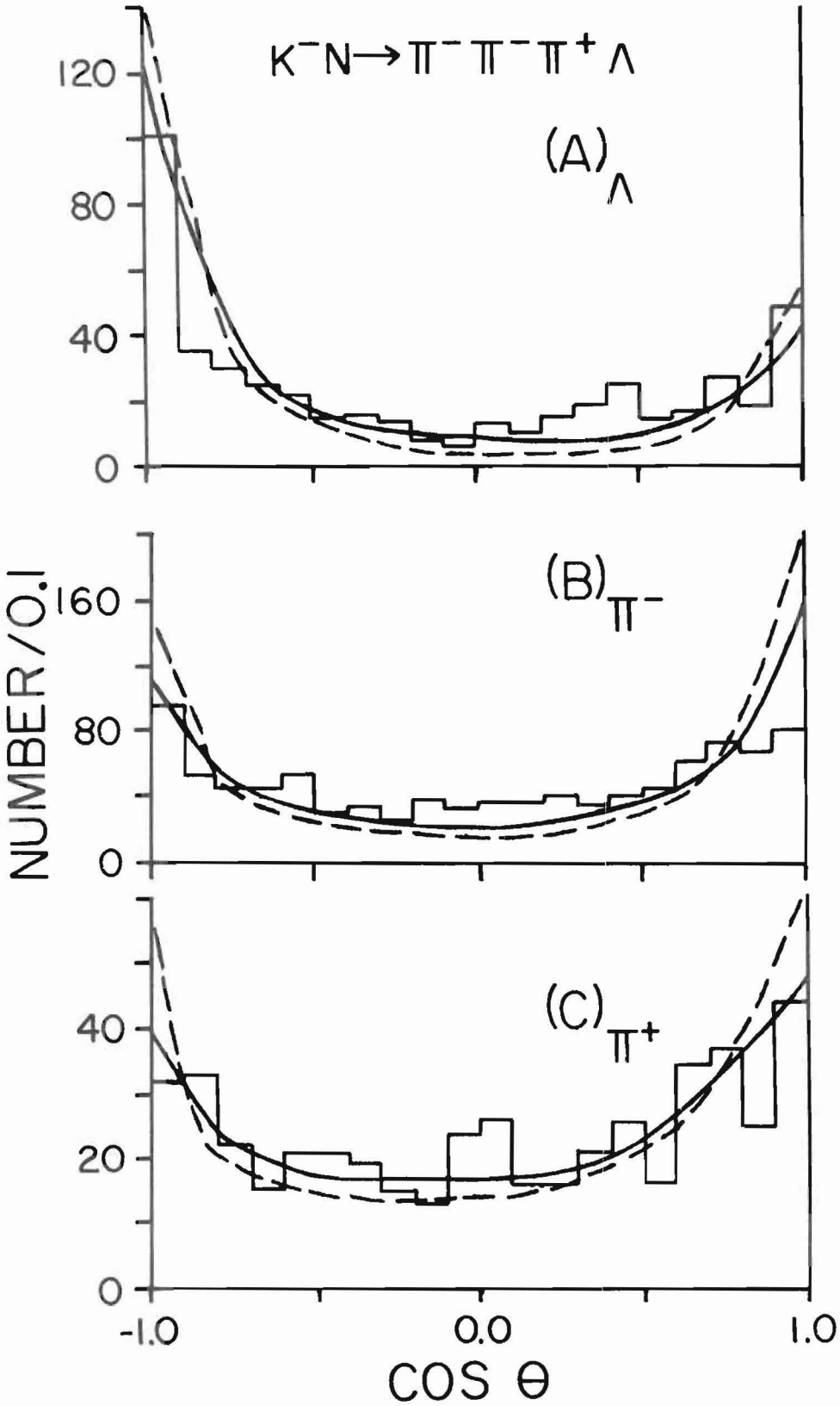
K⁻N→π⁻π⁻π⁺Λ
(A)Λ
(B)π⁻
(C)π⁺
NUMBER/0.1
120
80
40
0
160
80
0
40
20
0
-1.0
0.0
1.0
COS θ

Figure 43.--The single particle center of mass longitudinal momentum distributions of Reaction (I-2) for (A) Σ°, (B) π^{-}, and (C) π^{+}.

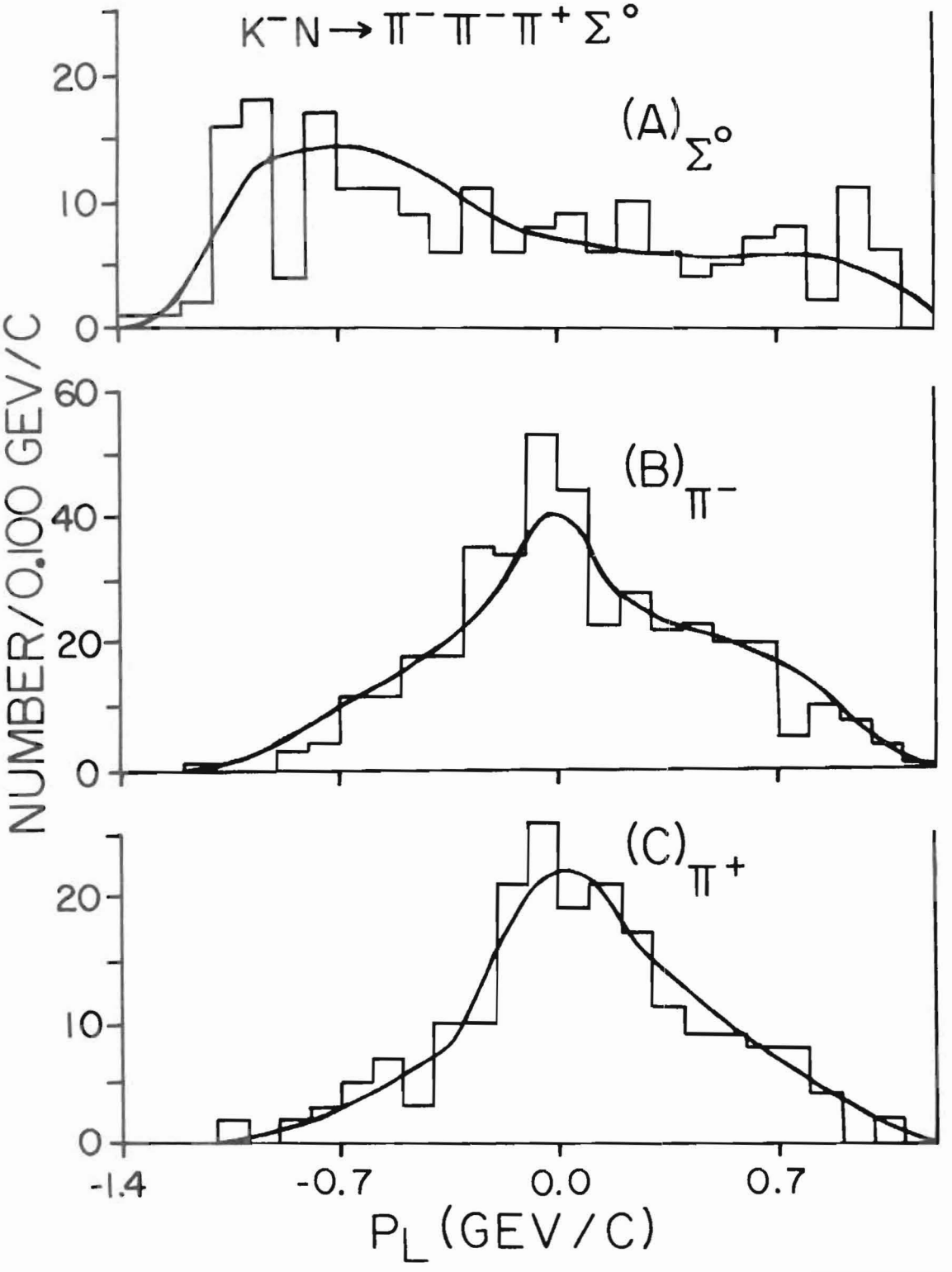
K⁻N → π⁻π⁻π⁺Σ°
(A) Σ°
(B) π⁻
(C) π⁺
NUMBER/0.100 GEV/C
20
10
0
60
40
20
0
20
10
0
-1.4
-0.7
0.0
0.7
P_L (GEV/C)

Figure 44.--The single particle center of mass transverse momentum distributions of Reaction (I-2) for (A) Σ°, (B) π^{-}, and (C) π^{+}.

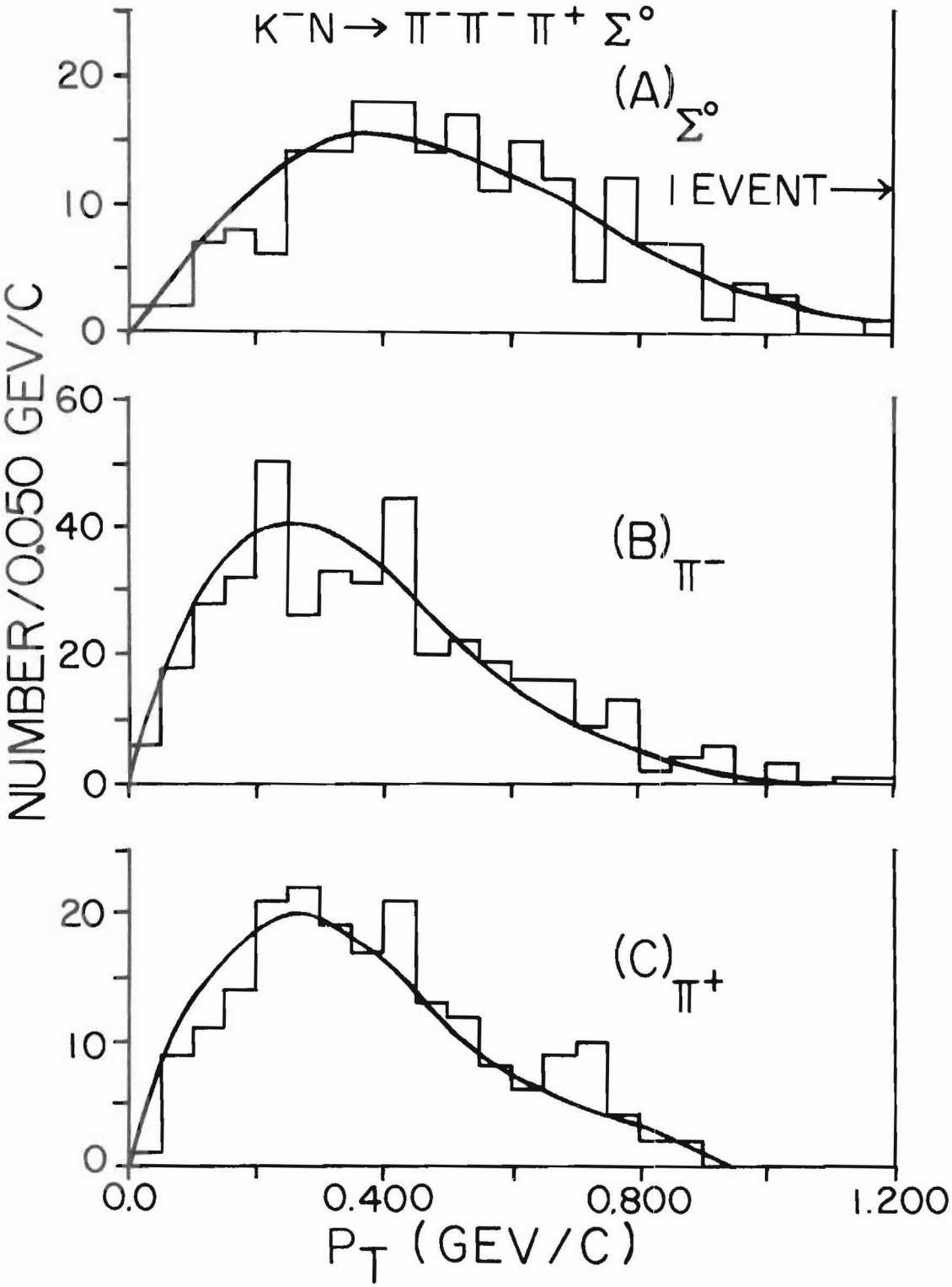
K⁻N → π⁻π⁻π⁺ Σ°
(A) Σ°
1 EVENT →
(B) π⁻
(C) π⁺
NUMBER/0.050 GEV/C
0
10
20
40
60
0.0
0.400
0.800
1.200
P_T (GEV/C)

Figure 45.--The single particle center of mass production angular distributions of Reaction (I-2) for (A) Σ°, (B) π^{-}, and (C) π^{+}. The dashed lines give the CLA model results when we use values for b_i that are 0.5 times the ones we regularly used.

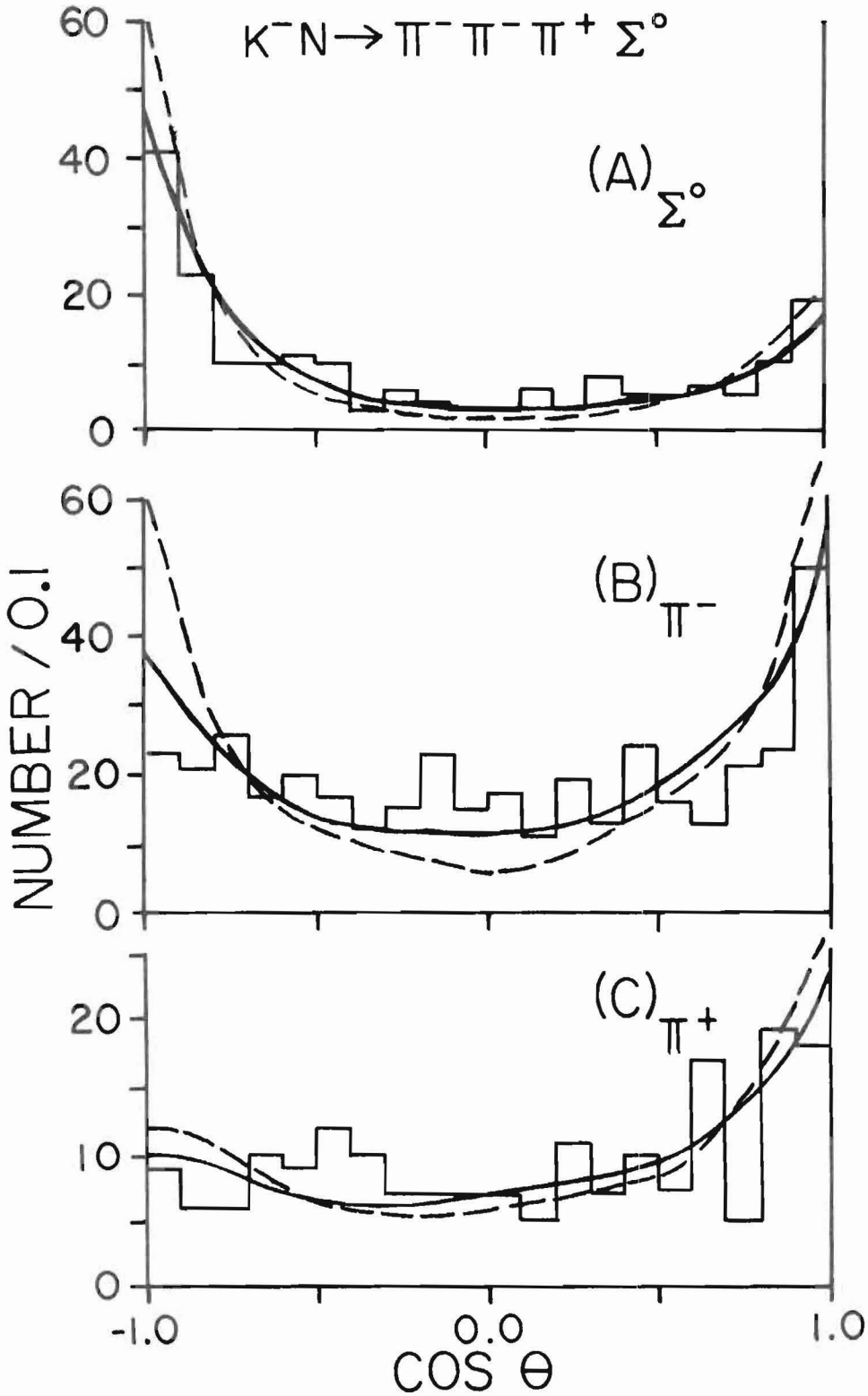
$K^- N \rightarrow \pi^- \pi^- \pi^+ \Sigma^0$
(A) Σ^0
(B) π^-
(C) π^+
NUMBER / 0.1
60
40
20
0
60
40
20
0
20
10
0
-1.0
0.0
1.0
COS θ

Figure 46.--The single particle center of mass longitudinal momentum distributions of Reaction (I-3) for (A) Λ, (B) π^-, (C) π°, and (D) π^+.

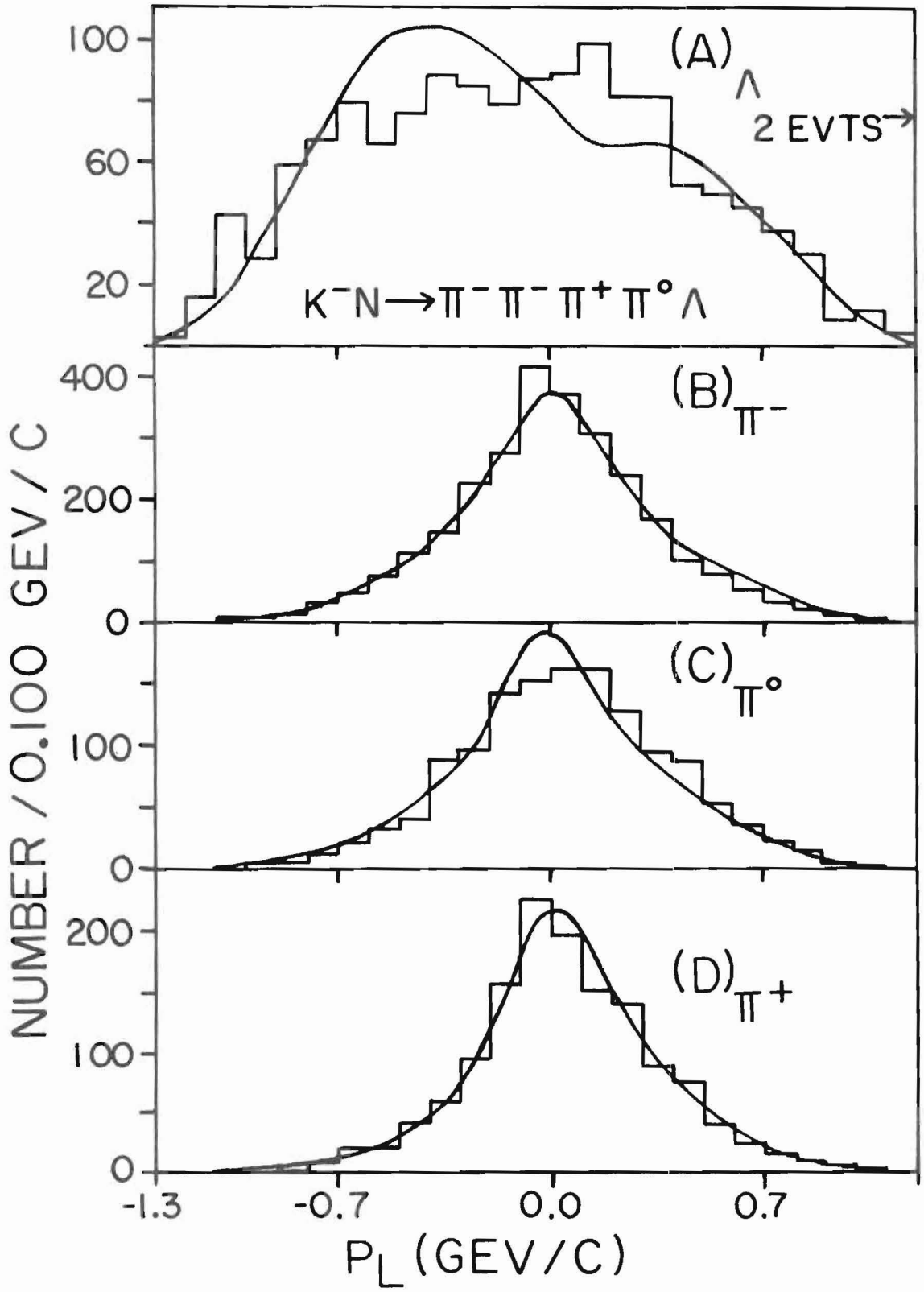
(A)
Λ
2 EVTS
K⁻N → π⁻ π⁻ π⁺ π° Λ
(B) π⁻
(C) π°
(D) π⁺
NUMBER / 0.100 GEV / C
P_L (GEV/C)
-1.3
-0.7
0.0
0.7
100
60
20
400
200
0
100
0
200
100
0

Figure 47.--The single particle center of mass transverse momentum distributions of Reaction (I-3) for (A) Λ, (B) π^-, (C) π°, and (D) π^+.

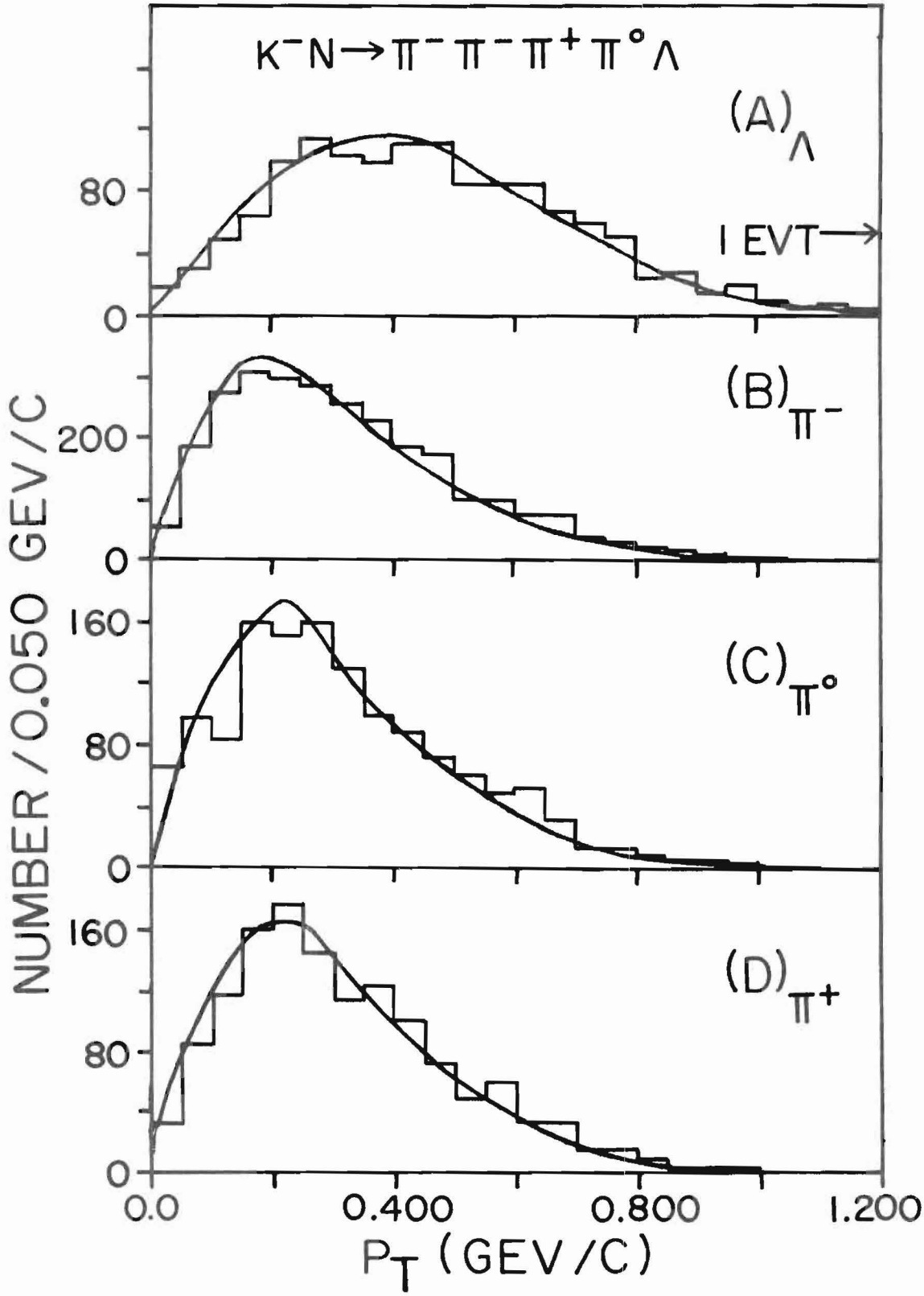
K⁻N→π⁻π⁻π⁺π°Λ
(A)Λ
1 EVT→
(B)π⁻
(C)π°
(D)π⁺
NUMBER /0.050 GEV/C
0
80
200
160
0.0
0.400
0.800
1.200
P_T (GEV/C)

Figure 48.--The single particle center of mass production angular distributions of Reaction (I-3) for (A) Λ, (B) π^-, (C) π°, and (D) π^+ where the dashed lines give the CLA model results when we use values for b_i that are 0.5 times the ones we regularly used.

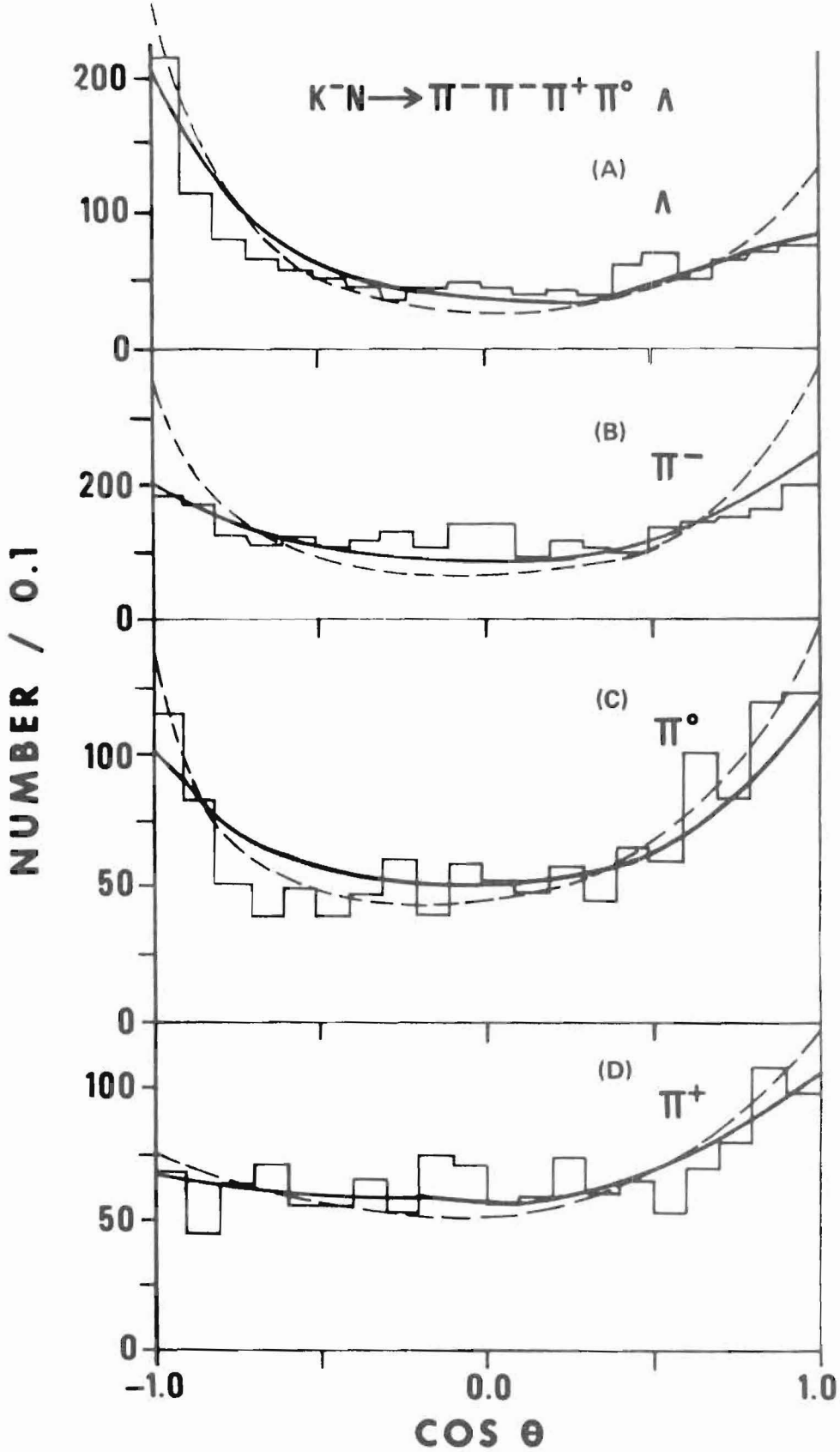
K⁻N → π⁻π⁻π⁺π° Λ
(A)
Λ
(B)
π⁻
(C)
π°
(D)
π⁺
NUMBER / 0.1
200
100
0
200
0
100
50
0
100
50
0
−1.0
0.0
1.0
COS θ

TABLE 4

AVERAGE VALUES AND ERRORS FOR TRANSVERSE (P_T) AND LONGITUDINAL (P_L) MOMENTA OF THE SINGLE PARTICLES IN THE OVERALL CENTER OF MASS AS OBTAINED FROM THE DATA AND GIVEN BY THE CLA MODEL

Reaction	Particle	$P_T \pm \Delta P_T$ (MeV/c)		$P_L \pm \Delta P_L$ (MeV/c)	
		Data	Model	Data	Model
(I-1)	π^-	407 ± 8	353 ± 3	32 ± 16	97 ± 11
	π^+	376 ± 11	355 ± 5	57 ± 20	84 ± 10
	Λ	523 ± 13	471 ± 5	-120 ± 32	-277 ± 15
(I-2)	π^-	393 ± 12	359 ± 2	70 ± 22	72 ± 7
	π^+	387 ± 15	371 ± 3	64 ± 31	98 ± 8
	Σ°	509 ± 18	491 ± 4	-204 ± 50	-242 ± 12
(I-3)	π^-	323 ± 4	307 ± 2	9 ± 7	32 ± 5
	π^+	317 ± 5	305 ± 3	43 ± 9	49 ± 5
	π°	321 ± 6	308 ± 3	56 ± 10	27 ± 6
	Λ	465 ± 7	448 ± 4	-116 ± 16	-140 ± 9

However, quantitatively the model disagrees with the data. This can be seen by comparing the average values for P_L and P_T. The distributions in cos θ also show qualitative agreement between the CLA model and the data. However, there is not quantitative agreement. The chi-squared probability that the CLA model agrees with the data for each single particle cos θ distribution is shown in Table 5.

TABLE 5

CHI-SQUARED PROBABILITY THAT CLA MODEL AGREES WITH DATA FOR SINGLE PARTICLE COS θ DISTRIBUTIONS

Reaction (I-1)		Reaction (I-2)		Reaction (I-3)	
π^-	< 0.01%	π^-	0.03%	π^-	< 0.01%
π^+	43 %	π^+	65 %	π^+	7 %
Λ°	< 0.01%	Σ°	55 %	π°	0.01%
				Λ°	< 0.01%

The reader will also note that the multiparticle production angular distributions we displayed along with our mass plots showed qualitative agreement with the CLA model.

In all three of our reactions the hyperon shows peaking in the backward direction. The nucleon in the reactions $K^-N \rightarrow \pi^-\pi^-P\overline{K}^\circ$, $K^-N \rightarrow \pi^-\pi^-\pi^+N\overline{K}^\circ$, and $K^-N \rightarrow \pi^-\pi^-P\pi^\circ\overline{K}^\circ$ of course also shows strong peaking in the backward direction.[5] The ratio of the number of baryons in the forward hemisphere of the center of mass system to the total number of baryons for each of these six reactions is given in Table 6 for both the data and the CLA model. We observe that the CLA model is correct in

saying that this ratio is larger for the hyperons than for the nucleons although the values it gives for these ratios are quantitatively correct for only two of the six. CLA stress that the Reggeized multiperipheral model explains the fact that this ratio is larger for hyperons than for nucleons in events of the same multiplicity. The diagrams that describe these three reactions with nucleons in the final state contain strangeness zero meson, strange meson, and nucleon exchange where we have listed them in order of decreasing Regge intercepts. But the diagrams that describe

TABLE 6

FRACTION OF BARYONS IN THE FORWARD HEMISPHERE OF THE CENTER OF MASS SYSTEM

	Forward Baryons / Total Baryons	
	Data	CLA Model
$K^-N \to \pi^-\pi^-\pi^+\Lambda^\circ$	0.43 ± 0.02	0.30
$K^-N \to \pi^-\pi^-\pi^+\Sigma^\circ$	0.37 ± 0.03	0.33
$K^-N \to \pi^-\pi^-\pi^+\pi^\circ\Lambda$	0.43 ± 0.01	0.37
$K^-N \to \pi^-\pi^-P\overline{K}^\circ$	0.16 ± 0.02	0.09
$K^-N \to \pi^-\pi^-\pi^+N\overline{K}^\circ$	0.24 ± 0.02	0.13
$K^-N \to \pi^-\pi^-P\pi^\circ\overline{K}^\circ$	0.18 ± 0.02	0.20

our three reactions with hyperons in the final state only contain strange meson and nucleon exchange. Nucleon exchange will play a relatively more important role in ours because strange meson exchange offers

less competition than the exchange of a higher lying strangeness zero meson trajectory. Also, the hyperon may be produced at any vertex of a multiperipheral diagram. But the external line for the final state nucleon must be further away from the vertex of the K^- beam particle than the external $\overline{K}^\circ$ line. If this were not so, one would have to invoke the exchange of a positive strangeness baryon and there is no definitive evidence for the existence of such an object.[26]

CHAPTER VI

COMPARISON OF DATA WITH MODEL OF PLAHTE AND ROBERTS

The Plahte and Roberts model attempts to predict the relative amounts of resonance present in the data. Figure 49 shows the mass distributions of $\Lambda\pi^-$ and $\Lambda\pi^+$ for Reaction (I-1) versus the predictions. We see that the model predicts approximately twice as much $Y^{*\pm}(1385)$ as is observed in the data. However, in the case of $\rho^\circ(765)$ there is good qualitative agreement with the data as shown in Figure 50. This model and the data agreed quantitatively about the amount of $\rho^\circ(765)$ produced in Reaction (I-2). For Reaction (I-3) it predicted excessive resonance production. In fact, our data have a total of 0.6 pairs of particles per event in the $Y^{*\pm 0}(1385)$ and $\rho^{\pm 0}(765)$ resonances while the model predicted 1.5. The most striking disagreement was in the $\pi^+\pi^\circ$ mass distribution, which is shown in Figure 51.

The CLA and this model's single particle production angular distributions are very similar for Reactions (I-1) and (I-2). For Reaction (I-3) the CLA model gave better results. In particular, the Plahte and Roberts model failed to give both Λ° peaking in the backward direction and π° peaking in the forward direction.

We conclude that this model of Plahte and Roberts as we have parameterized it does not give a good description of our data. We remind the reader that we have only included the effects of isospin

Figure 49.--Mass distributions of Reaction (I-1) where the smooth curve is the prediction of the Plahte and Roberts model normalized to the data for the particle combinations (A) $\Lambda\pi^-$ and (B) $\Lambda\pi^+$.

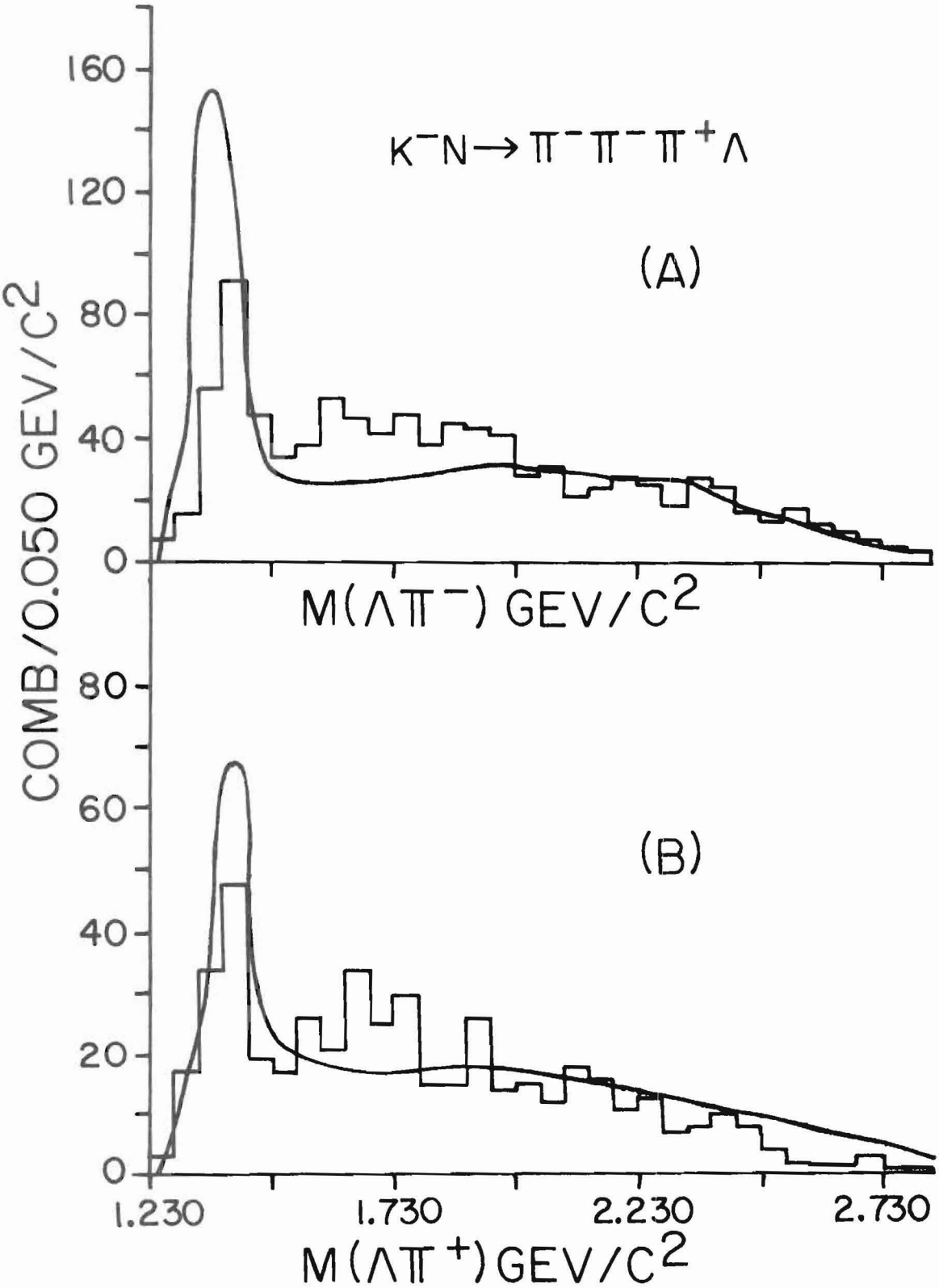
$K^-N \rightarrow \pi^-\pi^-\pi^+\Lambda$
(A)
(B)
COMB/0.050 GEV/C^2
160
120
80
40
0
80
60
40
20
0
1.230
1.730
2.230
2.730
$M(\Lambda\pi^-)$ GEV/C^2
$M(\Lambda\pi^+)$ GEV/C^2

Figure 50.--The $\pi^+\pi^-$ invariant mass distribution for Reaction (I-1) where the smooth curve is the prediction of the model of Plahte and Roberts normalized to the data.

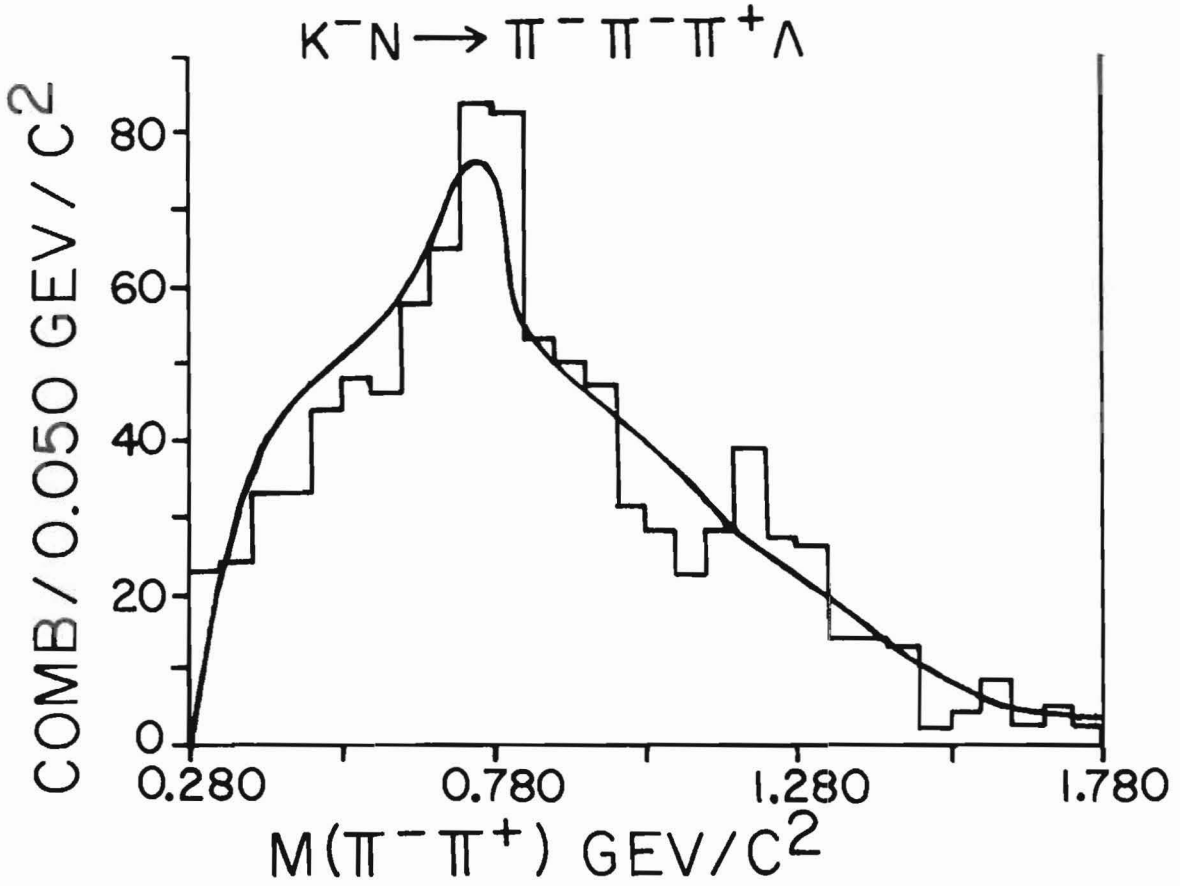
K⁻N → π⁻π⁻π⁺Λ
COMB / 0.050 GEV / C²
80
60
40
20
0
0.280
0.780
1.280
1.780
M(π⁻π⁺) GEV/C²

Figure 51.--The distribution in $M(\pi^+\pi^\circ)$ for Reaction (I-3) where the smooth curve is the prediction of the Plahte and Roberts model normalized to the data.

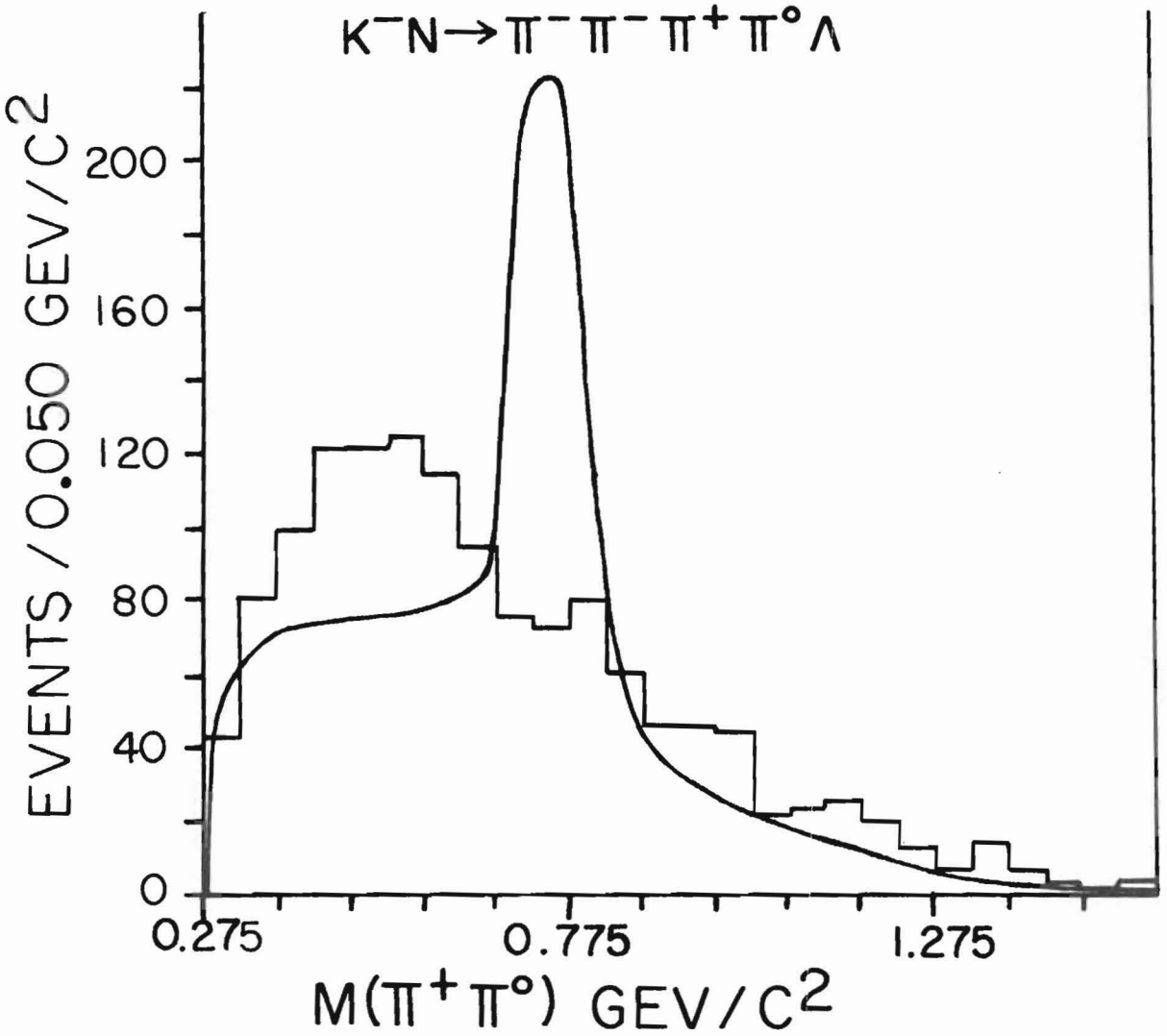
K⁻N→π⁻π⁻π⁺π°Λ
EVENTS / 0.050 GEV/C²
200
160
120
80
40
0
0.275
0.775
1.275
M(π⁺π°) GEV/C²

in an approximate manner.

CHAPTER VII

CONCLUSIONS

The cross-sections for Reactions (I-1), (I-2) and (I-3) and for the production of well known resonances in them have been measured. Other experiments at nearby energies have indicated the existence of a Y^* resonance having a mass of (1.626 ± .007) GeV/c^2, and a width of (0.066 ±0.014) GeV/c^2.[19,21] We find no compelling evidence for the presence of this resonance in our data. However, we cannot exclude the possibility of its existence. We have also searched our data for the $\Lambda_2(1330)$ resonance. This resonance is well known, but has only recently been reported in K^-N data. That was at nearby incident beam momenta.[24,25] We find no compelling evidence for the existence of this resonance in our data.

The cross-sections for Reactions (I-1) and (I-2) at an incident beam momentum of 3.0 GeV/c have been published.[29] These are (530 ± 50) and (180 ± 40) μbarns respectively while ours are (180 ± 30) and (90 ± 16) μbarns. The cross-section for Reaction (I-3) and its resonance production have also been published[27] for 3.0 GeV/c. These are shown in Table 7 and can be compared with our cross-sections shown in Table 2. For the 3.0 GeV/c data $\rho(765)$ and $\Sigma^\circ(1750)$ are not observed. However, the quasi-two-body state $Y^{*-}(1385)\omega^\circ(784)$ is observed at 3.0 GeV/c but we do not detect it in our data. Also, we have no compelling evidence for $Y^{*+}(1385)$ in this reaction, but it is seen at the lower momentum.

TABLE 7

CROSS-SECTIONS AND PERCENTAGES FOR RESONANCES OBSERVED IN THE REACTION $K^-N \rightarrow \Lambda\pi^-\pi^-\pi^+\pi^\circ$ AT AN INCIDENT BEAM MOMENTUM OF 3 GeV/c[27]

Final State	Percent	Cross-Section (μbarns)
$Y^{*+}(1385)\pi^-\pi^-\pi^\circ$ $\hookrightarrow \Lambda\pi^+$	10.5 ± 2.5	78 ± 20
$Y^{*-}(1385)\pi^+\pi^-\pi^\circ$ $\hookrightarrow \Lambda\pi^-$	30 ± 5	225 ± 40
$Y^{*\circ}(1385)\pi^+\pi^-\pi^-$ $\hookrightarrow \Lambda\pi^\circ$	13 ± 3	98 ± 25
$Y^{*-}(1385)\omega(784)$ $\hookrightarrow \Lambda\pi^-$ $\hookrightarrow \pi^-\pi^+\pi^\circ$	14 ± 3	105 ± 25
$\Lambda\omega(783)\pi^-$ $\hookrightarrow \pi^-\pi^+\pi^\circ$	10 ± 3	75 ± 25
$\Lambda B^-(1235)$ $\hookrightarrow \pi^-\pi^-\pi^+\pi^\circ$	1 ± 1	8 ± 8
$\Lambda B^-(1235)$ $\hookrightarrow \omega(784)\pi^-$	12.5 ± 3	94 ± 25
$\Lambda\pi^+\pi^-\pi^-\pi^\circ$	9	68
TOTALS	100.0	751 ± 65

Comparisons between the CLA model and the distributions of the data for center of mass production angle of various particle combinations, and single particles were made. The results of this model were also compared with the data for the single particle distributions in longitudinal momentum and transverse momentum. We found good qualitative, but not quantitative agreement. This lends encouragement to the idea of multiperipheralism and supports the idea that further theoretical work using the ideas employed in the model may lead to better quantitative agreement and increased understanding of the strong force.

The CLA model does not attempt to predict the relative amounts of resonance production. We compared the data to a calculation based on a model of Plahte and Roberts and found strong disagreement on this point. However, it must be borne in mind that this calculation took the conservation of isotopic spin into account in only an approximate manner.

APPENDIX

APPENDIX

CROSS-SECTION PER EVENT

The cross-section per event was found by averaging the results of two methods. The value obtained was (0.220 ± 0.033) μbarns per event. Roll numbers 765 and 766 were scanned twice by our best scanners. For every fifth frame a count of the interactions and a count of the beam tracks was taken. The results are given in Table 8. The sensitivity S_B, which is the number of events per unit cross-section, of these two

TABLE 8

CROSS-SECTION DATA FOR ROLLS 765 AND 766

ROLL 765	ROLL 766	
88	110	$(\overline{K} + \Lambda^\circ)$ Vees
91	113	$(\overline{K} + \Lambda^\circ)$ Vees corrected for events that did not pass geometry program
492	423	Events with even number of prongs (Every fifth frame)
14.0	13.5	Average number of beam tracks
1182	1165	Total frames

rolls with no spectator cut and using the beam track count was found from

$$S_B = \frac{N_t X_{av} T}{f_\mu} , \qquad \text{(A-1)}$$

where

N_t = 4.15×10^{22} neutron-targets/cm^3,

f_μ = (1/.95) is the assumed correction for muon contamination in the beam,

T = 3.22×10^4 is the total number of beam tracks,

and X_{av} = 128 cm is the average length which a beam track travels in the chamber before interacting.

The average beam track length in the bubble chamber was obtained from

$$X_{av} = \ell[1 - e^{-X/\ell}] \qquad \text{(A-2)}$$

where

X = 146 cm is the fiducial length used in the bubble chamber,

and ℓ = 532 cm is the interaction mean free path.

The value obtained for S_B was 0.162 events per μbarn. It should be pointed out that X_{av} did not take account of the beam attenuation due to decay of the K^-. However this would have changed S_B by only approximately two per cent and this is a relatively unimportant correction. Furthermore, the final sensitivity was obtained from an average of S_B and the sensitivity determined by a second method and including the correction for the K^- decay would have changed the final result by only about one per cent.

The sensitivity, S_I, of the two cross-section rolls was found by use of the following equations:

$$\sigma_S(\text{even prongs}) = \sigma_S(K^-P) + \sigma_{SP}(K^-N), \qquad \text{(A-3)}$$

$$\sigma_S(K^-P) = \sigma_T(K^-P) - \sigma_{ELU}(K^-P), \tag{A-4}$$

$$\sigma_{SP}(K^-N) = \sigma_T(K^-N) f_S H, \tag{A-5}$$

and

$$S_I = \frac{N_e}{\sigma_S(\text{even prongs})} . \tag{A-6}$$

The total cross-sections $\sigma_T(K^-P)$ = 24.8 mb and $\sigma_T(K^-N)$ = 21.1 mb were obtained for our beam momentum by linear interpolation between the counter results at 3.98 and 6 GeV/c. These are given in Table 9. The meaning of the other symbols is as follows:

$\sigma_z(X)$ = cross-section for X where

- z = S means X was observed in the bubble chamber,
- z = T means the total cross-section for X,
- z = ELU means the elastic unseen cross-section for X where we have considered a proton of momentum less than 0.100 GeV/c as being unseen,
- z = SP means X was observed in the bubble chamber with a spectator proton,

$\sigma_{ELU}(K^-P)$ = 0.3 mb,

N_e = 4575 is the number of even pronged events observed for the two cross-section rolls,

f_S = 0.325 is the fraction of observed spectators, and

H = 0.918 is a correction for the hiding of the neutron by the proton of the deuteron.[6,7]

Using Equations (A-3) through (A-6) we obtained S_I = 0.149 events per

TABLE 9

TOTAL CROSS-SECTIONS[7,30] FOR K^-P, K^-D AND K^-N
FOR VARIOUS BEAM MOMENTA

Total Cross-Section (mb)	Beam Momentum (GeV/c) 2.48	2.97	3.98	4.91	6	8	10
K^-P	26.9 ± 0.5	25.3 ± 0.4	25.4 ± 0.7	24.8	24.0 ± 0.3	23.6 ± 0.2	22.5 ± 0.2
K^-D	47.8 ± 0.6	46.2 ± 0.4	44.7 ± 0.5	44.4	44.1 ± 0.3	41.7 ± 0.3	41.5 ± 0.3
K^-N	22.6 ± 0.9	22.4 ± 0.7	20.5 ± 0.9	21.1	21.9 ± 0.4	19.7 ± 0.4	20.6 ± 0.4

↑
Interpolated

μbarn. Earlier we obtained $S_B = 0.162$ events per μbarn. These results are consistent and we average them to obtain a sensitivity for the two cross-section rolls of $S = 0.155$ events per μbarn. The cross-section per event for the total sample is then

$$(1/S)(N_v/N_t) \tag{A-7}$$

where

$N_v = 204$ is the number of $(\overline{K}^\circ + \Lambda^\circ)$ vees for the two cross-section rolls and

$N_t = 5991$ is the total number of $(\overline{K}^\circ + \Lambda^\circ)$ vees in the sample.

Thus we obtain a cross-section per event for the experiment of (0.220 ± 0.033) μbarn/event.

LIST OF REFERENCES

1. Chan Hong-Mo, J. Loskiewicz and W. W. M. Allison, Nuovo Cimento 57A, 93 (1968).

2. E. Plahte and R. G. Roberts, Nuovo Cimento Letters 1, 187 (1969).

3. J. G. Androulakis, et al., Nucl. Inst. and Methods 20, 100 (1963).

4. J. W. Burren and J. Sparrow, National Institute for Research in Nuclear Science Report NIRL/R/14 (1963), and A. G. Wilson, NIRL/M/38 (1962); "Geometry Program Manual," Science Research Council, R. H. E. L., Chilton, Didcot, Berkshire, England (1968); "Kinematics Program Manual," Science Research Council, R. H. E. L., Chilton, Didcot, Berkshire, England (1968); "Geometry Testing Program Optical Constants," Science Research Council, R. H. E. L., Chilton, Didcot, Berkshire, England (1968).

5. R. R. Price, Ph.D. Dissertation, Vanderbilt University, 1971 (unpublished).

6. R. J. Glauber, Phys. Rev. 100, 242 (1955).

7. W. Galbraith, et al., Phys. Rev. 138B, 913 (1965).

8. T. B. Borak, Ph.D. Dissertation, Vanderbilt University, 1969 (unpublished).

9. L. Hulthén and M. Sugawara, in "Handbuch der Physik," edited by S. Flugge (Springer-Verlag, Berlin, 1957), Vol. 39, p. 1.

10. Riccardo Levi Setti, "Elementary Particles," The University of Chicago Press, Chicago, 83-85 (1966).

11. J. D. Jackson, in "High Energy Physics," edited by C. DeWitt and M. Jacob (Grodon and Beach, New York, 1965), p. 329.

12. A. Weinberg, Vanderbilt University, Nashville, Tennessee (private communication).

13. It happens for reasons too trivial to discuss here that those 27 events of Reaction (I-3) that are also ambiguous with Reaction (I-2) are not in the plot. There was no justifiable reason to rerun the computer program to include them.

14. G. Bassompierre, et al., Nuclear Physics B9, 295 (1969).

15. H. Pilkuhn, "The Interactions of Hadrons," John Wiley and Sons, Inc., New York, 35 (1967).

16. J. P. Chandler and C. A. Tilger, Nuclear Instruments and Methods 51, 117 (1967).

17. J. Orear, et al., Physical Review Letters 21, 389 (1968).

18. David J. Crennell, et al., Physical Review Letters 21, 648 (1968).

19. David J. Crennell, et al., "Proceedings of the Lund International Conference on Elementary Particles," edited by G. von Dardel (Berlingska Boktryckeriet, Lund, Sweden, 1969).

20. R. Barloutaud, et al., Nuclear Physics B16, 201 (1970).

21. A. C. Ammann, et al., Physical Review Letters 24, 327 (1970).

22. H. Pilkuhn, "The Interactions of Hadrons," John Wiley and Sons, Inc., New York, 32 (1967).

23. Gerson Goldhaber, et al., Physical Review Letters 12, 336 (1964).

24. A. F. Garfinkel, et al., Physics Letters 33B, 536 (1970).

25. David J. Crennell, et al., Physical Review Letters 22, 1327 (1969).

26. Matts Roos, et al., Physics Letters 33B, 1 (1970).

27. W. Hoogland, et al., Physics Letters 33B, 631 (1970).

28. J. D. Jackson, Reviews of Modern Physics 37, 484 (1965).

29. D. Merrill, et al., Nuclear Physics B18, 403 (1970).

30. V. Cook, et al., Physical Review 123, 320 (1961).